# APPLICATION OF IN SITU Rb-Sr DATING AND GEOCHEMICAL INVESTIGATIONS ON A NEW, 1.52-1.56 GA. OLD PEGMATITE FIELD IN THE ARCHIPELAGO OFF GOTHENBURG, IDEFJORDEN TERRANE, WESTERN SWEDEN

**Laszlo Zorc**

**Degree of Master of Science (120 credits)
with a major in Earth Sciences
45 hec**

**Department of Earth Sciences
University of Gothenburg
2023 B1261**

**Faculty of Science**

UNIVERSITY OF GOTHENBURG

# APPLICATION OF IN SITU Rb-Sr DATING AND GEOCHEMICAL INVESTIGATIONS ON A NEW, 1.52-1.56 GA. OLD PEGMATITE FIELD IN THE ARCHIPELAGO OFF GOTHENBURG, IDEFJORDEN TERRANE, WESTERN SWEDEN

**Laszlo Zorc**

Table of Contents

# Abstract

In this study, Rb-Sr geochronology was used to determine the crystallization/cooling ages of muscovites and biotites from mapped primitive barren and rare element pegmatites in the Stora-Le-Marstrand Formation in the southwestern archipelago of Gothenburg. The results indicate that primitive barrens can be linked to the DG2 deformation event that occurred 1.56-1.54 Ga and suggest an anatectic origin and limits the migmatisation event to 1547 Ma. The study also found that the Leucosome sample from the SLM Fm. and the barrens have similar geochemical fractionation indicators, which supports the theory that these barrens originate from the partial melt of the SLM Fm. A correlation was identified between the degree of fractionation and the cooling age of the barrens, with younger barrens showing greater fractionation as seen in parameters such as Ba/Rb, Rb/Sr and trace element concentrations of Li, Ta and Cs in muscovites, biotites, garnets and feldspars. Rb-Sr ages of biotites were used as an exhumation age indicating that the area of the SLM Fm. west of Gothenburg reached a temperature of 300-350°C at around 938 to 973 Ma, which is consistent with the end of the Sveconorwegian orogeny. The study also found that the beryl-bearing rare element pegmatites on the island of Donsö are of cogenetic origin yielding calculated cooling ages of 1520 ± 6.4 2s Ma, the study suggest the source for these pegmatites may be another deformation event or the last intrusive stage of the Hisingen suite. The study also found that fast data acquisition with the handheld XRF is suitable for a rough estimate of the degree of fractionation and that the Rb-Sr dating process can be made faster and easier by using the initial Sr isotope ratios of 0.715 ± 0.015 (for enriched magmatic rocks) by Rösel & Zack (2022). Overall, this study provides new insights into the formation and evolution of the pegmatites in the Idefjorden terrane and highlights the potential of using Rb-Sr geochronology for dating pegmatites. The correlation between fractionation degree and cooling age of the barrens and rare element pegmatites, as well as the determination of exhumation ages from biotites samples, add to our understanding of the geodynamic processes occurred in this part of the Idefjorden terrane.

# Introduction

As the world shifts towards more sustainable energy sources, the demand for rare metals such as Li, Nb, Ta, Sn, W, and rare earth elements (REE) has increased significantly (Linnen et al., 2012). This has sparked interest in re-evaluating pegmatites as potential sources of these critical elements in Europe (Beurlen et al., 2014; Müller et al., 2022). To ensure a sustainable supply of these critical materials in the future, it is crucial to gain a better understanding of the petrogenesis of pegmatite deposits.

Southern Norway and western Sweden are known for their occurrence of rare element pegmatites of the NYF & LCT group, which manly formed during the Sveconorwegian orogeny. However, with the absents of parental plutons the formation of rare element pegmatites in a metamorphic terrain is still not well understood (Romer & Smeds 1996; Müller, 2017). In the archipelago southwest of Gothenburg, various magmatic intrusions like, gabbros, granites and granitic pegmatites containing exotic minerals such as beryl, columbite and chrysoberyl can be found. These pegmatites are mineralogically similar to known Sveconorwegian pegmatites such as Skuleboda, Högsbo, Timmerhult and Gulebo, but are cross-cutted by 1.44 Ga old Koster dykes (e.g., Ursholmen island), indicating a different origin.

Age dating of pegmatites in southwestern Sweden is mainly done with U-Pb on columbite and euxenite minerals, which do not occur in every pegmatite (Smeds, 1990; Romer & Smeds, 1996). However, with recent improvements in the *in situ* Rb-Sr dating method (Zack & Hogmalm 2016; Hogmalm et al. 2017), using a laser ablation inductively coupled plasma spectrometer, it is now possible to precisely date Rb-enriched phases such as muscovites and biotites found in almost every pegmatite. Therefore, the aims of this study are:

(1) To map and characterize unknown pegmatite bodies in the southern archipelago of Gothenburg using a handheld XRF device to estimate the fractionation degree of K-feldspars and classify the pegmatites.

(2) To date muscovite and biotite samples from barrens and rare element pegmatites to draw conclusions on their genesis and utilizing the Rb-Sr ages of biotites as exhumation ages to estimate the thermal history of the area and its relation to the Sveconorwegian orogeny.

(3) Develop fractionation trends based on compatible and incompatible elements in the crystal chemistry of muscovite, biotite, garnet and feldspar. The results will be used to

provide evidence for whether these pegmatites have a residual melting or partial melting origin.

(4) Investigating the potential of established initial Sr isotope ratios by Rösel & Zack (2022) as a tool to make the Rb-Sr dating process faster and more efficient in pegmatite geochronology.

(5) Evaluating the potential of the handheld XRF as a tool for quick and cost-effective analysis of pegmatites in the field.

Overall, this study aims to contribute to a better understanding of the petrogenesis and geochronology of pegmatites in the Idefjorden terrain, and to provide important information for the sustainable exploration and utilization of these critical elements in the future.

# 1. Pegmatites

Pegmatites are holocrystalline igneous intrusive rocks, predominantly of granitic composition (quartz, feldspar, ± muscovite, ± biotite), with crystal sizes >3 cm, although the variation in crystal sizes within a pegmatite is very heterogeneous and can vary from a few μm to several meters (London, 2008). Larger, pegmatite lenses, but also pegmatite veins often show a well-developed zonal arrangement of mineral precipitates where the mineral formations of the inner zones replace or displace those of the outer zones, but never the reverse. In addition, pegmatites can exhibit monomineralic zones, often present of Quartz in the center or by graphic skeletal intergrowths when two phases crystallize simultaneously (e.g., tourmaline - quartz, k-feldspar – quartz; London, 2018). None of these features are necessarily present in every pegmatite, but they often occur together. According to London (2005), the zonar structure and structural features of pegmatites can be explained by rapid crystal growth from a supercooled and thus supersaturated melt. In the process, crystallization fronts were formed at the boundaries of the magma bodies, where mainly the growth of quartz and k-feldspar took place. Incompatible elements, such as Li, Be, B and F, are not incorporated into these mineral phases, but are pushed in front of the crystallization front, so that the zonal enrichment of the corresponding rare minerals occurred. In this context, it is interesting that unusually short cooling times have been estimated for many plutonic pegmatites, which would explain the supercooling of the melt (London, 2005). As an example, the Harding pegmatite in New Mexico is said to have cooled to solidus within a

few months of its emplacement (Chakoumakos & Lumpkin, 1990). For the Little Three pegmatite vein near Ramona (California), a cooling time of 25 days was estimated (Morgan & London, 1999), and the 30 cm thick gemstone pegmatites of Himalaya-San Diego, County are even said to have needed only little more than a week to reach solidus temperature (Webber et al. 1997, 1999). A particular interest of pegmatites, besides their gigantic crystal size and potential for gemstones, is their enrichment with rare elements such as Nb, Ta, Li and Sn (Simmons and Webber, 2008). Pegmatites are also exploited for silicates such as feldspar and quartz for glasses and ceramics (Černý, 1991; Linnen et al. 2012; London & Kontak, 2012). With the increasing interest in commercial exploitation of pegmatites for rare elements, it is important to understand the sources and processes involved in pegmatite formation. Although the geochemical and structural characteristics of granitic pegmatites vary, they share a common genetic feature: crystallization from volatile melts with varying enrichments of lithophilic rare elements (Černý, 1991; London, 2008).

## 1.1. Formation of Pegmatites

The formation of pegmatites has been discussed for many years. At present, there are two hypotheses that aim to explain how pegmatite forming melts are generated (e.g., London, 2005; Černý et al. 2012; London & Morgan, 2012; Simmons et al. 2016; Shaw et al. 2016; Wise et al. 2022) namely, through late-stage fractional crystallization processes associated with granitic plutons (residual pegmatites; London, 2005) and alternatively, the anatectic model, with low degrees of partial melting, where the bulk rock composition of source rocks controls the pegmatite chemistry (see figure 1; Barros and Menuge, 2016; Demartis et al. 2011; Fei et al. 2020; Gourcerol et al. 2019; Müller et al. 2017; Simmons et al. 2016; Webber et al. 2019; Wise et al. 2022). Both the differentiation and anatectic models are considered valid for the generation of barren pegmatites (Černý & Ercit, 2005; Simmons & Webber, 2008). There is however an ongoing debate concerning the genesis of rare-metal pegmatite especially in places where granites are not observed around the rare element pegmatites. Despite these differing views on the origin of pegmatites, there is general agreement that they form by primary crystallization from a volatile, siliceous melt (Jahns & Burnham, 1969; Černý, 1991; London, 1990).
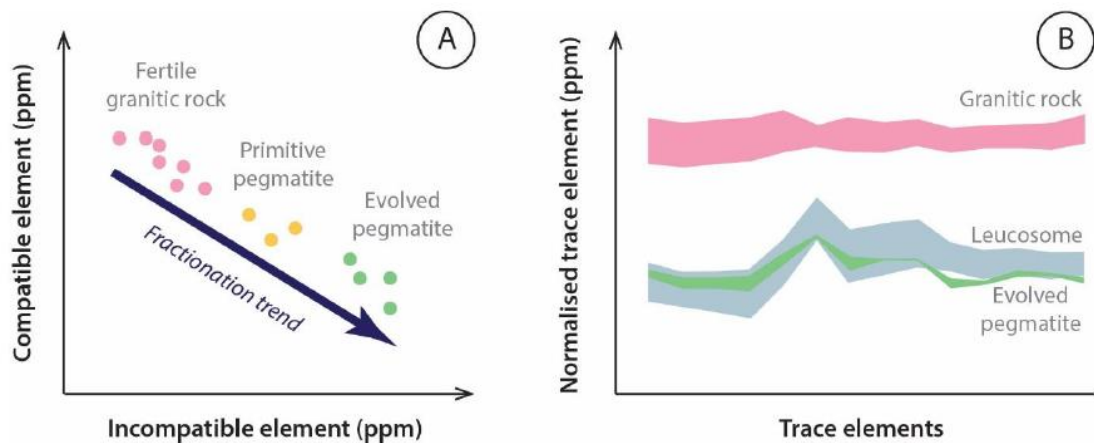
*Figure 1: Assumed geochemical signatures of pegmatites formed by continuous crystallization of a pluton (A) or by partial melting (B). (A) A simplified model of geochemical fractionation from fertile granitic rocks to evolved rare element pegmatites with intervening barren pegmatites. This is applicable to either whole-rock or mineral geochemistry (e.g. Wise & Brown, 2010; Černý et al. 2012). (B) Comparison between the broadly similar trace element signatures of evolved pegmatites and leucosomes from adjacent migmatites and the contrasting compositions of a nearby granitic pluton in Maine, after Simmons et al. (2016).*

### 1.1.1. Residual pegmatites

The first model to form rare-element pegmatite is by extended fractional crystallization of a granitic, water-rich magma at the scale of a pluton (Figure 2; London, 2005). This model is widely accepted and is based on the close spatial association and trace element similarity between the pegmatites and granitic plutons (O'Connor et al. 1991; London, 2005; Martin & De Vito, 2005). This means that the composition of the source magma has a major influence on the final composition of the resulting rare element pegmatites (Černý, 1991). For a pegmatite to have formed according to this genetic model, several conditions must be fulfilled (Černý, 1991; Černý & Ercit, 2005; Martin & De Vito, 2005; London, 2005; Linnen et al. 2012):

- a relative chronology supporting a continuous crystallization process
- the presence of physical links between pegmatite bodies and parental pluton
- an identity of pegmatite bodies inside and beyond the outer contact of the pluton in a proximal position
- continuity in textural, mineralogical, and geochemical parameters
- a limited timeframe allowing the persistence of residual melt
- correspondence of bulk compositions to experimentally determined minima or eutectics in geochemically evolved systems, and relevance of temperatures of crystallization to these experimental findings.

Several authors support this genetic model of pegmatite formation by extended fractional crystallization of a fertile granite, even where a parent granite body is not present (e.g., Crouse & Černý, 1972; Jahns & Ewing, 1976; Černý and Ercit, 2005; Stilling et al. 2006; Hulsbosch et al. 2014; London, 2014; Roda-Robles et al. 2018). This poses the question whether it is valid to assume that, if a pegmatite cannot be proven to be spatially, temporally, or genetically related to parent granites, an unseen granitic body exists at depth (Shaw et al. 2016). Considering this question, Martin & De Vito (2005) suggested that a detailed understanding of tectonic settings and magmatic chronology is necessary to understand the origin of pegmatites in question.

### 1.1.2. Anatectic pegmatites

In several places, the anatectic model offers a better explanation for the field and structural characteristics of pegmatite fields than the residual melt model. Various orogenies provide different examples of the relationship between pegmatite fields and anatectic areas (Deveaud et al. 2015; Müller et al. 2017). This model relates the formation of rare-element pegmatites through small degree partial melting of crustal sources (figure 2), which results in the enrichment of incompatible elements and rare metals in the pegmatites (Simmons et al. 1995, 1996, Simmons & Webber, 2008; Shaw et al. 2016). The formation of pegmatites through the partial melting of crustal rocks is based on (Norton & Redden, 1990; Martin & De Vito, 2005):

- a common similarity between the pegmatites and host-rock major bulk geochemistry
- the occurrence of leucosomes with pegmatitic textures in metamorphic terranes
- the difficulty of relating highly evolved magma compositions to plausible granitic sources by geochemistry and geochronology

Anatectic pegmatite genesis often works as an alternative explanation model in areas where these requirements are not fulfilled. For example, if no potential parental granite is exposed or the granite body occurs to far away from the pegmatites (Shaw et al. 2016; Müller et al. 2017) or the pegmatites show a clear age deviation than an adjacent granite (Müller et al. 2017; Webber et al. 2019). Other areas where anatexis is used as an explanation are the absence of chemical zoning around the granite body (Müller et al. 2017; Fuchsloch et al. 2018; Webber et al. 2019) or a big different in geochemistry patterns between the pegmatites and the granitic parent body (Fuchsloch et al. 2018; Konzett et al. 2018). The anatectic model is especially appropriate to LCT pegmatites

and is based on the idea that fluxing and incompatible elements are often present in a sedimentary sequence that melts to form large volumes of granitic magma, which could later fractionate to form pegmatite melts; if low-degree partial melts are generated instead, the same elements could partition into them and form pegmatite melts directly without fractionation from a larger body of granitic magma (Simmons & Webber, 2008). The heat source comes from an adjacent granitic intrusion or mafic underplating in an orogenic setting. Although this model is still an area of on-going research, it has already been supported by various authors (e.g., Norton & Redden, 1990; Simmons et al. 1995, 1996; Kontak et al. 2005; Martin & De Vito, 2005; Deveaud et al. 2015; Müller et al. 2017). Nevertheless, some inconsistencies remain, such as pegmatite melts must be emplaced/travel rapidly enough to preserve a thermal contrast with host rocks, which is the condition for the development of their characteristic textures (e.g. Devineau et al. 2020; London & Morgan, 2012).
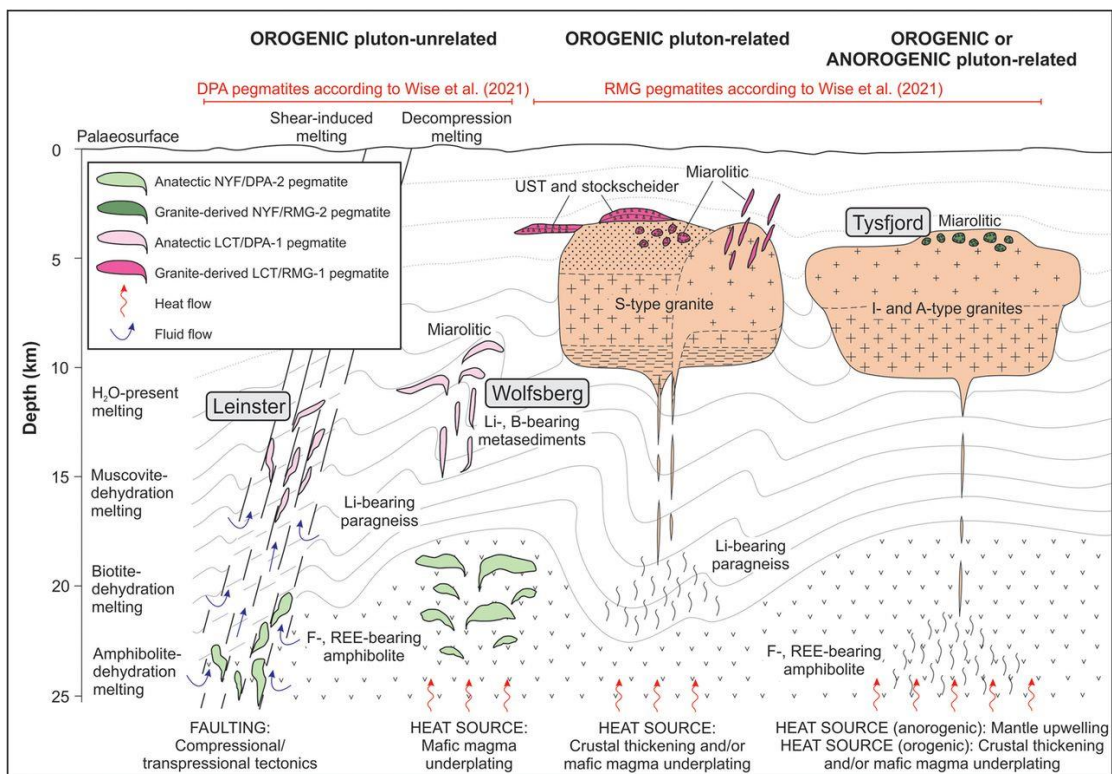


*Figure 2: Schematic crustal profile illustrating the contrasting controls on the formation of pegmatites in a pluton-related, compared with a pluton-unrelated, scenario. In the case of pluton-unrelated settings, the degree of partial melting and source rock composition control the formation of barren or rare element pegmatites. The indicated dehydration melting depths correspond to geothermal gradients of 35–40°C km$^{-1}$. Müller, Axel et al. Geological Society, London, Special Publications (2022), 526 (1)*

## 1.1.Internal evolution of pegmatites

Various processes have been proposed to explain the zoning observed in pegmatites. It was previously considered that the crystal size observed in pegmatites could be explained by slow cooling in a silicate melt or by the interaction between an aqueous vapor phase and a silicate melt (Jahns & Burnham, 1969). However, recent studies suggest that pegmatites are undercooled liquids crystallize on a timescale of days to months or years (Nabelek et al. 2010; London, 2014, 2018). This is thought to be possible due to the presence of fluxing elements including H, B, P, F and Li, which lower the viscosity and solidification temperature of granitic melts while enhancing diffusion and facilitating rapid crystal growth (London & Morgan 2012). Under these conditions, crystal nucleation rates decrease, and ion diffusion increases, which can lead to the formation of large crystals characteristic of pegmatites (Nabelek et al. 2010). Undercooling due to heat dissipation from a magmatic body and a delay in nucleation between cooling and the onset of crystallization lead to supersaturation of the melt with fluxes and incompatible elements (Nabelek et al. 2010; London 2014). Rapid crystallization and supercooling lead to the formation of a boundary layer of excluded elements in front of the crystallization growth front through a process known as constitutional zone refinement (CZR) (London, 2014; London 2018)

## 1.1.1. Constitutional zone refining

Constitutional Zone Refining (CZR) is a process where incompatible elements (mostly related to feldspar and quartz) are enriched in the residual fluid of a crystallizing pegmatite body (London, 2014, 2018). As crystallization proceeds, the solidus of the boundary layer decreases as it becomes enriched in fluxing elements such as F, H, Li, P, B and other incompatible elements relative to the composition of the source melt (Figure 3; London, 2018). The accumulation of fluxing elements at the crystal growth front forms complexes with incompatible elements in the melt, leading to an increased size of the crystallizing phases. This process explains the huge crystal size and pronounces enrichment of rare metals in the intermediate zones of pegmatites (London, 2014, 2018). CZR is detectable in fully developed zoned pegmatites. Here, the outer zones of a pegmatite body, which contain graphic textures and fine crystalline minerals, are dominated by the effects of supercooling, while the increasingly coarse and blocky inner zones result from flux build-up in the boundary layer (London, 2018; London & Morgan, 2012).
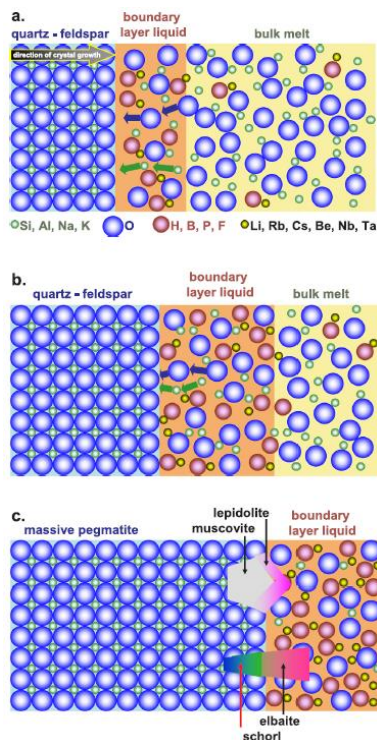
*Figure 3: Schematic diagram illustrating crystal growth in the boundary layer, local saturation, and fluxed constitutional zone-refining (CZR). (a) In CZR, compatible components dissolve from the bulk melt through the boundary layer and accumulate on the surfaces of the rock-forming minerals. (b) Excluded components become enriched in the boundary layer fluid as fluxes lower the solidus temperature and increase the miscibility of all components. (c) As soon as the components of the main melt are exhausted, crystallization from the boundary layer fluid occurs, leading to abrupt changes in the composition of the minerals (mica, tourmaline) that grow in this interval (London, 2018).*

## 1.1.2. Melt-melt immiscibility

Melt inclusion studies initiated by Thomas et al. (2000) indicate the coexistence of two immiscible melts during the crystallization of pegmatite magmas. One melt is a high viscosity, silicate-rich, low water and flux peraluminous melt (Type-A) and the second is a low viscosity, high water and flux, low silicate, (per)alkaline melt (Type-B) (Thomas et al. 2012). The two melts thus represent conjugate melt fractions resulting from the immiscibility of melt and melt in extremely water-rich parent melts. Although Type A and Type B melts coexist, the physical and chemical differences between the melts have a significant impact on the distribution of elements between them (Thomas & Davidson, 2012). Thomas et al. (2012) and Thomas & Davidson (2012) concluded that melt-melt immiscibility occurs in pegmatites near the crystallization front and eliminates the need for a flowed-through boundary layer and processes of constitutional zone refinement during crystallization of a pegmatite melt, as proposed by London (2018). Indeed, it is the density contrasts between Type A and Type B melts that allow their separation under gravity and thus can explain the differences in mineralogy, texture and bulk composition of zoned pegmatites.

## 1.1.3. Tracer in Pegmatite Fractionation

Various mineralogical features, such as the K/Rb or Ba vs Rb/Sr ratio of K-feldspar and the Mn/Fe ratio of garnets are commonly regarded as diagnostic of rare-metal

pegmatites (Černý et al. 1985). They are interpreted as the result of fractional crystallization from a parent granite (London, 2008; Černý et al. 2012). However, it seems clear that other processes such as low degrees of partial melting could produce a similar set of characteristics. Barium has almost the same size as potassium and rubidium, which means that the K-feldspar precipitation controls the Ba distribution in differentiated granitic suites. Therefor Ba/Rb and K/Ba ratio in K-Feldspar is one of the most sensitive indicators of fractionation in magmatic systems (Taylor & Heier 1960, Taylor et al. 1967). Ba contents of leucogranites are generally less than 500 ppm in Kfsp and in pegmatitic granites usually below 100 ppm (Kolbe & Taylor 1966, Taylor et al,1967). By that a high Ba content means a less fractionated melt composition. However, within the pegmatites, the content of Ba in Kfsp can vary greatly from core to rim. For example, the beryl-columbite pegmatite in Věžná, Czech Republic has 1000 ppm Ba in Kfsp within the border zone and only 40 ppm in the core zone (Černý and Burt, 1984). Another indicator of a fractionated melt is the Rb/Sr ratio. It is commonly used to determine the degree of differentiation (fractional crystallization and/or partial melting) that a magmatic system has undergone (Černý et al. 1985; Clark and Černý, 1987; Halliday et al. 1991). Because strontium is compatible and rubidium is incompatible in feldspars, as magmatic systems evolve the Rb/Sr ratio of the melt tends to increase particularly in highly evolved granitic and pegmatitic systems (e.g. Černý et al. 1985; Clark and Černý, 1987; Halliday et al. 1991). Micas are, behind K-feldspar and Quartz, the third most common minerals in pegmatites (Černý and Burt, 1984), which makes them useful for comparing pegmatites both within the same field and on a regional scale. Additionally, micas carry important trace elements like Li, Rb and F that can be used to evaluate the fractionation degree of the pegmatites (Černý and Burt, 1984; Neiva, 2013; Marchal et al. 2014).

## 1.2. Pegmatite Classification

The classification of pegmatites is broad and complex, which has led to a development of numerous different classification schemes over the last decades (Müller et al. 2018); however, the simplest division is that of barren and rare-element pegmatites, with the latter hosting appreciable amounts of rare minerals such as beryl, columbite, spodumene, tourmaline and other rare minerals (London, 2014). Many approaches to classify pegmatites have been proposed in the past, however, the most widely accepted is the depth-zone classification scheme from Černý & Ercit (2005) (see table. 1), modified

after Ginsburg et al. (1979). This "depth-zone classification" is based on a combination of depth of emplacement, metamorphic grade, mineralogy, and rare element content with an average estimation of the pressure and temperature conditions of the host rocks.

*Table 1: Černý´s depth-zone classification of granitic Pegmatites (from Černý et al. 2012)*

| Class | Family | Subclass | Type | Subtype |
|---|---|---|---|---|
| Abyssal | NYF | HREE | | |
| | NYF | LREE | | |
| | NYF | U | | |
| | LCT | BBe | | |
| Muscovite | | | | |
| Muscovite-rare element | NYF | REE | | |
| | LCT | Li | | |
| Rare element | NYF | REE | allanite-monazite | |
| | | | euxenite | |
| | | | gadolinite | |
| | LCT | Li | beryl | beryl-columbite |
| | | | | beryl-columbite-phosphate |
| | | | complex | spodumene |
| | | | | petalite |
| | | | | lepidolite |
| | | | | elbaite |
| | | | | amblygonite |
| | | | albite-spodumene | |
| | | | albite | |
| Miarolitic | NYF | REE | topaz-beryl | |
| | | | gadolinite-fergusonite | |
| | LCT | Li | beryl-topaz | |
| | | | spodumene | |
| | | | petalite | |
| | | | lepidolite | |

The Černý-Ercit classification describes three petrogenetic categories within the pegmatite classes Abyssal, Muscovite, Muscovite-rare element, rare-element and Miarolitic. The LCT-Family (Lithium-Cesium-Tantalum), the NYF-Family (Niobium-Yttrium-Fluorine), and ''Mixed'' (LCT- & NYF-Family), is based on the progressive accumulation of rare elements mainly derived from the fractionation of S-, A-, and I-type granite plutons (Černý 1991; Černý and Ercit, 2005). These families are divided into types and subtypes based largely on accessory mineralogy, rare element composition, and emplacement depth of the pegmatites. Černý´s classification was originally meant to describe the geochemical signature of granite-pegmatite systems or populations and were not intended to be applied to individual pegmatites (Černý & Ercit, 2005), which leads to unwarranted confusion and misclassification of some pegmatite localities (Wise et al., 2022). Therefore, Wise et al. 2022 propose a new, simpler classification based on mineral composition that uses a more comprehensive set of accessory minerals and defines three pegmatite groups that are genetically related to granite plutons and the anatexis of metaigneous and metasedimentary protoliths. Group 1 and 2 pegmatites

are formed from the residual melts of S-, A- and I-type granite magmatism (RGM) as well as being direct products of anatexis (DPA), while Group 3 pegmatites are formed only by anatexis (table 2).

*Table 2: Classification of RMG and DPA Pegmatites*

**RMG (Residual melts of granite magmatism)**

| | S-type granite | A-type granite | I-type granite |
|---|---|---|---|
| Typical source rock | | | |
| Granite chemistry | Peraluminous | Peralkaline & metaluminous to mildly peraluminous | Peraluminous to metaluminous |
| Relation of pegmatites to source | Interior to marginal | Interior to marginal | Interior to marginal |
| Pegmatite type | Group 1 | Group 2 | Groups 1 & 2 |
| Typical geochemical signatures | Be, Nb, Ta, P, Sn, Li, Cs, B | REE, Be, Nb, F | B, Be, REE, Nb, Ti, Li, Ca |
| Examples* | Winnipeg River, MB, Canada | Pikes Peak, CO, USA | Třebíč pluton, Czech Republic |
| | Cañada pegmatite, Spain | Mt. Perdosu, Italy | Strzegom granite, Poland |
| | Kalba field, Kazakhstan | Amis complex, Namibia | O'Grady batholith, NWT, Canada |
| | Malkhan field, Russia | Luumaki, Finland | Greer Lake, MB, Canada |

**DPA (Direct products of anatexis)**

| | | | |
|---|---|---|---|
| Typical source rock | Granulite to amphibolite facies metamorphic rocks | Granulite to amphibolite facies metamorphic rocks | Granulite to amphibolite facies metamorphic rocks |
| Relation of pegmatites to source | Segregations of anatectic melts | Segregations of anatectic melts | Segregations of anatectic melts |
| Pegmatite type | Group 1 | Group 2 | Groups 3 |
| Typical geochemical signatures | Be, Nb, Ta, P, Li, B | REE, U, Be | Al, Be, B |
| Examples* | Góry Sowie, Poland | Evje-Iveland, Norway | East Antarctica, Antarctica |
| | Oxford field, ME, USA | Lewisian Gneiss Complex, Scotland | Thomas mine, NC, USA |
| | Cape Cross-Uis, Namibia | Fraser Lake, SK, Canada | Dolní Bory, Czech Republic |
| | Leinster pegmatite belt, Ireland | Ploskaya, Kola Peninsula, Russia | Batchellerville, NY, USA |

Group 1 pegmatites are typically enriched in Li, Rb, Cs, Be, Ga, Sn, Ta > Nb, B, P and F with three types: (i) beryl ± phosphate-bearing type, (ii) Li-rich spodumene- or petalite-dominant type, and (iii) lepidolite or elbaite as the primary Li phase bearing type. These three types can, depending on the degree of fractionation, contain further accessory minerals (see table 3; Group 1). Many of the rare-element minerals listed here host or are enriched in Lithium and are typically associated with cleavelanditic albite, particularly in the more evolved units of pegmatite bodies (Wise et al. 2022). The pegmatites of Group 2 are at first sight difficult to distinguish from simple versions of group 1 pegmatites. They are mostly composed of feldspar and quartz, but the presence of small amounts of accessory minerals, such as fluorite, helvite, magnetite or hyalitopal, distinguishes them from group 1 pegmatites. Feldspars are predominantly potassium than sodium rich, local amazonite, while biotite over muscovite is the dominant mica class. Garnets are mostly spessartine rich. In principle, Fe mineral affinity can be recognized, such as biotite, fayalite, magnetite, allanite, ilmenite, hematite, epidote etc. (see table 3). Group 3 pegmatites are strongly peraluminous and consist essentially of quartz, K-feldspar, plagioclase, biotite, and almandine with accessory rare minerals such as muscovite, biotite, garnet, or tourmaline. Unique to this group is the presence of andalusite, sillimanite or cordierite, as well as chrysoberyl > beryl as the primary Be carrier.

*Table 3: Group 1-3 pegmatite classification with prominent accessory minerals of RMG (residual melts of granite magmatism) and DPA (direct products of anatexis) granitic pegmatites modified after Wise et al. (2022)*

## RMG

### Rock-forming

| Group 1 (S-type affiliation) | | Group 2 (A-type affiliation) | | Group 1 & 2 (I-type affiliation) | |
|---|---|---|---|---|---|
| Biotite | Fe, Mg | Biotite | Fe, Mg, Na | Biotite | Fe, Mg |
| Almandine | | Fayalite | | Almandine | |
| Muscovite | Al | Arfvedsonite/Riebeckite | | Muscovite | Al |
| | | Magnetite | | | |
| | | Spessartine | Mn | | |
| | | Muscovite | Al | | |

### Rare-element

| Group 1 (S-type affiliation) | | Group 2 (A-type affiliation) | | Group 1 & 2 (I-type affiliation) | |
|---|---|---|---|---|---|
| Schorl | Fe, B | Allanite | REE, Y, Be, Nb, Ta, P | Schorl | B |
| Beryl | Be | Gadolinite | | Beryl | Be |
| Columbite-group | Nb, Ta, Sn | Fergusonite | | Columbite-group | Nb, Ta |
| Tapiolite-(Fe) | | Samarskite | | Allanite | REE, Y, Nb, Ta |
| Cassiterite | | Euxenite | | Monazite/Xenotime | P |
| Graftonite group | P, Li, F | Columbite-group | | Topaz | F |
| Triphylite-lithiophilite | | Monazite | | Fluorite | |
| Amblygonite-montbrasite | | Xenotime | | Elabite | Li, B, Ca |
| Elbaite | Li, B | Beryl | Be | Liddicoatite | |
| Lepidolite | | Phenakite | | Lepidolite | |
| Spodumene | | Zinnwaldite | Li, Fe | Danburite | |
| Petalite | | Topaz | F | Hambergite | Be, B |
| Pollucite | Cs | Fluorite | | Epidot | Ca |
| | | Cryolite | | Stillbite/Laumonite | |

### Accessory minerals

| Group 1 (S-type affiliation) | | Group 2 (A-type affiliation) | | Group 1 & 2 (I-type affiliation) | |
|---|---|---|---|---|---|
| Apatite | | Aegirine | Hyalite opal | Amazonite | Petalite |
| Cleavelandite | | Amazonite | Molybdenite | Amethyst | Pollucite |
| Zircon | | Amethyst | Schorl | Anatase | Pyrochlore-group |
| | | Helvine Group | Triplite | Apatite | Rhodizite |
| | | | Zircon | Axinite | Stibiotantalite |
| | | | | Cleavelandite | Titanite |
| | | | | Ilmenite | Zinnwaldite |
| | | | | Kunzite | Zircon |

## DPA

### Rock-forming

| Group 1 | | Group 2 | | Group 3 | |
|---|---|---|---|---|---|
| Biotite | Fe (±Mg) | Biotite | Fe (±Mg) | Cordierite | Mg |
| Almandine | | Magnetite | | Kyanite | Al |
| Muscovite | Al | Hornblende | | Anadlusite | |
| | | Almandine | | Sillimanite | |
| | | Muscovite | Al | Muscovite | |

### Rare-element

| Group 1 | | Group 2 | | Group 3 | |
|---|---|---|---|---|---|
| Schorl | B | Uraninite | U | Schorl | B |
| Beryl | Be | Allanite | REE, Nb, P | Dumortierite | |
| Amblygonite-montbrasite | P | Monazite | | Grandldierite | |
| Lepidolite | Li, B, F | Titanite | Ti | Borasilite | |
| Spodumene | | Beryl | Be | Chrysoberyl | Be |
| Elbaite | | Columbite-group | Nb, Ta | | |
| Pollucite | Cs | | | | |

### Accessory minerals

| Group 1 | | Group 2 | | Group 3 | |
|---|---|---|---|---|---|
| Apatite | Petalite | Amazonite | Schorl | Almandine | Rutile |
| Cleavelandite | Zircon | Epidote | Topaz | Beryl | Sapphirine |
| Columbite-group | | Fluorite | Zircon | Corundum | Surinamite |
| Cassiterite | | Hematite | | Gahnite | Xenotime |
| Graftonite group | | Ilmenite | | Ilmenite | Zircon |
| Triphylite-lithiophilite | | Molybdenite | | Monazite | |

1.2.1.Internal anatomy of pegmatite bodies

The internal structure of pegmatites was first described by Cameron et al. (1949) and their terminology is still in use to date. In addition, the internal structure of pegmatites is proposed as another criterion to complement the classification of Wise et al. 2022. Pegmatite melts which are less fractionated have commonly a homogenous composition with no or little signs of internal zoning of the pegmatite body. Highly fractionated pegmatite melts form granitic pegmatites with heterogenous compositions, which exhibit characteristic zoning throughout the pegmatite bodies (Simmons et al. 2003). During this fractional crystallization, grain sizes gradually increase from the border zones towards the core. Generally, three types of pegmatite bodies are recognized, based on the texture and complexity of the mineral assemblage present in the pegmatite: They are distinguished in unzoned, homogeneous - simple zoned, and heterogeneous - complex zoned pegmatites (Cameron et al. 1949).

Homogeneous – simple zoned pegmatites

This group of pegmatites is defined as bodies that are simple aggregates of quartz, feldspar with minor amounts of mica, and accessory minerals such as tourmaline that cannot be divided readily into units of contrasting mineralogy or texture (Cameron et al. 1949; Hugo, 1970). Whereas unzoned pegmatites have only a border zone, simple zoned pegmatites consist of semi-concentric to asymmetric zones with distinct texture and mineralogy, including a border zone, wall zone, one or several intermediate zones, and a core.

Heterogeneous – complex pegmatites

Complex zoned pegmatites bodies show to some degree a systematic arrangement of their constituents, each of which consists of two or more structural and lithologic units which differ in mineralogy and/or texture (Cameron et al. 1949; Hugo, 1970). A complex zoned pegmatite shows in principle the same type of zoning as simple zoned pegmatites with the difference that late-stage (metasomatic) replacement parts superimpose and replace the primary zoning. In addition to unzoned, simple zoned, and complex zoned pegmatites, a miarolitic and a layered type are distinguished today.

i.   Border zone

The border zones are the first to crystallize, while wall zones and intermediate zone crystallize later. It occurs as a thin layer (mm to cm thick) in the outermost parts of a

pegmatite body (figure 4) and is aplitic to finely crystalline (~ 2-5 mm). It occurs in contact with the pegmatite's host rocks and is like the chilled margin of intrusive rocks. The border zone is commonly composed of feldspar, quartz, and mica.
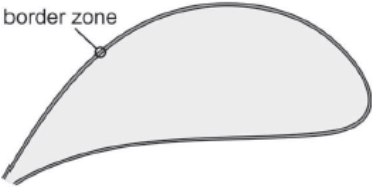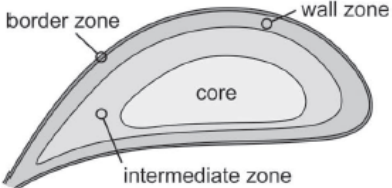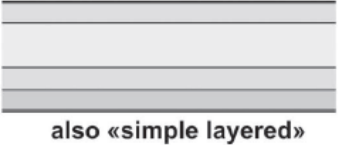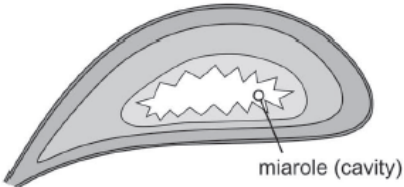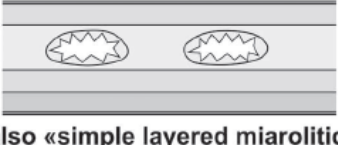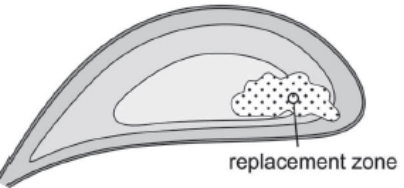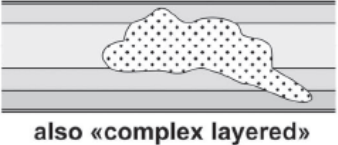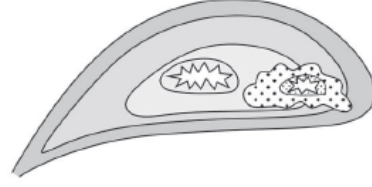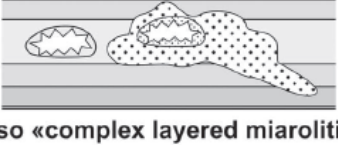
| type | irregular to stock-, tongue-, and ovoid-like | sheet- and dyke-like (aspect ratio >10:1) |
|------|----------------------------------------------|-------------------------------------------|
| unzoned | | |
| simple zoned | | also «simple layered» |
| simple zoned miarolitic | | also «simple layered miarolitic» |
| complex zoned | | also «complex layered» |
| complex zoned miarolitic | | also «complex layered miarolitic» |

*Figure 4: Illustration of the differently zoned pegmatite bodies from unzoned, simple zoned to complex zoned. Miarolitic pods only occur in shallowly intruded pegmatites where the low pressure allows the formation of cavities.*

ii.    Wall zone

The wall zone adjoins the border zone (figure 4). Compared to the border zone, the wall zone is thicker (few cm to several m) and coarsely crystalline (~ 1 cm to several m). The mineralogy of the wall zone is essentially the same as the border zone and these two zones may be considered as textural variants of the same mineralogical zone (Cameron et al. 1949; London, 2014).

    iii.    Intermediate zone

The intermediate zone is marked by a sharp increase in grain size inwards from the border and wall zones (figure 4) and is identifiable by the dominance of a particular mineral. The intermediate zone is typically dominated by perthitic K-feldspar, plagioclase, muscovite, and quartz with garnet, beryl, lepidolite or montebrasite for LCT pegmatites. Although the intermediate zone is less commonly developed than other zones in a pegmatite body, this zone is most prominent in the thickest part of a pegmatite body and pinches out and disappears where the pegmatite thins. One or more intermediate zones may be developed in a single pegmatite body.

    iv.    Core zone

The core zone represents the innermost unit of a zoned pegmatite body (figure 4). It is dominated by monomineralic quartz, perthitic microcline, sodic plagioclase, and rare minerals such as beryl.

# 2. Geological setting

## 2.1. Idefjorden lithotectonic unit

The Idefjorden lithotectonic unit lies to the west of the Mylonitzone (MZ) and extends over a length of about 450 km and a width of 140 km (see figure 5). The unit is made up of plutonic and volcanic rocks formed during the Gothian accretionary orogeny mainly between 1.66 and 1.52 Ga and associated with metasedimentary rocks (Åhäll and Connelly 2008; Bingen et al. 2005; Bergström et al. 2020). Evidence for older units is absent (Brewer et al. 1998; Åhäll & Connelly, 2008; Petersson et al. 2015). The Idefjorden terrane is bounded by the Telemarkia and Kongsberg terranes to the west and the Eastern Segment to the east (Bingen et al. 2008b). The igneous protoliths are mostly granites to tonalites (Bingen et al. 2005; Åhäll & Connelly, 2008; Petersson et al. 2013), of which the Mjösjö dacite (1.66 Ga) and the Härsjön gneiss (1.64 Ga) of the Horred Formation are the oldest (Åhäll & Connelly 2008; Petersson et al. 2015). The Gothenburg-Åmål belt (GAB; 1.63-1.59 Ga) consists of supracrustal rocks (volcanics, volcaniclastics and sediments) of the Åmål Formation metamorphosed to gneisses with greenschist and amphibolite facies. The Gothenburg Suite, which has a similar age, consists of granitic and mafic bodies intruded into supracrustal rocks of the Horred and Åmål Formations (Brewer et al. 1998; Åhäll & Connelly 2008; Petersson et al. 2015). The 1.59-1.52 Ga Stora Le-Marstrand (SLM) Formation consists of migmatised

metasupracrustal rocks and metabasalts that postdate the Gothenburg-Åmål Belt (Åhäll & Daly 1989; Åhäll & Connelly 2008).
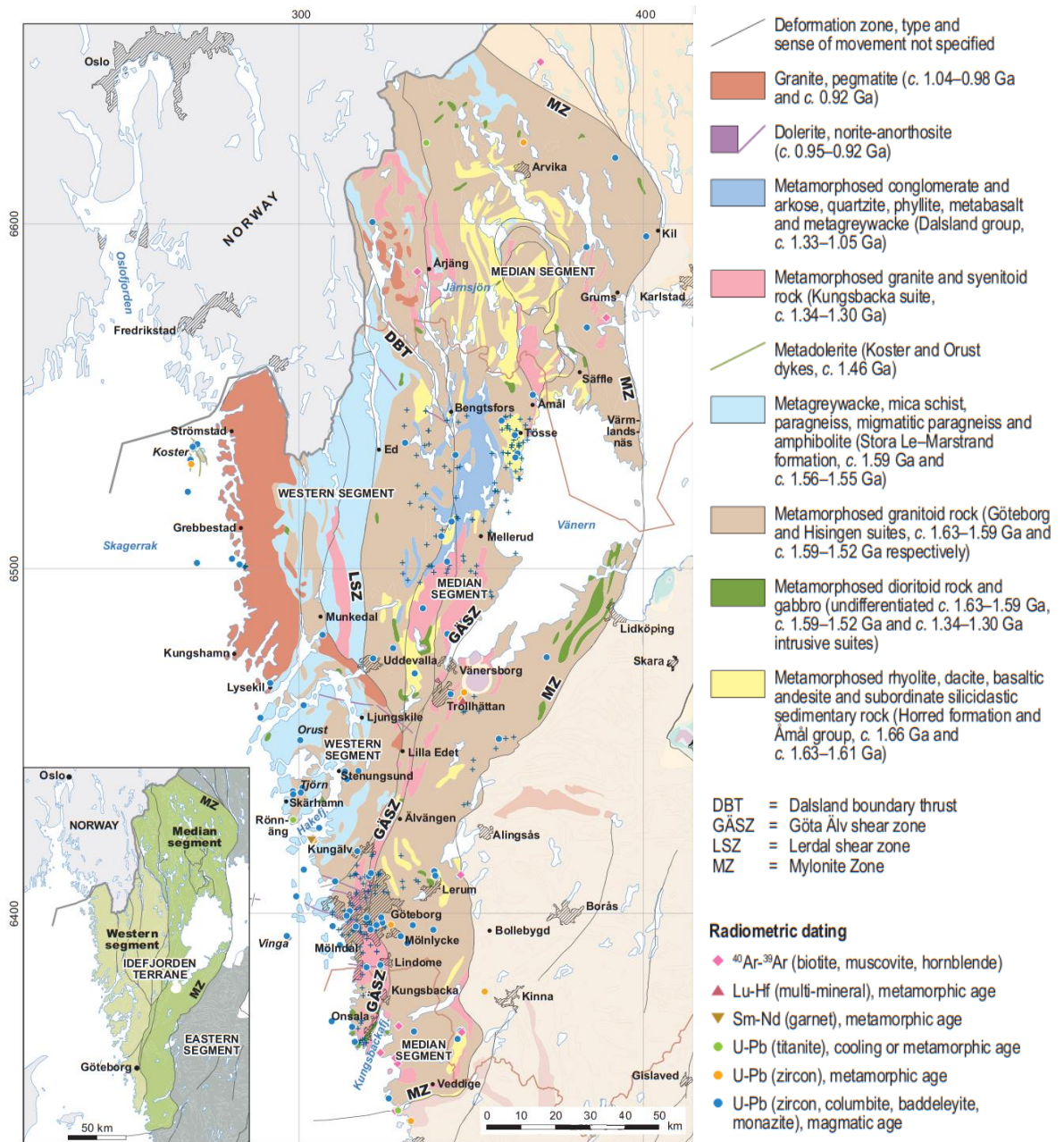


*Figure 5: 1:1 million bedrock geological map of the Idefjorden terrane and western segment by (SGU, Bergman et al. 2012). The rocks included in the Idefjorden terrane are shown in darker tones and presented in the legend. Shown in light blue is the SLM fm. in the westernmost part of the Idefjorden terrane, which was intruded by the Göteborg and Hisingen suite (shown in light brown). The main shear zones and the mylonite zone are also shown. The red rectangle marks the mapping area studied in this work. Sample sites for radiometric age determination (123 samples) in the Idefjorden terrane, based on the respective databases at the Geological Survey of Sweden, are also shown. A complete table of all age data is available in (Bergström et al. 2020).*

1.52 Ga), which are intermediate granitoids/tonalites and mafic-rock suites intruding the Horred, Åmål and SLM formations. Deformation varies from migmatised to unde-formed (Åhäll & Connelly 2008), with the southern part of the Göta Alv Shear Zone (GASZ) roughly defining the boundary between greenschist-bearing granites west of

the shear zone and veined amphibolitic rocks east of the shear zone (Austin Hegardt 2010). Rocks formed after the Gothian orogeny and before the Sveconorwegian orogeny occur as variably deformed and metamorphosed lithological units, including the Brevik Gabbro (1.50 Ga) and the Stigfjorden granite (1.51-1.49 Ga) (Åhäll & Connelly 1998), the Orust tholeiitic dolerite dyke swarm (1.46 Ga), the Kungsbacka bimodal suite of granitic and gabbroic bodies (1.34-1. 30 Ga), the 1.28 Ga Bunketorp Granite, the 1.25 Ga Segmon Granite and the 1.21 Ga Sandsjön Granite Gneiss (Åhäll & Connelly 1998; Austin Hegardt et al. 2007; Åhäll & Connelly 2008; Bingen et al, 2020).

## 2.2. The Gothian Orogeny

The Gothian orogeny is made up of three different complexes/formations, younging towards the west and includes the eruption and emplacement of subduction-related magmatic rocks with magnesian and calc-alkaline trends during the time interval 1.66–1.52 Ga (Åhäll and Connelly 2008; Brewer et al. 1998); (1) the oldest 1.66–1.64 Ga metavolcanic Horred Complex, (2) the 1.63–1.59 Ga metavolcanic and metasedimentary Åmål Complex, which is associated with the Göteborg granite suite, and (3) the 1.59–1.52 Ma metasedimentary and metavolcanic Stora Le-Marstrand Complex, which is interpreted as an infilling of a back-arc basins (Brewer et al. 1998) with siliciclastic material, including turbiditic greywackes, at around 1.59 Ga and at 1.57–1.55 Ga and is associated with the 1.59–1.52 Ga plutonic Hisingen Suite (Åhäll and Connelly 2008). Metamorphic events involving crustal shortening and anatexis, the latter consistent with a hot orogenic system, occurred during the time intervals at around 1.59 Ga ($D_{G1}$) and at 1.56–1.54 Ga ($D_{G2}$) (Åhäll & Connelly 2008; Austin Hegardt et al. 2010). The magmatic activity, a rapid uplift, erosion, the deposition of siliciclastic rocks, and the deformation and metamorphism all occurred in a close time span to each other during various stages of the orogenic activity. Thermobarometry calculations in grt-amph-plg, grt-amph and grt-ms-bt-plg reactions on samples from one of the small islands south of Tjörn, yield to metamorphic conditions of c. 8 kbar and 600-700°C (Austin Hegardt et al. 2010). The rocks of the Gothian orogen were later overprinted and reworked by the Sveconorwegian orogeny.

## 2.3. The Sveconorwegian Orogeny

The Sveconorwegian orogen is divided into different lithotectonic units, which are separated by generally north-south striking crustal-scale shear zones. The units are from west to east; Telemarkia, Bamble, Kongsberg, Idefjorden and Eastern Segment (Bingen

et al. 2005; Bingen et al. 2008b), which have been reworked during processes associated with the 1.14-0.92 Ga Sveconorwegian orogeny (Bingen et al. 2008b). The boundary between the Eastern Segment and the Idefjorden terrane is defined by a major ductile shear zone, the Mylonite Zone, which is shallowly west-dipping in the south and subvertical in the north (Stephens et al. 1996; Viola et al. 2011; Petersson et al. 2013). Bingen et al. (2008a) described four main tectonometamorphic stages of Sveconorwegian orogeny: (1) The Arendal phase, 1.14 Ga, involved granulite- and upper amphibolite-facies metamorphism at intermediate pressure, in Bamble and Kongsberg Terranes (Engvik et al. 2016). (2) The 1.05-1.02 Ga Agder phase with greenschist- to upper amphibolite-facies metamorphism and affected Telemarkia and Idefjorden Terranes. (3) The Falkenberg phase, at 0.99-0.97 Ga, caused high-pressure and high-temperature metamorphism of the Eastern Segment (e.g., Johansson et al. 1991; Johansson & Kullerud 1993; Wang & Lindh, 1996; Andersson et al. 1999), and eclogite-facies conditions are recorded in an eclogite-bearing nappe (Möller, 1998, 1999). (4) The Dalane phase is the post-collisional stage after 0.97 Ga and includes an anorthosite-mangerite–charnockite–granite (AMCG) intrusive suite in terranes west of the Mylonite Zone. There are two phases of Sveconorwegian ductile deformation, described as $D_{SN1}$ and $D_{SN2}$ and associated with upper and lower amphibolite facies metamorphism, correspond to the D3 and D4 deformational events described by Austin Hegardt et al. (2010) and Park et al. (1991). Coarse grained granitic veins on the island of Tjörn are present along the foliation and are generally coarser grained compared with the older MG2 migmatite veins. Metamorphic conditions at 11.5 kbar and 750°C during $D_{SN1}$ have been inferred using thermobarometry calculations from garnet–amphibole– plagioclase and garnet–amphibole reactions in samples of post-$D_{G2}$ amphibolite dykes hosted by paragneiss and yield a Sm–Nd garnet age of c. 1.03 Ga for this event (Austin Hegardt et al. 2010). A second phase of Sveconorwegian deformation $D_{SN2}$ is another structural feature in the western segment. This deformation is characterized by NE-SW trending folds with subhorizontal axial surfaces and pronounced lineation development. In the area of most intense $D_{SN2}$ deformation on a small island south of Tjörn, chevron-like folding and crenulation cleavage are particularly well developed in the mica-rich beds of paragneisses belonging to the SLM Formation (Austin Hegardt et al. 2010). Based on 40Ar-39Ar (muscovite) geochronology, these authors proposed that $D_{SN2}$ structures developed at about 980 Ma.

## 2.4. Stora-le-Marstrand formation

The Stora Le Marstrand (SLM) formation occurs from the southern archipelago of Gothenburg, along the coast, to south-eastern Norway and correlates with the Veme Complex west of the Oslo Rift. The siliciclastic metasediments have a semi-pelitic composition and can be associated with a greywacke as protolith (Daly, 1978). Through metamorphic overprinting, this has been locally transformed into mica schist and fine-grained paragneiss. Linear banding in the paragneiss indicates an assemblage of carbonate layers and sand-rich psammites (Bergström et al. 2020). During extended metamorphism, the banded paragneiss transforms into a diatexic migmatite. In addition to the metasediment with varying degrees of overprinting, a few mafic rock bodies occur in the SLM, consisting of banded calc-silicate-rich amphibolites. These occur as elongated lenses, mostly parallel to the SLM foliation (N-S) and range from a few meters to several meters thick. These banded amphibolites are interpreted as relics of basaltic subvolcanic sills and ash deposits and been interpreted as the result of oceanic back-arc magmatism (Brewer et al. 1998). Other mafic rocks include local Gabbros and bimodal dikes of mafic and felsic magma mingling interpretated as the result of mafic underplating (eg. on Vrangö; Ackevall, 2016). Due to the strong metamorphic overprint, the SLM Formation cannot be further subdivided stratigraphically. However, by dating detrital zircons, a distinction can be made between the deposition ages and their origin (Åhäll & Connelly, 2008). The dominant dendritic zircons in the SLM have an age of ~ 1.6 Ga, which originate from the Åmål Group and the Gothenburg Intrusion Series (Åhäll & Connelly, 2008). The oldest zircons found are 2-1.8 Ga old, although dendritic zircons from the Archean have also been found (Cornell et al. 2000; Austin Hegardt et al. 2010; Andersen et al. 2004). Therefore, the SLM formation has been subdivided into an older eastern SLM 1 and a younger, western SLM 2 part. The siliciclastic rocks of the SLM 1 Fm. were deposited between 1.59-1.52 Ga (Åhäll & Connelly, 2008) but prior to emplacement of a pluton belonging to the Hisingen intrusive suite at 1588 Ma (Connelly & Åhäll 1996; Åhäll et al. 1998). The more spatially restricted siliciclastic rocks of SLM 2 exposed in the westernmost areas of the Koster Archipelago contain detrital zircon grains that have an origin age of 1.57-1.55 Ga (Åhäll & Connelly 2008). Austin Hegardt et al. 2010 established a deformation sequence using geochronology and structurgeology in metagreywacke, Leucosomes and paleosomes, tonalite and amphibolite dykes from Nordön Island (~5 km east of Marstrand). The first Gothian

deformation event $D_1$ is recorded in the parallel foliations $S_1$ and represents a compaction with local folding $F_1$ at 1598-1587 Ma and therefore represents the $D_{G1}$ event. The subsequent $D_{G2}$ event is recorded in the isoclinal folds $S_2$, which are related to migmatisation $M_2$ and dated at $1545 \pm 11$ Ma (Austin Hegardt et al. 2010), as well as the Intrusion of Amphibolite Dykes $1547 \pm 11$ Ma. Furthermore, Austin Hegardt et al. 2010 define a $D_3$ event related to the Sveconorwegian orogen at $1029 \pm 6$ Ma, recorded in $S_3$ tight folding of the already deformed migmatites including the amphibolite intrusion. The whole package of multiple metamorphic overprinted rocks is subsequently intruded by a pegmatite interpreted as post-orogenic dike N-S trending at $994 \pm 3$ Ma (Ar-Ar in muscovite).

## 2.5. Hisingen-suite

The Hisingen suite consists of plutonic rocks which are emplaced between 1.59-1.52 Ma and intruded into the siliciclastic metasedimentary rocks of the SLM formation in the Western segment (Bergström et al. 2020). Based on field observations/crosscutting relationships within the SLM rocks, the Hisingen suite pluton intruded after the early Gothian deformation phase (1.59 Ga; $D_{G1}$). The Series of Intrusions can be divided into three phases according to field characteristics and ages (Åhäll & Connelly 2008). These calc-alkaline intrusions indicate resumption of continental arc magmatism after the accretion of SLM 1 rocks. The Hisingen Suite shows progressively younger ages towards the west (Åhäll & Connelly, 2008). The first stage of Hisingen magmatism (1.59–1.56 Ga) is dominated by large, intermediate granitoid to tonalitic intrusions emplaced along the transition zone between the GAB (Göteborg-Amal- Belt) and SLM 1 rocks. The middle stage (1.56–1.55 Ga) of intrusions is marked by an overall change in style to smaller and more planar intrusions. This phase is contemporaneous with the formation and accretion of the volcaniclastic SLM 2 rocks in the Koster segment and southwards at 1.57–1.55 Ga and with local deformation and elevated crustal temperatures in the south, associated with the $D_{G2}$ Gothian deformation phase (1.56–1.55 Ga). The SLM 2 (greywacke) type deposits and the interbedded mafic volcanics were migmatised before the Hisingen intrusions were emplaced in the Koster segment at $1546 \pm 7$ and $1545 \pm 5$ Ma (Åhäll & Connelly 2008). The last stage of Hisingen magmatism (1553–1522 Ma) is dominated by intermediate granitoid intrusions emplaced in western parts of the Idefjorden terrane, including the Koster segment.

## 2.6. Pegmatites in the Idefjorden terrane

The pegmatites in the Idefjorden terrane are divided into three pegmatite fields (see Table 4; Müller et al. 2017): Halland field (Grebbestad, Skuleboda, Timmerhult, Skantorp, Gundlebo), Gothenburg field (Högsbo) and Østfold field (Karlshus & Vintergruben). U-Pb age dating in columbite-group minerals and euxenite result in the following ages of formation: Timmerhult (1038.7 ± 3.4 Ma, Romer & Smeds (1996); Skantorp (1041 ± 1.6 Ma, Romer & Smeds (1996); Högsbo (1029.7 ± 1.4 Ma, Jonason, 2016); Skuleboda (984.3 ± 6.4 Ma, Romer & Smeds (1996); 1035 Ma, Herzog et al. (1960); 910 Ma; Welin & Blomqvist (1964); Gundlebo (987 ± 8 Ma, Jansson, 2018) & Riddaho (941.6 ± 1.4 Ma, Romer & Smeds (1996). More recent Rb-Sr dating on Muscovite and Lepidolith confirm these numbers (table 4; Jansson, 2018). These ages were interpreted to be syn-tectonic to post-orogenic, disproving earlier assumptions about a genetic link with the Bohus granite (920 Ma) (e.g. Brotzen, 1961). Romer & Smeds (1996) argued that the apparent younger age towards the east reflects crustal thickening that occurred from west to east during the Sveconorwegian orogeny. However, all known rare metal pegmatites in the Idefjorden terrane have a formation age of 1041-906 Ma. Older Gothian-age pegmatites were discovered by Lundegårdh, which are located in the eastern part of the Kållered-Mölndal area and in the Styrsö archipelago are considered to be a product of the final Gothian migmatisation (Lundegårdh, 1953). Nevertheless, his assumption that these are Gothian-age pegmatites is based only on field observations and has not yet been substantiated with geochronological data.

*Table 4: Known rare element pegmatites in the idefjorden terrane with age and dating method*

| Pegmatite field | Pegmatite age (Ma) | Age dating methods | Data source |
|---|---|---|---|
| Østfold | 906 ± 6 Karlshus | U-Pb columbite | Müller, 2017 |
| | 909 ± 1 Vintergruben | U-Pb columbite | Müller, 2017 |
| Halland | 922 ± 3 Grebbestad | U-Pb columbite | Müller, 2017 |
| | 942 ± 1 Riddaho | U-Pb columbite | Romer & Smeds, 1996 |
| | 984 ± 6; 982 ± 14 Skuleboda | U-Pb columbite; Rb-Sr ms | Romer & Smeds, 1996; Jansson, 2018 |
| | 987 ± 8; 987 ± 11 Gundlebo | U-Pb columbite; Rb-Sr ms | Romer & Smeds, 1996; Jansson, 2018 |
| | 1039 ± 3; 1038 ± 11 Timmerhult | U-Pb columbite; Rb-Sr ms | Romer & Smeds, 1996; Jansson, 2018 |
| | 1041 ± 2 Skantrop | U-Pb columbite | Romer & Smeds, 1996 |
| Gothenburg | 1030 ± 1 Högsbo | U-Pb columbite | Jonason, 2016 |

# 3. Rb-Sr system

Geochronology on pegmatites and associated inferences from isotope geochemistry are understudied fields when compared to mineralogy, petrography and geochemistry. Intrinsic characteristics of pegmatite melts including their low viscosity and reactivity with host rocks, facilitating emplacement away from the source and the assimilation of wall rocks, are likely to disturb isotopic systems and bring challenges for age determinations (McCauley & Bradley 2014). All isotopic methods used for radiometric dating have inherent limitations, but additional specific problems arise when applied to pegmatites, as discussed by these authors: for the Ar-Ar method, the closure temperature of 350-425 °C for muscovite can be too low in certain terranes (Harrison et. al., 2009); the U-Pb method, even though the most robust in principle, relies on trace minerals such as zircon (>900 C°; Lee et. al., 1997) and monazite that might be inherited from older adjacent wall rocks, have suffered metamictisation or present other complex isotopic histories. Nb-Ta oxides from the columbite group proved to be useful, but do not occur in every pegmatite. However, it is now possible to obtain accurate age data from muscovites and biotites due to two key improvements in the Rb-Sr method, such as the redetermination of the $^{87}$Rb decay constant (Villa et al., 2015) and the development of an *in-situ* method (Zack & Hogmalm, 2016), which has significantly advanced the potential of this isotopic system for dating pegmatites. The routine developed by Zack & Hogmalm (2016) is based on the different reactivity of Rb and Sr, using suitable reaction gases that can separate the two elements. This brings key improvements to the method such as: the virtual elimination of isobaric overlap, the possibility of high spatial resolution and the consequent improved quality of measurements and calculated ages, especially in cases of within-crystal variation in Rb/Sr ratio and/or initial $^{87}$Sr/$^{86}$Sr ratio.

By using the half-life of 48.8 Ma for $^{87}$Rb to $^{87}$Sr it is possible to determine ages of K-rich minerals. Rubidium resembles the behavior of K where they have similar ionization potential and electronegativity, but the larger radius of Rb is the main reason for K-Rb fractionation. Strontium, on the other hand, can incorporate into prominent Ca minerals and K minerals such as mica, feldspars, and in small amounts into amphiboles. Strontium exhibits properties to K and Ca. This means that Sr is preferentially incorporated into the K, Na, and Ca sites of feldspars, but also to some extent into the K sites of mica. The fractionation and incorporation of strontium into Ca and K phases is

controlled mainly by its large size and therefore tends to favor calcium and potassium (Černý et al. 1985). Depending on the age and the amount of rubidium in a mineral, the radiogenic [87]Sr isotope accumulates in the crystal system. However, as also non-radiogenic strontium [86]Sr, [88]Sr and [84]Sr as well as radiogenic [87]Sr are incorporated in the mineral during growth, the age cannot be calculated by the measured [87]Rb/[87]Sr alone. Utilizing the decay constant of the decay rate $\lambda^{87}=1.3972\pm0.0045$ x10[11] from Villa et al. 2015, and the amount of remaining [87]Rb, radiogenic [87]Sr, and stable [86]Sr in at least two minerals with different initial Rb/Sr ratios, an isochron can be constructed with a slope corresponding to the age of fixation of radiogenic decay in the minerals, this problem ca be avoided (Nicolaysen, 1961). In this case, the Rb-Sr age is given by evaluating the resulting isochrone in the Nicolaysen diagram, which expresses the time-dependent variation of [87]Sr relative to [86]Sr and where the age t is defined as the slope of the isochron:

$$t = 1 / \lambda \cdot \ln\{1 + \left[\left(\frac{^{87}Sr}{^{86}Sr}\right) - \left(\frac{^{87}Sr}{^{86}Sr}\right)_{inital}\right]\left(\frac{^{87}Rb}{^{86}Sr}\right)\}$$

where ([87]Sr/[86]Sr) results from the following:

$$\left(\frac{^{87}Sr}{^{86}Sr}\right) = \left(\frac{^{87}Sr}{^{86}Sr}\right)_{Initial} + \left(\frac{^{87}Rb}{^{86}Sr}\right)_{total} \cdot (e^{\lambda t} - 1)$$

However, since neither the time nor the initial [87]Sr/[86]Sr is known, this methodology only works with many analyses on different mineral grains to estimate the initial strontium in the Nicolaysen diagram. Since this is not possible in every case, the method is limited in its application, with respect to single spot dating. However, by a precise determination of the initial strontium isotope composition also single-spot ages can be obtained (Rösel & Zack, 2022). If the initial [87]Sr/[86] Sr cannot be constrained through independent analyses from the sample, Rösel & Zack, 2022 recommend using following ranges for three different sample types: (1) 0.703±0.003 (for mantle derived magmatic rocks), (2) 0.715±0.015 (for enriched magmatic rocks) and (3) 0.730±0.030 (for crustal rocks).

## 3.1. Closure temperature

The Rb-Sr system records the time of reaching solidus, at which a mineral incorporates the two elements and crystallizes. The closure temperature below which the daughter

isotopes no longer diffuse out of the host mineral depends on the grain size and the cooling rate. Empirical calculations of closure temperatures in biotite, muscovite, and K-feldspar were performed in closed systems by Jenkin, 1997 and Villa, 1998. Closure temperatures for the Rb-Sr geochronometer in muscovite are above 500 °C and can reach 600-650 °C in coarse-grained pegmatite crystals (Cliff, 1985; Villa, 1998), making the mineral suitable for pegmatite geochronology. Biotite and K-feldspar have lower closure temperatures, about 300-350 °C, which may be used as exhumation ages (Dodson, 1979; Jenkin, 1997).

## 3.2. Opening and resetting temperature

The temperature at which daughter isotope loss begins during reheating is defined as the opening temperature and is particularly important for dating because it limits the maximum temperature a mineral can withstand without experiencing thermal overpressure. The resetting temperature describes the resetting temperature of a certain mineral and is defined as the temperature at which 99% of the daughter isotopes have been lost compared to 1% of the opening temperature. For muscovite, the reset temperature is assumed to occur in the range of 550 - 800°C at a grain size of 50 to 1000 µm, while for biotite it should occur in the range of 200 - 400°C (Dodson, 1973; Jäger, 1979; Del Moro et al. 1982; Jenkin, 1997).

# 4. Methods

## 4.1. Field work

The fieldwork lasted a total of 6 weeks and was mainly carried out on the islands of the south-eastern archipelago and the Gothenburg mainland. As there is no detailed geological map including pegmatite bodies in the area so far, there were no geological landmarks, and all pegmatites (except D3; see table 5) were discovered in this study and described. A total of 57 pegmatites and barrens were found. In addition to the location of the pegmatites, the size, orientation, mineral content, and the surrounding host rock were also documented (see Appendix).

*Table 5: Documented pegmatites with associated coordinates. Highlighted pegmatites were sampled.*

| Location | Latitude | Longitude | Location | Latitude | Longitude |
|----------|----------|-----------|----------|----------|-----------|
| ***Vrångö 1*** | 57.57188 | 11.777453 | Styrsö 1 | 57.612021 | 11.792579 |
| Vrångö 2 | 57.572068 | 11.778386 | Styrsö 2 | 57.611906 | 11.790407 |
| Vrångö 3 | 57.567379 | 11.781313 | Styrsö 3 | 57.60804 | 11.787176 |
| Vrångö 4 | 57.563148 | 11.786681 | Styrsö 4 | 57.604274 | 11.78862 |
| ***Vrångö 5*** | 57.562882 | 11.790854 | ***Styrsö 5*** | 57.603894 | 11.787892 |
| Vrångö 6 | 57.564496 | 11.791761 | Styrsö 6 | 57.602597 | 11.785889 |
| ***Vrångö 7*** | 57.576598 | 11.793243 | ***Styrsö 7*** | 57.601214 | 11.784887 |
| Vrångö 8 | 57.57964 | 11.792326 | Styrsö 8 | 57.599007 | 11.784371 |
| Vrångö 9 | 57.588401 | 11.784966 | Styrsö 9 | 57.597746 | 11.777434 |
| Vrångö 10 | 57.587458 | 11.784512 | Styrsö 10 | 57.598246 | 11.77753 |
| Vrångö 11 | 57.585435 | 11.780121 | Styrsö 11 | 57.597965 | 11.777565 |
| Vrångö 12 | 57.585777 | 11.779275 | Styrsö 12 | 57.613581 | 11.755154 |
| Vrångö 13 | 57.586278 | 11.777561 | Styrsö 13 | 57.61377 | 11.754365 |
| ***Vrångö 14*** | 57.58701 | 11.775689 | Styrsö 14 | 57.613119 | 11.752178 |
| Vrångö 15 | 57.584077 | 11.775405 | ***Styrsö 15*** | 57.614007 | 11.754536 |
| Vrångö 16 | 57.589416 | 11.78451 | Styrsö 16 | 57.614329 | 11.755967 |
| Donsö 1 | 57.593035 | 11.801368 | Styrsö 17 | 57.611728 | 11.760062 |
| Donsö 2 | 57.592974 | 11.801731 | Styrsö 18 | 57.610271 | 11.77913 |
| ***Donsö 3*** | 57.605068 | 11.807219 | Styrsö 19 | 57.611294 | 11.77211 |
| ***Donsö 4*** | 57.602002 | 11.799806 | ***Styrsö 20*** | 57.611145 | 11.7756 |
| Donsö 5 | 57.600954 | 11.799007 | Styrsö 21 | 57.605811 | 11.758944 |
| ***Donsö 6*** | 57.604104 | 11.799184 | ***Styrsö 22*** | 57.606123 | 11.756125 |
| Donsö 7 | 57.606537 | 11.796921 | Ursholmen 1 | 58.832669 | 10.990619 |
| ***Donsö 8*** | 57.607414 | 11.803425 | N. Koster | 58.911982 | 11.005238 |
| Donsö 9 | 57.608533 | 11.804987 | Saltö 1 (Bohus) | 58.877858 | 11.116257 |
| Donsö 10 | 57.610621 | 11.808118 | ***Langholmen*** | 57.62227 | 11.813807 |
| ***Donsö 11*** | 57.611143 | 11.810579 | ***Rivö 1*** | 57.658148 | 11.79896 |
| Donsö 12 | 57.60851 | 11.816039 | ***Rivö 2*** | 57.659853 | 11.796702 |
| Donsö 13 | 57.608402 | 11.816705 | ***Skeppstadsholmen*** | 57.694456 | 11.77877 |

Furthermore, about 4-8 measurements were taken on K-feldspar crystals distributed in the different pegmatite bodies with a portable XRF device to gather information on the degree of fractionation. Samples were also taken from each pegmatite. The sample material depends on the mineral composition of each pegmatite. Efforts were always made to collect Kfsp, Mus and Bio and, if present, Grt, Ber and associated minerals such as apatite and chrysoberyl. The results of the mapping were compiled, and a map was created in ArcMap 10.8.1 (see figure 11). In total, from the 57 mapped pegmatites, 22 muscovite samples from 14 different pegmatites, 19 K-feldspar samples, 14 plagioclase samples, 2 muscovites from leucosomes, one biotite from leucosomes, 8 biotites from pegmatite, 10 garnets from pegmatites, and 3 garnets from melt pools were collected and prepared in 1-inch pugs (see figure 6).

## 4.2. Sample preparation

A total of 9 epoxy pugs were made, with the mica samples arranged parallel to the c-axis along copper tape to get more samples into one pug. The pugs are then grounded down to 1 µm.
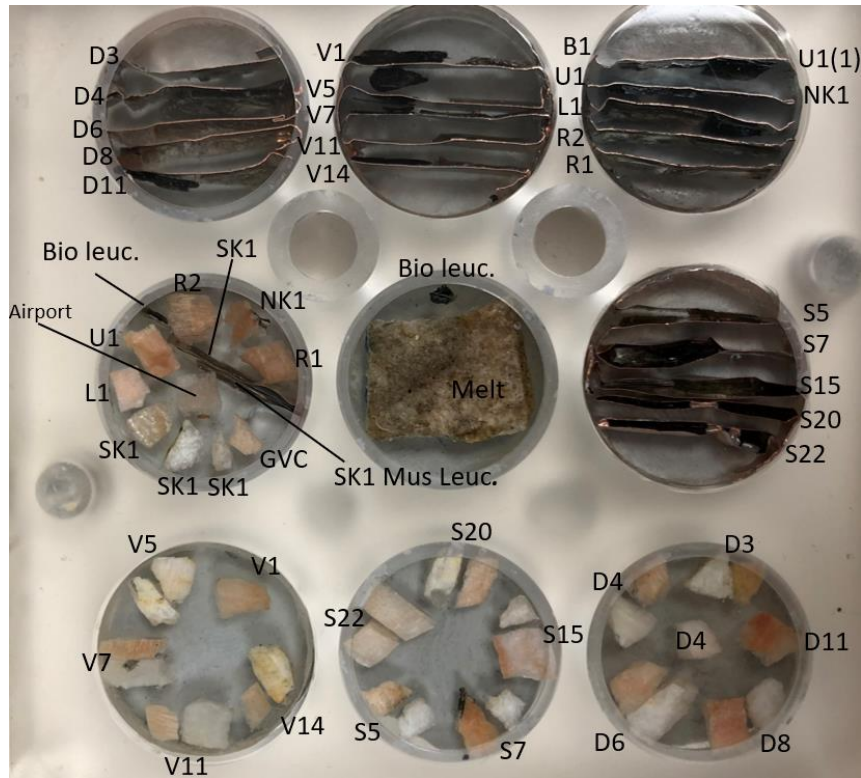


*Figure 6: Picture of the ground pugs in the sample holder of the LA-ICP-MS.*

The arrangement of the mica samples was made according to the example of the pug for mica standards (see figure 7). Mica sheets from the samples presented in this study are thick enough to facilitate enough space for spot sizes of at least 50 µm, which offers a good ratio between the amount of samples in a pug and the CPS obtained from each spot.
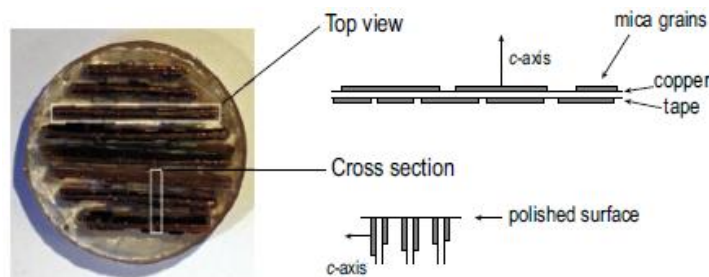


*Figure 7: Shows 1-inch-round epoxy mount with eight mica samples routinely analysed in Gothenburg, including a large single muscovite crystal from Högsbo as well as several biotite flakes from La Posta-Bt and McClure-Bt used in this study. Individual mica grains were affixed on copper-tape for reasons of stability. The copper tapes were arranged upright and parallel to each other with approximately 1.5 mm prior to casting with epoxy and to polishing to expose the grains (Rösel & Zack, 2022)*

## 4.3. Portable XRF

For XRF field analysis, a portable Olympus Delta X-Ray Fluorescence with a rhodium anode and an excitation source of 4 W was used. This instrument allows voltages from 15 to 50 kV and currents from 5 to 100 μA and has a spot size of 5 mm. The spot of interest was screened with two energy beams that corresponded to two different phases 30 keV (phase 1), and 50 keV (phase 2) to enhance peak intensities and improve sensitivity. Measurements of a 30 s duration were made in 221 different spots on Kfsp using the inbuilt Soil mode. Each spot was measured once. At the beginning of each fieldwork day the pXRF was calibrated with a "innov X Systems - 316" cobalt standard as well as an Amazonite crystal to estimate the precision of the analysis. Because the pXRF was used to estimate the degree of fractionation of each pegmatite, only K, Rb, Sr, Ba and Pb were measured and documented. Potassium was only to ensure that it was a Kfsp and not a plagioclase. Rb, Sr and Ba were used to estimate fractionation degrees.

## 4.4. Geochemistry and Rb-Sr dating

The geochemical analyses were carried out using an ESI 213 NWR laser ablation system (LA) with a connected Agilent 8800QQ inductively coupled plasma spectrometer (ICP-Ms) system at the Department of earth science at the University of Gothenburg. Since the focus of the study is geochronology, the data obtained could also be used for geochemistry. In total, measurements were made on 4 days, sampling mica, feldspars, and garnets. Zack & Hogmalm (2016) and Hogmalm et al. (2017) developed a method based on the possibility to separate Rb from Sr by using reaction gases such as $O_2$, $N_2O$ and $SF_6$, with which Sr is reactive but Rb is not. The reaction gases can be introduced into the reaction cell, which is located between the two quadrupoles of the ICP-MS; the first quadrupole (before the reaction) admits only one desired mass at a time, and the second quadrupole (after the reaction) measures the reaction products. While the Sr isotopes are measured as mass-shifted products (e.g., $^{86,87,88}Sr^{16}O$), Rb does not react, and the measured mass remains the same (e.g., $^{85}Rb$ measured at mass 85; see figure 8). With the reaction cell, the isobaric interference from $^{87}Rb$ to $^{87}Sr$, which was previously the greatest obstacle to LA-ICP-MS-Rb-Sr dating, is almost eliminated. NIST SRM 610 and BCR-2G glasses (for low-Rb phases) are used as standards, and a nano powder tablet of phlogopite mica-Mg for the muscovite analysis. These are used to correct matrix effects and are systematically analyzed between samples after ten sample points. Furthermore, standards from the Högsbo-Ms pegmatite with an age of 1037±11

Ma (Hogmalm et al. 2016), from La Posta-Bt granodiorite with an age of 91.6 Ma (Zack & Hogmalm, 2016), from Mica-Fe with an age of 307.6 ± 0.4 (Grove & Harrison, 1996), from McClure-Bt with an age of 523.98 ± 0.12 Ma (Schoene & Bowring, 2006), and Wilson Prom. -Bt with an age of 395 ± 4 Ma (Elburg, 1996) were used to check the accuracy of the calculated single spot ages.
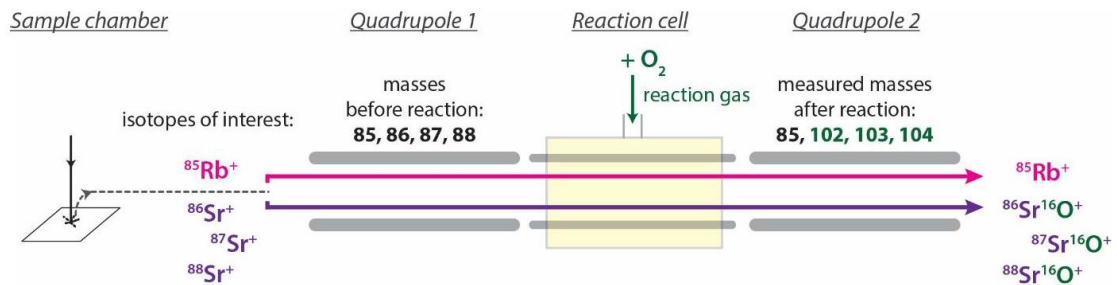


*Figure 8: Simplified scheme of Rb-Sr isotope analyses using two quadrupoles and reaction gas, or MS/MS mode. A small amount of material is ablated from the sample chamber, and the plasma is directed to the ICP-MS. In the first quadrupole, masses of isotopes of interest are redirected one at a time to the reaction cell, which in this case are 85 for Rb and 86, 87 and 88 for Sr. A reaction gas such as $O_2$ is inserted in the reaction cell, and mass-shifted isotopes can be measured after the reaction. No mass shifted Rb (mass 101) is measured in quadrupole two, as it does not react with gases. Mass-shifted SrO can be measured at masses 102 (86 from Sr summed with 16 from O), 103 (for $^{87}Sr$) and 104 (for $^{88}Sr$). Modified from the Agilent handbook.*

After the data acquisition, the Glitter software v4.5 was used for signal revision to eliminate occasional spikes, inclusions and produce subtracted background count rates for the masses of interest. In the data processing, spots on mica were sorted out that had a 4:1 relationship of IV-ions(Si and IVAl)/monovalent-ions (K, Na and Rb) with the criterion of: 3.8-4.2 "good", 3.5-4-5 "okay", >4.5 and <3.5 "bad". Bad spots were not used for geochemical analysis or age dating. In total, 4 of 32 spots on Högsbo-Ms and 11 of 36 spots on biotites of samples S22, V5 and V1 were sorted out. Isotopic ratios were then calculated using conversion factors derived from the known isotopic ratios of the high Rb, low Sr muscovite standards ([1]Mica-Mg: $^{87}Rb/^{86}Sr$ = 154.6 ± 1.932 and $^{87}Sr/^{86}Sr$ = 1.8525 ± 0.00242) and low Rb and medium Sr phases ([2]NIST SRM 610: $^{87}Rb/^{86}Sr$ = 2.3300 ± 0.0049 and $^{87}Sr/^{86}Sr$ = 0.709699 ± 0.000018 and [3]BCR-2G:

$^{87}\text{Rb}/^{86}\text{Sr} = 0.3901 \pm 0.00097$ and $^{87}\text{Sr}/^{86}\text{Sr} = 0.705003 \pm 0.0000087$) ([1]Hogmalm et al. 2017; [2]Jochum et al. 2011; [3]Jochum et al. 2005). The Rb and Sr concentrations were determined separately by normalizing against the Si count rates in the NBS610 glass standard and its known SiO2 content. The calculation of $^{87}\text{Sr}/^{87}\text{Rb}$ ratios for single-spot Rb-Sr ages were calculated using the drift and mass bias corrected $^{87}\text{Sr}/^{86}\text{Sr}$ and $^{87}\text{Rb}/^{86}\text{Sr}$ integration periods. The $^{87}\text{Sr}\sim/^{86}\text{Sr}\sim$ ratio is divided by a factor of circa 1.03 to calculate the mass bias corrected $^{87}\text{Sr}/^{86}\text{Sr}$. This correction factor is based on repeated analysis on the primary reference material used (NIST SRM 610, BCR-2G or Mica-Mg). The $^{87}\text{Sr}/^{87}\text{Rb}$ ratio for each data point within the integration period was calculated in accordance with the formulation on an isochron by Nicolaysen (1961) (see. Chapter 3. Rb-Sr system). Data reduction was undertaken with a Data Reduction Scheme (DRS) written for Iolite v. 3.71 (Paton et al. 2011) and the "Geochron1" setting.

*Table 6: Shown are machine settings and analytical conditions for the LA-ICP-Ms during the four days of analyses*

| Run | 201119 | 201130 | 211217 | 220831 |
|---|---|---|---|---|
| Fluence [J cm$^{-2}$] | 5.1 | 5.1 | 5.8 | 4.9 |
| Repetition rate [Hz] | | 10 | | |
| Spot [µm] | | 50 | | |
| Sampling mode/pattern | | static spot ablation | | |
| Carrier gas | | He | | |
| Cell carrier gas flow [l min$^{-1}$] | 650 | 850 | 750 | 750 |
| Addition of N2 [ml min$^{-1}$] | | 4 ml min-1 | | |
| **ICP-MS** | | | | |
| Model type | | Agilent 8800QQQ | | |
| Sample type | | Ablation aerosol | | |
| Analytical mode | | Mass shifted | | |
| **Plasma** | | | | |
| RF power [W] | 1550 | 1550 | 1550 | 1550 |
| RF matching [V] | 1.8 | 1.8 | 1.8 | 1.8 |
| Sample depth [mm] | 4 | 3.8 | 4 | 3.9 |
| Nebulizer Gas [l min$^{-1}$] | 0.78 | 0.84 | 0.85 | 0.83 |
| Lenses | | | | |
| Extract 1 [V] | -5 | -12 | -12 | -5 |
| Extract 2 [V] | -210 | -250 | -220 | -210 |
| Omega bias [V] | -150 | -150 | -150 | -150 |
| Omega lens [V] | 10 | 8 | 8 | 10 |
| Q1 entrance [V] | -10 | -12 | -10 | -12 |
| Q1 exit [V] | -6 | 0 | 1 | -4 |
| Cell focus [V] | -14 | -3 | -2 | -10 |
| Cell entrance [V] | -120 | -140 | -120 | -140 |
| Cell exit [V] | -85 | -85 | -85 | -85 |
| Deflect [V] | 0 | 0 | 0 | 0 |
| Plate bias [V] | -70 | -70 | -70 | -70 |
| **Q1** | | | | |
| Q1 bias [V] | 1 | 1 | 1 | 1 |
| Q1 prefilter bias [V] | -12 | -7 | -12 | -7 |
| Q1 postfilter bias [V] | 0 | 0 | 0 | 0 |
| **Cell** | | | | |
| reaction gas | | N2O and He | | |
| reaction gas flow | 23% | 22% | 20% | 22% |
| OctP bias [V] | -11 | -10 | -8 | -10 |
| OctP RF [V | 200 | 200 | 200 | 200 |
| Energy discrimination [V] | -6 | -4 | -2 | -4 |
| **Q2** | | | | |
| Q2 Bias | -17 | -14 | -9 | -14 |

## 4.5. Analytical setup

The Rb/Sr and Sr/Sr compositions were measured at the facilities at the Department of Earth Sciences at the University of Gothenburg. The ESI NWR213 laser ablation system is coupled to an Agilent 8800 ICP-QQQ-MS, which was used in this study (see Zack & Hogmalm 2016, Hogmalm et al. 2017). Data from four measurement sessions (201202, 201130, 211217, 220831) are presented in this study, where "211217" (Day 1) and "220831" (Day 2) were used for dating. The machine was tuned trough ablating and analyzing the standard NIST SRM 610 in static spot ablation mode. The analyses were carried out in MS/MS mode with the octopole bias set to negative voltage. Machine settings was 35% (201202 & 201130), 48% (211217) and 60% (220831) output with 50 µm spot size at 10 Hz and a fluence of 4.9-5.8 J/cm2 (see full machine settings and analytical conditions in table 6). Mass-shifted mode with dwell time settings for analyzed elements is shown in table 7.

*Table 7: Q1 and Q2 settings along with dwell time for all analyzed elements*

| Element | Q1 (m/z) | Q2 (m/z) | Dwell times (ms) |
|---|---|---|---|
| Li | 7 | 7 | 5 |
| Na | 23 | 23 | 2 |
| Mg | 24 | 24 | 2 |
| Al | 27 | 27 | 2 |
| Si | 28 | 60 | 2 |
| P | 31 | 47 | 2 |
| K | 39 | 39 | 2 |
| Ca | 44 | 60 | 2 |
| Ti | 48 | 80 | 2 |
| V | 51 | 83 | 2 |
| Cr | 52 | 68 | 2 |
| Mn | 55 | 71 | 2 |
| Fe | 56 | 72 | 2 |
| Co | 59 | 59 | 2 |
| Zn | 66 | 66 | 2 |
| Rb | 85 | 85 | 30 |
| Rb | 85 | 101 | 2 |
| Sr | 86 | 102 | 150 |
| Sr | 87 | 102 | 5 |
| Sr | 87 | 103 | 200 |
| Y | 89 | 105 | 2 |
| Zr | 90 | 122 | 2 |
| Nb | 93 | 125 | 2 |
| Sn | 118 | 118 | 2 |
| Cs | 133 | 133 | 2 |
| Ba | 137 | 153 | 2 |
| Ce | 140 | 156 | 2 |
| Hf | 178 | 210 | 2 |
| Ta | 181 | 213 | 2 |
| W | 182 | 198 | 2 |
| Tl | 205 | 205 | 2 |
| Pb | 208 | 208 | 2 |

# 5. Results

## 5.1. Field Observation

The rocks and geological setting on the Southern Archipelago west of Gothenburg are characterized by a complex diversity, ranging from undeformed metasediments, almost entirely melted migmatites of the same metasediment, mafic and felsic intrusions, banded amphibolites, young diabas dikes, to cross-cutting pegmatite dikes and lenses. Exposed are undeformed metasediments of the SLM fm., with relict sedimentary structures consisting of 5-30 cm thick, rarely cross-bedded bedding with alternating lighter psammitic and darker pelitic components. The undeformed metasediment occurs both

as quartzite layers with >75% Qz and as metapelitic units with < 30% Qz and >40% feldspar. In addition to quartz and feldspar, mica is also present in the SLM Fm. rocks, with biotite occurring more frequently than muscovite. In areas of more extensive migmatisation the metagreywacke transforms into a paragneiss, where Qz, Kfsp, Plg, and Ms recrystallize in coarse-grained (up to 3 cm crystals) leucosomes as small pockets or layers (see figure 9 A & 14 F). The paragneiss is typically well banded and veined, and is predominantly semipelitic in composition, containing the assemblage of quartz + plagioclase ± biotite ± muscovite ± microcline ± garnet ± chlorite. During extended metamorphism, the banded paragneiss transforms into a diatexic migmatite with various generations of leucosomes, which partially cross each other as migrating melt (see figure 9 B & C). Rarely features like banded amphibolite xenoliths float in the migrating diatexite are preserved (see figure 9 E & 14 D). Locally, the metasediment melts completely and recrystallizes as a S-type like porphyritic granite with K-feldspars up to 1.5 cm in size (see figure 9 F). Depending on the local source rock, the migrating melt is composed of qz and plg with either more or less Kfsp. In addition to the felsic metasediment with varying degrees of migmatisation, metamorphic mafic rock bodies occur within the SLM Fm., consisting of banded calc-silicate-rich amphibolites. These occur as elongated lenses, mostly parallel to the SLM foliation (N-S) and range from a few meters to several meters thick. Within the amphibolites, elongated lenses of quartz and calc-silicates (epidote rich) occur (see figure 9 E), more rarely garnets. These amphibolites have the same structural imprints as the metasediment. Other mafic rocks include undeformed local gabbros and bimodal dikes of mafic and felsic magma mingling, containing paragneiss xenoliths, intruded into the metasediment, which are then cross-cutted by pegmatite dikes (see figure 9 C & 14 E). Intrusive felsic rocks ranging from granodiorite, rarely granite to tonalite and vary in grain size from fine to coarse-grained. In addition to quartz, plagioclase and k-feldspar, macroscopically visible garnet and mica also occur in the leucocratic intrusive bodies. In some localities the leucogranites and nearby pegmatites are both rich in Qz and Plg, whereas Kfsp is absent. In such areas the pegmatites are similar in composition to the leucosomes in the metasediment consisting of Qz, Plg and Mica.
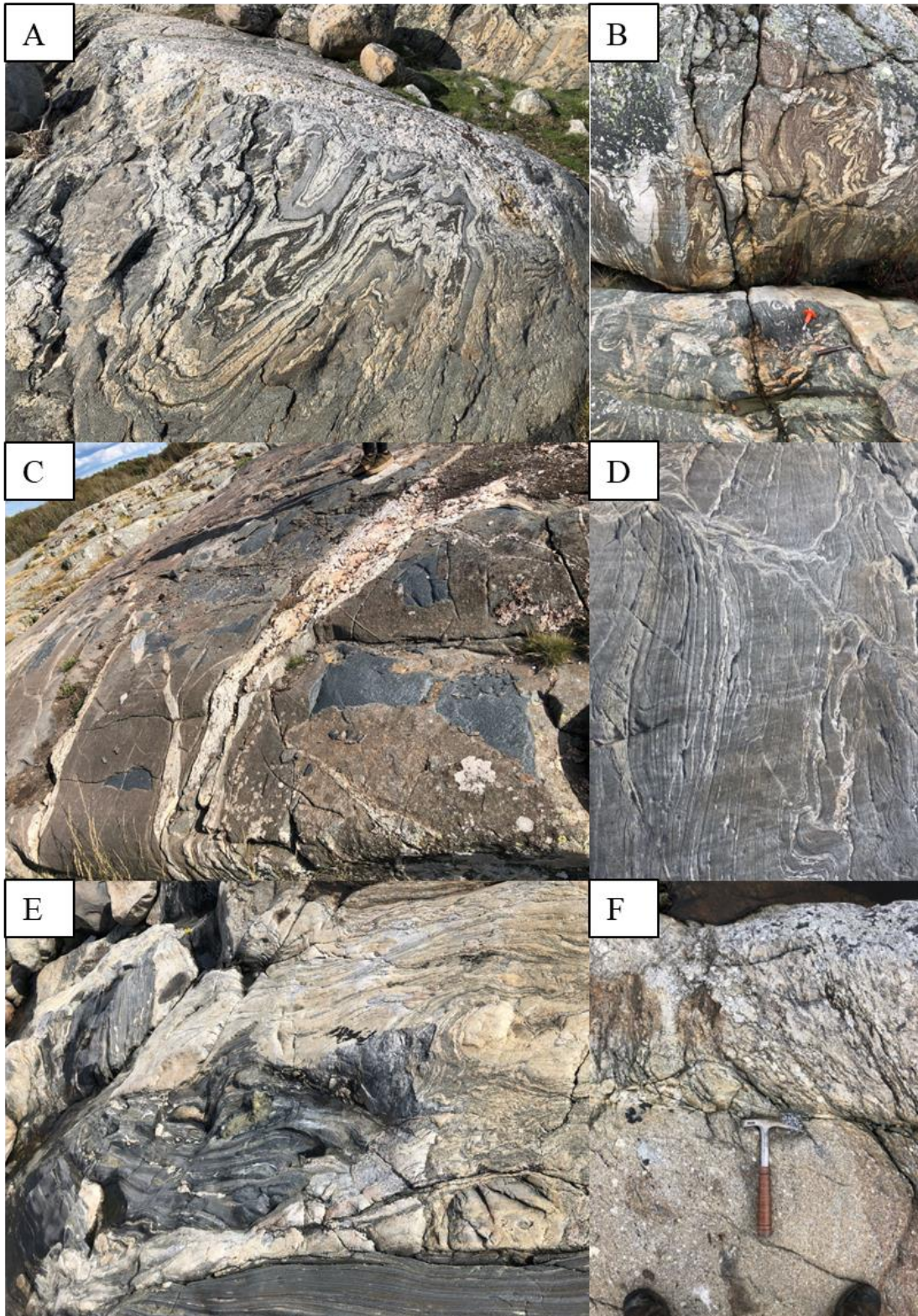
*Figure 9: Photos of SLM Fm. And field relations taken from the mapping area in the southern archipelago west of Gothenburg. A&B: strongly deformed metasediment shows S1, S2 and S3 structure. C: Mafic body crosscutted by felsic pegmatitic dykes. D: Less deformed metagrauwacke. E: Sheared paragneiss and epidote-rich amphibolite at Lotsutkiken. F: Granitic porphyritic Intrusion crosscuts SLM paragneiss structures on Ursholmen.*
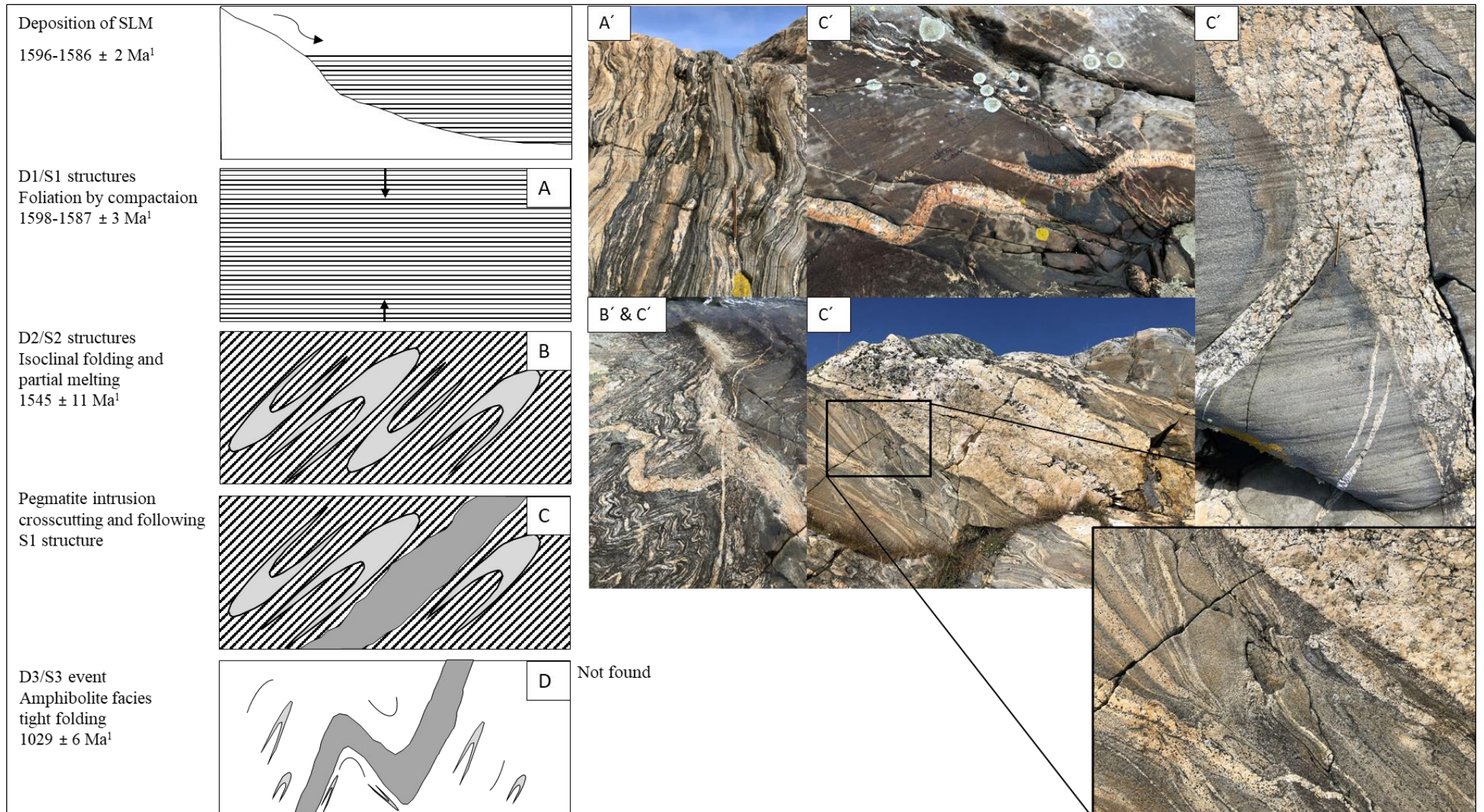
Figure 10: Shown are the deformation events determined by Hegardt (2010) on the island of Nordön, 20 km north of the area covered by this study. The structures S1 and S2 are common, represented by illustration A and picture A' for S1 and B & B' for S2. In general, the pegmatites crosscut the S1 and S2 structures, but sheared smaller branches (see photo above centre, side branch of Sk1 Type II pegmatites) were also found. However, these cannot be assigned to the D3 event defined by Hegardt (2010), as this event has been dated to Sveconorwegian age.

## 5.2. Pegmatites

A total of 57 pegmatites were mapped on the islands of Styrsö, Donsö, Vrangö, Rivö, Langholmen and on the Skeppstadsholmen peninsula and are summarized in figure 11. The study area is located within the SLM formation, which is described in the chapter above. Two types of pegmatite were identified during the field work.
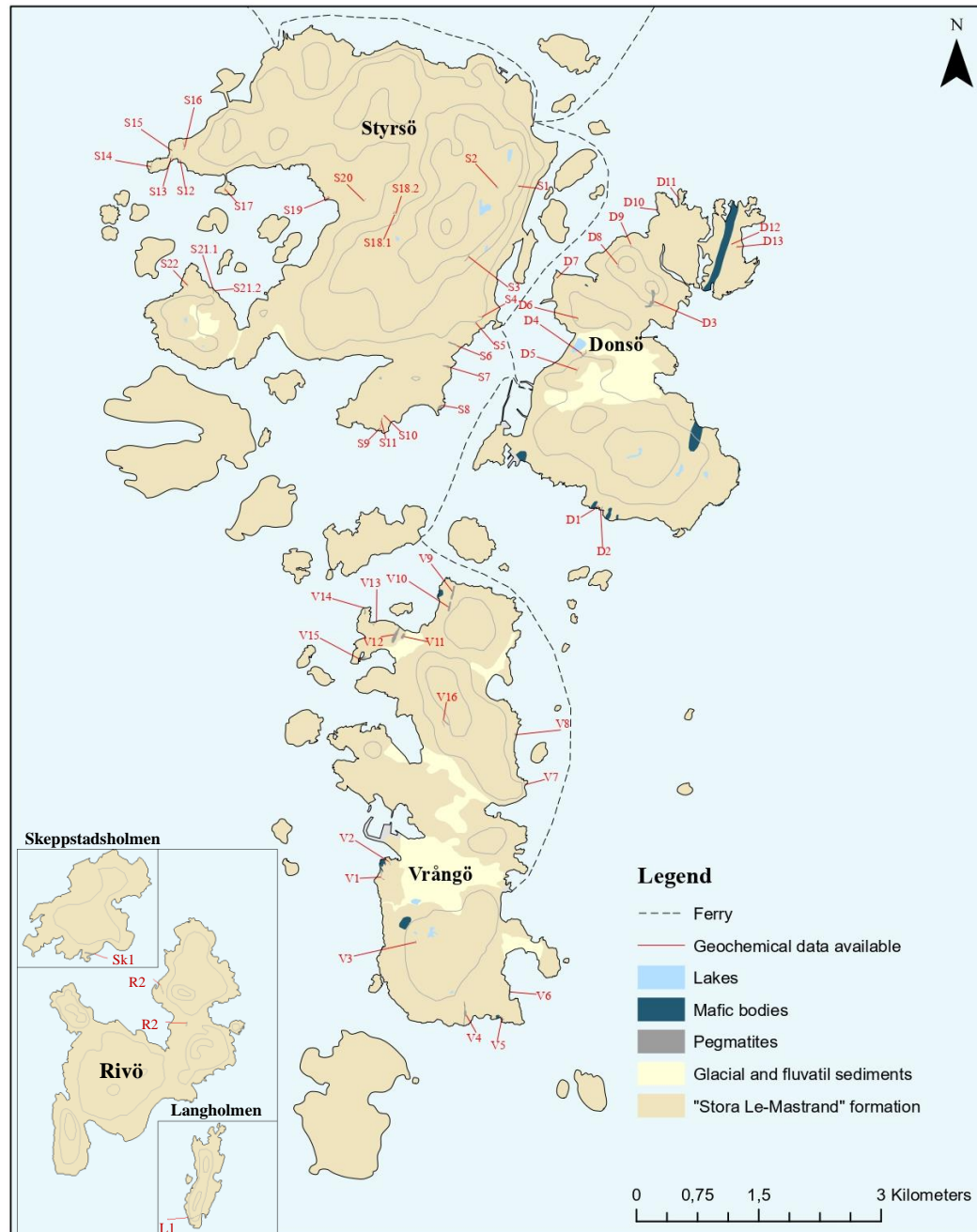


*Figure 11: General map of the study area in the southern archipelago of Gothenburg. V1-14, D1-13, S1-22, R1-2, L1 and Sk1 are Type I and II pegmatites found during the fieldwork. Rivö, Skeppstadsholmen and Langholmen are not shown at their actual location on the map for the sake of completeness. The coordinates a of the pegmatites can be found in table 5.*

**Typ I:** Kfsp + Qz + Plg + mica

Is a primitive barren, characterized by a low Rb/Sr ratio in Kfsp. It is exclusively granitic in composition and limited to quartz, sanidine/microcline, albite, rarely biotite and muscovite. The width and length of the barrens is not a distinguishing criterion, compared to the more fractionated pegmatites, and ranges from a width of > 1m, length > 5 m to thick dikes, with branches and sharp contact, that are up to 10 m wide and up to 70 m long (e.g. Langholmen; see figure 12 C). The barrens occur both along the foliation of the SLM (N-S) and crosscutting the SLM (W-E). This type is usually simple zoned with a fine-grained Border Zone consisting of plg + Qz + bio + kfsp < 2 cm. The barrens occur in two forms that are easily distinguishable by eye, with the proportion of Kfsp to Plg and the proportion of Ms to Bt being the decisive criterion (see figure 12, B & C). Barren with mainly K-feldspar and less plagioclase are predominantly also found with a higher proportion of muscovite, whereas the opposite is the case with plagioclase-rich barren have consequently more biotite. Sampled pegmatites L1, S7, S20, S22 and R2 representing this type.

**Typ II:** Kfsp + Qz + plg + mica + Grt + Ber +Ap + Cbe + (Clb + Fl)

The second type of pegmatite has a similar composition to the type I pegmatites, with accessory minerals such as garnet, beryl, apatite and chrysoberyl in addition to Kfsp, Qz, Plg and mica. Smeds, 1990 has also described columbite-tantalite and fluorite in pegmatite D3 (see figure 11), which however could not be found in this study. In addition to the occurrence of these mineral composition, this type has a higher Rb/Sr ratio in Kfsp than the Type I pegmatites. Pegmatites of this type are predominantly found on the island of Dönsö, with pegmatites D3, D4, D6, D8 and D11 best representing this type. Other pegmatites of this type are found at Styrsö (S15), Vrangö (V5), Rivö (R1) and Skeppstadsholmen (Sk1), the pegmatites on Donsö were the only ones with noticeable amounts of beryl. Beryl occurs mostly as Heliodor, rarely with a light greenish to blueish coloration and is found together with large crystals of Qz, Ms and Kfsp within the Core Zone (see figure 13, E & D). The beryl crystals are partially deformed (see figure 13, C), which would classify these rocks as "meta-pegmatites". Biotite is rarely present in this type whereas muscovite is very common. Biotite was only found in pegmatite D3 and D11. Muscovite was found along the border zone manly in the intermediate zone with crystal up to 30 cm. Accessory minerals such as, apatite and magnetite

were found in pegmatite D4 and D6. The presence of garnet was the first reason for dividing the pegmatites into type I and type II, which was considered an indicator of higher fractionation. Garnet forms clusters of crystals up to 2 cm in size within the intermediate and wall zones. Garnet has a deep red not transparent color. K-feldspar and Quartz often form intergrowth textures, such as graphic textures (see figure 13, A). The type II pegmatites are predominantly in the N-S strike of the SLM formation, but foliation and folding of the metasediment is corsscuted.
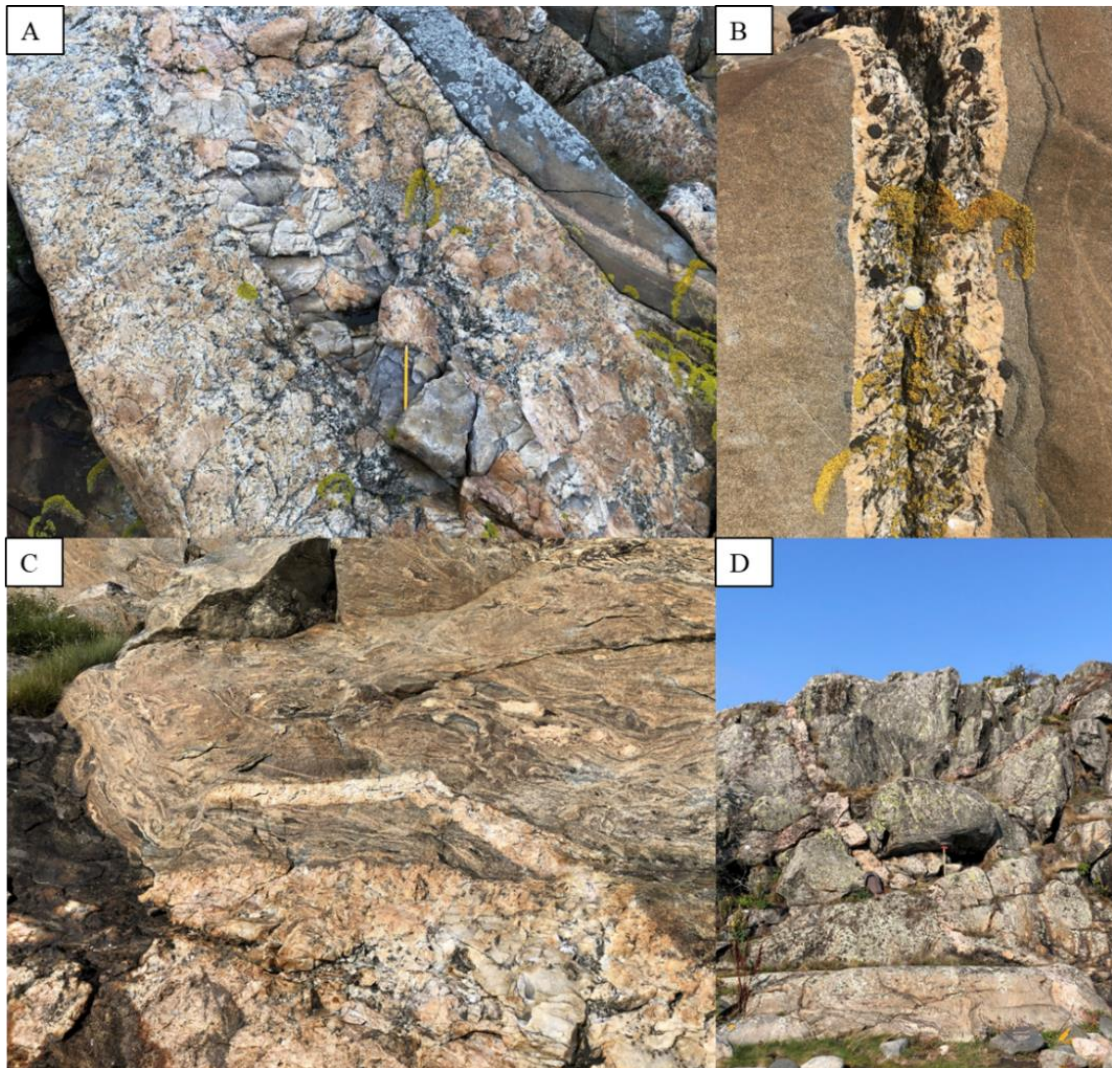


*Figure 12: A. Pegmatite Sk1 with distinct zonation of fine Qz, Kfsp and Ms in the boder zone. Grt layer in the intermediate zone and large Qz, Kfsp and Ms crystals in the core zone. B. Lateral branch of pegmatite V7 consisting of Plg and Ms in undefomed greywacke. C. Pegmatite L1 in strongly deformed paragneiss with fine boder zone and bulky core zone. The pegmatite corsscutted the structures of the paragneiss. D. Pegmatite D11 is only 50 cm wide and has many small yellow beryl crystals.*
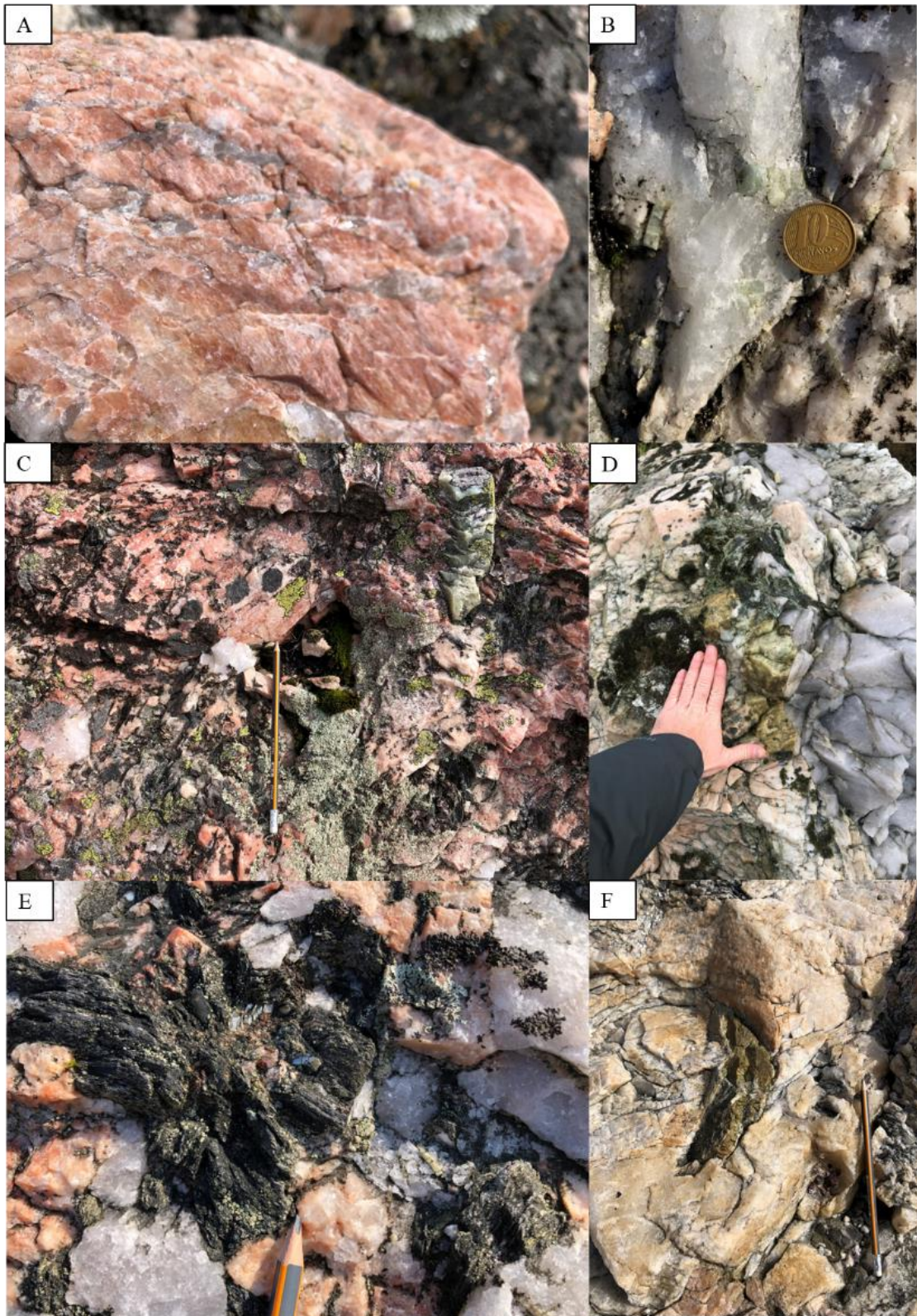
*Figure 13: A. Intergrowth of Kfsp and quartz is common in the intermediate zone. B. Beryl in Qz within the core zone in pegmatite D8. C. Large Kfsp crystal with 15 cm long beryl in pegmatite D8 surrounded by grt clusters. D. Pegmatite D4 with yellow greenish beryls and Ms clusters in the core zone. E. Typical radial cluster of Ms with grt in the intermediate zone. F. Chrysoberyl in the core zone consisting of Qz, Kfsp and Grt in pegmatite S15.*
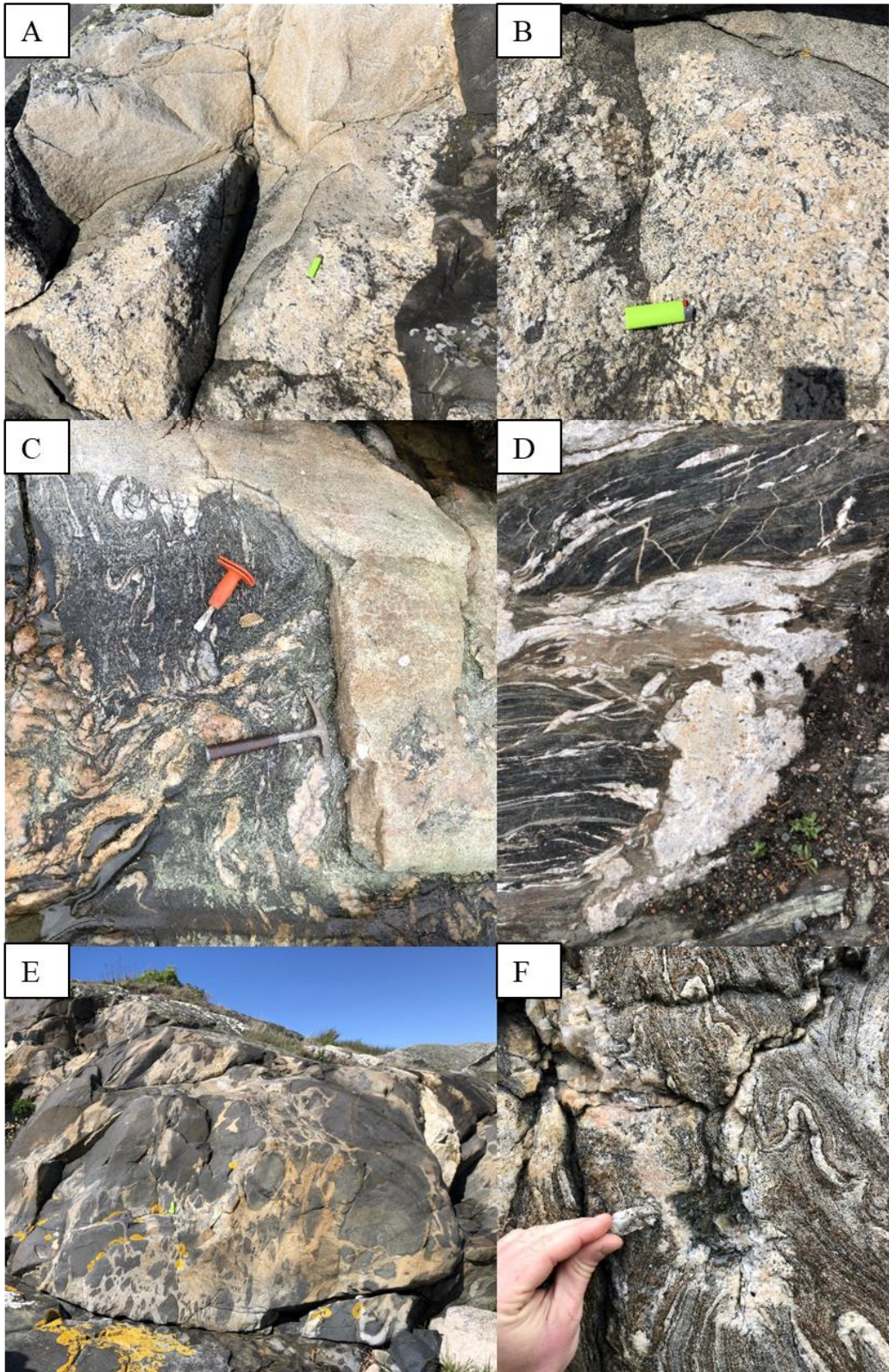
*Figure 14: Melt assemblages in the SLM metasediment. A: Granodioritic melt becomes more coarse-grained towards the margin with biotite up to 3 cm in size. Intruded into mafic and felsic magma mingling (E). B: Close-up of image A. C: Tonalitic intrusion crosscutting migmatite. D: Quartz and plagioclase rich melt intruded into banded amphibolite showing S3 structure. E: Magma-mingling of mafic and felsic melt intruded by pegmatites. F: Coarse-grained leucosome with muscovite up to 2 cm.*

**Meltpools/Aplite**

Melt pools are mainly found in areas of higher metamorphic overprint (eg. Vrangö, Skeppstadsholmen, Ursholmen). Melt formation next to amphibolites is predominantly Plg + Qz + Bio in composition with little to no Kfsp. Whereas melts within the paragneiss of the SLM have a granitic composition of Kfsp + Plg + Qz + Ms + Grt. Rarely, porphyritic structures with Kfsp crystals up to 1,5 cm in size form (eg. Ursholmen). The melt pools, usually a few square meters in size, crosscut the tectonic structures ($S_1$ & $S_2$) of the SLM Fm. (see figure 14, C). S3 structures within the migrating melt are characterized by tight, z-like folding of the aplitic dikes (figure 14, D). In the south of the island of Vrangö (10 m away from pegmatite V5) the granodioritic melt shows a coarse-grained texture towards the margin, which can be described as pegmatitic texture (see figure 14, A & B). The melt intrudes into an older intrusion of mafic and felsic material, which is described as magma-mingling (see figure 14, E). This type of intrusion has been dated to $1552 \pm 5$ Ma at another location with U-Pb in zircon (Ackevall, 2016).

## 5.3. pXRF mapping

A total of 221 measurements were performed with the pXRF on K-feldspar within the 57 pegmatites. The measured K-feldspar grains were scattered over each pegmatite body. The concentrations of K, Rb, Sr, Ba, and Pb were measured. Potassium was measured to ensure that it is a K-feldspar. Rb, Sr and Ba are used for preliminary determination of the fractionation degree. The potassium concentration in the feldspars varied from 2.95 wt% to 10.72 wt% with a mean value of 8.02 wt%. The rubidium concentration varies between 81 ppm and 689 ppm with a mean of 288 ppm. The strontium concentration varies between 10 ppm and 452 ppm with a mean value of 203 ppm. The barium concentration ranges from 26 ppm to 1388 ppm with a mean of 407 ppm. Lead content in the K-feldspars ranges from 13 ppm to 176 with a mean of 61 ppm. No correlation with pegmatite size and measured concentrations was observed. However, Rb, Sr and Ba contents in K-feldspar vary with the mineral composition of the respective pegmatite (see figure 15). When garnet was found in a pegmatite body, higher rubidium, lower strontium and barium concentrations are detected in the K-feldspars in the same body. A correlation between the mineral composition and the lead concentration could not be found.
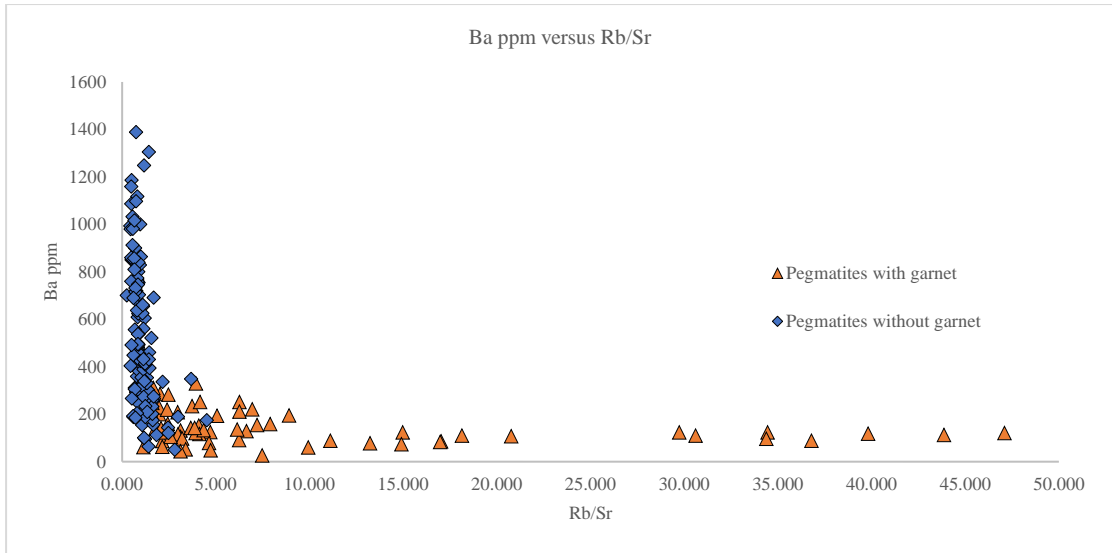
*Figure 15: Shown is the concentration of barium versus the Rb/Sr ratio of 122 measurements within all 57 pegmatite bodies. The measured K-feldspars in pegmatites with garnet show a lower concentration of barium and have a high Rb/Sr ratio compared to pegmatites without garnets.*
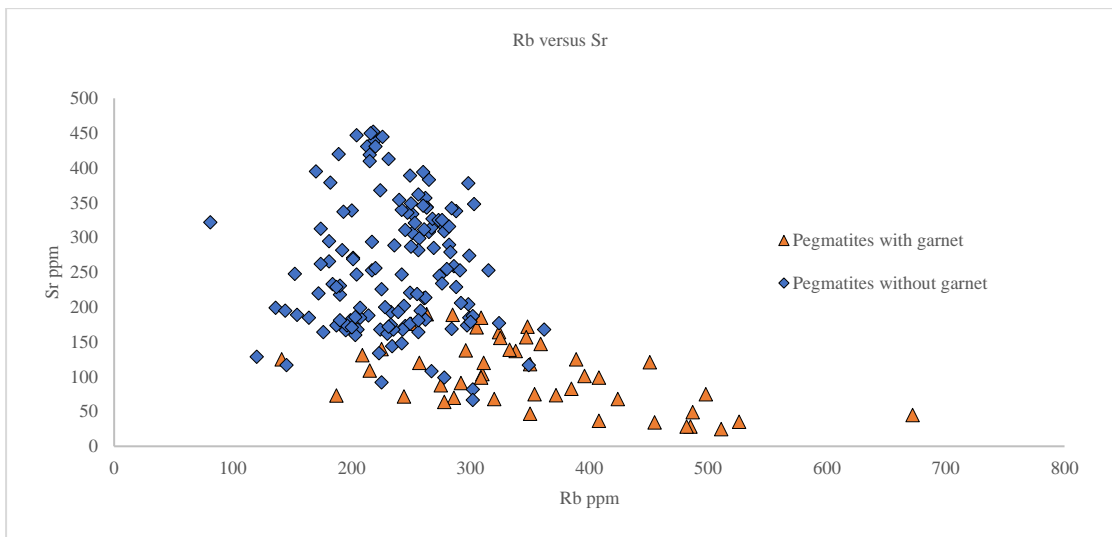


*Figure 16: Shown is the concentration of Sr versus Rb of 122 measurements in K-feldspar within all 57 pegmatite bodies. The measured K-feldspars in pegmatites with garnet show a lower concentration of Sr and have a higher Rb concentration compared to pegmatites without garnets.*

However, it cannot be generally assumed that the presence of a few garnet crystals indicates a high Rb/Sr ratio in all K-feldspars of the pegmatite body. Rather, it was observed that K-feldspars in the vicinity of garnet exhibit a higher Rb/Sr ratio. This is well demonstrated by the pegmatite S8. The Rb/Sr ratio is between 1.22 and 1.61 for six measurement points and 7.48 for spot, which was taken a few centimeters away from a garnet cluster. The first six measurements were taken within a radius of several meters. However, this observation could only be made in two pegmatites. Most K-

feldspar measurements showed a high Rb/Sr ratio in the presence of garnet in the pegmatite. Since every beryl-bearing pegmatite also contains garnet, no further subdivision is made in this respect.

## 5.4. Geochemistry

### 5.4.1. Mica

142 spots were obtained from 35 mica samples from 19 different pegmatites and two leucosomes within the SLM migmatite. The full LA-ICP-MS data set is found in Table 8. Five out of six Bt spots from pegmatite V5 and 1 out of 1 spot from pegmatite V1 were sorted out due to excessive chloritization (4:1 relationship; IV-ions/monovalent-ions; see table 8). Major element chemistry of the studied Muscovites is relatively consistent, whereas $SiO_2$ wt.%, $Al_2O_3$ wt.%, $K_2O$ wt%, FeO wt.% and MnO wt.% don't show any significant difference. In contrast, a difference in FeO and MnO concentration is seen in the biotite samples, with MnO being higher in type II pegmatites and FeO lower than in type I pegmatite. To classify the mica the chemical compositions determined from the mica grains were used. The data are plotted in the classification diagram from Tischendorf et al. (2001), which is based on the Mg, Li, Fe, and $^{VI}$Al (apfu) contents (Figure 17). Black mica generally plots as Mg-phlogopite, except of one mica spot from pegmatite V5. However, all other 5 spots have already been excluded from this mica sample and it can therefore be assumed that, despite an acceptable 4:1 relationship, this spot is also altered too much. White mica samples plot within the muscovite field and scratch the field of the Fe muscovite. For comparability of the analysis, in addition to the mica grains analyzed in this study, six other samples are included, which consist of the standards: Högsbo-Ms (Hogmalm et al. 2017), La posta-Bt (Zack & Hogmalm, 2016), Mc Clure Bt (Yang et al. 2014), Wilson Prom Bt (Elburg, 1996), Mica-Fe (Grove & Harrison, 1996) and Mica-Mg (Morteani et al. 2013; Hogmalm et al. 2017).

*Figure 17: Classification diagram of mica after Tischendorf et al. (2001). White Mica from Pegmatites (black triangle and red rhombus), black mica (black square), and standard samples are plotted.*

Table 8: Shown are oxides, trace element concentrations (ppm) and the stoichiometric mineral formula from the sampled muscovites and biotites of the respective pegmatites.

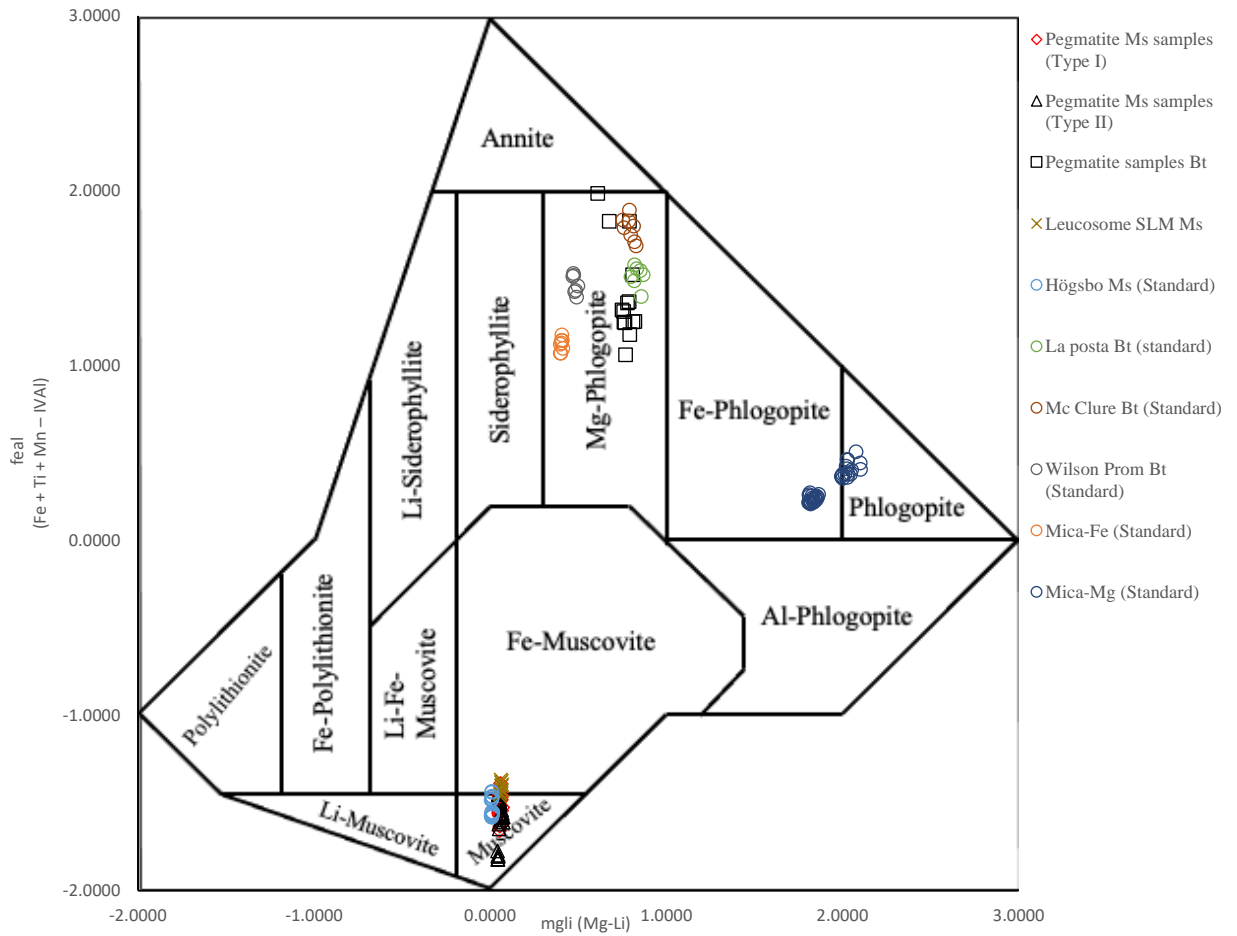| Location | D3 Ms | | | | | | D4 Ms | | | | | | D6 Ms | | | | | | D8 Ms | | | | | |
|---|---|---|---|---|---|---|---|---|---|---|---|---|---|---|---|---|---|---|---|---|---|---|---|---|
| Day | | | 2 | | | | 2 | 2 | 2 | 2 | 2 | 2 | 2 | 2 | 2 | 2 | 2 | 2 | 2 | 2 | 2 | 2 | 2 | 2 |
| Spot Nr. | 160 | 161 | 183 | 184 | 206 | 207 | 162 | 163 | 185 | 186 | 208 | 209 | 164 | 165 | 187 | 188 | 210 | 211 | 166 | 167 | 189 | 190 | 212 | 213 |
| SiO2 | 46.2 | 46.5 | 49.6 | 50.4 | 49.4 | 49.8 | 46.5 | 46.8 | 47.5 | 47.8 | 48.0 | 47.8 | 46.5 | 46.5 | 48.5 | 48.5 | 48.4 | 48.0 | 46.8 | 47.0 | 47.8 | 47.7 | 47.8 | 47.7 |
| Al2O3 | 34.9 | 34.7 | 31.6 | 30.7 | 31.6 | 31.8 | 34.9 | 34.9 | 34.2 | 34.2 | 34.0 | 34.2 | 35.0 | 35.4 | 33.6 | 33.4 | 33.7 | 34.1 | 35.1 | 34.8 | 34.4 | 34.5 | 34.5 | 34.3 |
| K2O | 12.1 | 12.1 | 12.2 | 12.2 | 12.1 | 12.0 | 12.6 | 12.6 | 12.3 | 12.4 | 12.2 | 12.3 | 12.1 | 12.0 | 12.2 | 12.1 | 12.0 | 11.8 | 12.3 | 12.5 | 12.1 | 12.1 | 12.1 | 12.2 |
| Na2O | 0.8 | 0.7 | 0.7 | 0.7 | 0.7 | 0.8 | 0.5 | 0.4 | 0.4 | 0.4 | 0.4 | 0.3 | 0.7 | 0.7 | 0.5 | 0.6 | 0.7 | 0.7 | 0.5 | 0.4 | 0.5 | 0.5 | 0.5 | 0.5 |
| CaO | 0.0 | b.d | 0.0 | 0.0 | 0.0 | 0.0 | b.d | b.d | 0.0 | 0.0 | 0.0 | 0.0 | 0.0 | 0.0 | 0.0 | 0.0 | 0.0 | b.d | 0.0 | 0.0 | 0.0 | 0.0 | 0.0 | 0.0 |
| MgO | 0.9 | 0.9 | 0.8 | 0.8 | 0.8 | 0.9 | 0.7 | 0.7 | 0.7 | 0.7 | 0.7 | 0.7 | 0.9 | 0.9 | 0.7 | 0.8 | 0.8 | 0.8 | 0.7 | 0.7 | 0.6 | 0.6 | 0.6 | 0.6 |
| MnO | 0.0 | 0.0 | 0.0 | 0.0 | 0.0 | 0.0 | 0.0 | 0.0 | 0.0 | 0.0 | 0.0 | 0.0 | 0.0 | 0.0 | 0.0 | 0.0 | 0.0 | 0.0 | 0.0 | 0.0 | 0.0 | 0.0 | 0.0 | 0.0 |
| FeO | 4.4 | 4.4 | 4.2 | 4.2 | 4.2 | 4.1 | 4.2 | 4.0 | 4.1 | 4.0 | 4.1 | 4.0 | 4.0 | 3.9 | 3.7 | 3.9 | 3.7 | 3.8 | 4.0 | 4.0 | 4.0 | 4.0 | 3.9 | 4.0 |
| Li | 87 | 80 | 70 | 55 | 59 | 55 | 45 | 36 | 33 | 31 | 29 | 26 | 26 | 25 | 22 | 22 | 22 | 22 | 16 | 10 | 17 | 11 | 14 | 14 |
| $^{85}$Rb | 1533 | 1520 | 1547 | 1600 | 1582 | 1484 | 711 | 705 | 680 | 680 | 681 | 694 | 666 | 640 | 629 | 639 | 656 | 650 | 1724 | 1729 | 1709 | 1699 | 1713 | 1755 |
| $^{86}$Sr | 1 | 1 | 1 | 3 | 2 | 0 | 2 | 2 | 2 | 2 | 1 | 2 | 2 | 2 | 3 | 2 | 2 | 2 | 1 | 1 | 1 | 1 | 0 | 1 |
| Ba | 24 | 22 | 32 | 72 | 57 | 16 | 13 | 12 | 12 | 13 | 10 | 14 | 15 | 19 | 15 | 15 | 17 | 14 | 3 | 4 | 3 | 2 | 2 | 2 |
| Cs | 86 | 84 | 87 | 101 | 94 | 79 | 24 | 29 | 23 | 27 | 23 | 33 | 26 | 25 | 23 | 24 | 25 | 25 | 116 | 114 | 114 | 111 | 112 | 116 |
| Ta | 36 | 51 | 118 | 85 | 108 | 56 | 7 | 7 | 6 | 6 | 6 | 6 | 8 | 8 | 7 | 7 | 7 | 7 | 32 | 32 | 31 | 30 | 28 | 32 |
| total | 99.34 | 99.37 | 99.14 | 99.14 | 98.88 | 99.32 | 99.36 | 99.38 | 99.38 | 99.41 | 99.44 | 99.42 | 99.27 | 99.27 | 99.36 | 99.31 | 99.28 | 99.27 | 99.43 | 99.43 | 99.43 | 99.44 | 99.44 | 99.43 |
| Number of ions based on 11 O | | | | | | | | | | | | | | | | | | | | | | | | |
| Si | 2.95 | 2.97 | 3.18 | 3.24 | 3.18 | 3.19 | 2.97 | 2.99 | 3.05 | 3.06 | 3.08 | 3.07 | 2.97 | 2.96 | 3.11 | 3.11 | 3.10 | 3.07 | 2.99 | 3.01 | 3.06 | 3.05 | 3.06 | 3.06 |
| $^{IV}$Al | 1.05 | 1.03 | 0.82 | 0.76 | 0.82 | 0.81 | 1.03 | 1.01 | 0.95 | 0.94 | 0.92 | 0.93 | 1.03 | 1.04 | 0.89 | 0.89 | 0.90 | 0.93 | 1.01 | 0.99 | 0.94 | 0.95 | 0.94 | 0.94 |
| ΣZ | 4.00 | 4.00 | 4.00 | 4.00 | 4.00 | 4.00 | 4.00 | 4.00 | 4.00 | 4.00 | 4.00 | 4.00 | 4.00 | 4.00 | 4.00 | 4.00 | 4.00 | 4.00 | 4.00 | 4.00 | 4.00 | 4.00 | 4.00 | 4.00 |
| $^{VI}$Al | 1.57 | 1.58 | 1.58 | 1.57 | 1.57 | 1.59 | 1.60 | 1.62 | 1.63 | 1.64 | 1.65 | 1.65 | 1.60 | 1.62 | 1.65 | 1.63 | 1.64 | 1.64 | 1.63 | 1.64 | 1.65 | 1.66 | 1.66 | 1.65 |
| Fe | 0.24 | 0.23 | 0.22 | 0.23 | 0.22 | 0.22 | 0.22 | 0.21 | 0.22 | 0.21 | 0.22 | 0.21 | 0.21 | 0.21 | 0.20 | 0.21 | 0.20 | 0.20 | 0.22 | 0.21 | 0.21 | 0.21 | 0.21 | 0.21 |
| Li | 0.01 | 0.00 | 0.00 | 0.00 | 0.00 | 0.00 | 0.00 | 0.00 | 0.00 | 0.00 | 0.00 | 0.00 | 0.00 | 0.00 | 0.00 | 0.00 | 0.00 | 0.00 | 0.00 | 0.00 | 0.00 | 0.00 | 0.00 | 0.00 |
| Mn | 0.00 | 0.00 | 0.00 | 0.00 | 0.00 | 0.00 | 0.00 | 0.00 | 0.00 | 0.00 | 0.00 | 0.00 | 0.00 | 0.00 | 0.00 | 0.00 | 0.00 | 0.00 | 0.00 | 0.00 | 0.00 | 0.00 | 0.00 | 0.00 |
| Ti | 0.01 | 0.01 | 0.02 | 0.02 | 0.03 | 0.01 | 0.01 | 0.01 | 0.01 | 0.01 | 0.01 | 0.01 | 0.02 | 0.02 | 0.02 | 0.02 | 0.02 | 0.02 | 0.01 | 0.01 | 0.01 | 0.01 | 0.01 | 0.01 |
| Mg | 0.09 | 0.09 | 0.08 | 0.08 | 0.08 | 0.08 | 0.07 | 0.06 | 0.07 | 0.07 | 0.07 | 0.07 | 0.08 | 0.08 | 0.07 | 0.07 | 0.07 | 0.08 | 0.06 | 0.06 | 0.06 | 0.06 | 0.06 | 0.06 |
| ΣY | 1.91 | 1.92 | 1.90 | 1.90 | 1.91 | 1.91 | 1.91 | 1.92 | 1.94 | 1.94 | 1.95 | 1.95 | 1.92 | 1.94 | 1.93 | 1.93 | 1.94 | 1.95 | 1.92 | 1.92 | 1.94 | 1.94 | 1.94 | 1.93 |
| K | 0.99 | 0.99 | 1.00 | 1.00 | 0.99 | 0.98 | 1.03 | 1.02 | 1.01 | 1.01 | 1.00 | 1.01 | 0.99 | 0.98 | 1.00 | 0.99 | 0.98 | 0.96 | 1.00 | 1.02 | 0.99 | 0.99 | 0.99 | 1.00 |
| Na | 0.09 | 0.09 | 0.09 | 0.09 | 0.09 | 0.10 | 0.06 | 0.05 | 0.05 | 0.05 | 0.05 | 0.04 | 0.09 | 0.09 | 0.07 | 0.08 | 0.08 | 0.09 | 0.07 | 0.05 | 0.07 | 0.06 | 0.06 | 0.06 |
| Ca | 0.00 | b.d | 0.00 | 0.00 | 0.00 | 0.00 | b.d | b.d | 0.00 | 0.00 | 0.00 | 0.00 | 0.00 | 0.00 | 0.00 | 0.00 | 0.00 | b.d | 0.00 | 0.00 | 0.00 | 0.00 | 0.00 | 0.00 |
| Rb | 0.01 | 0.01 | 0.01 | 0.01 | 0.01 | 0.01 | 0.00 | 0.00 | 0.00 | 0.00 | 0.00 | 0.00 | 0.00 | 0.00 | 0.00 | 0.00 | 0.00 | 0.00 | 0.01 | 0.01 | 0.01 | 0.01 | 0.01 | 0.01 |
| ΣX | 1.09 | 1.08 | 1.10 | 1.10 | 1.09 | 1.09 | 1.09 | 1.08 | 1.06 | 1.06 | 1.05 | 1.05 | 1.08 | 1.06 | 1.07 | 1.07 | 1.06 | 1.05 | 1.08 | 1.08 | 1.06 | 1.06 | 1.06 | 1.07 |
| mgli | 0.08 | 0.08 | 0.07 | 0.08 | 0.08 | 0.08 | 0.06 | 0.06 | 0.06 | 0.06 | 0.06 | 0.07 | 0.08 | 0.08 | 0.07 | 0.07 | 0.07 | 0.08 | 0.06 | 0.06 | 0.06 | 0.06 | 0.06 | 0.06 |
| feal | -1.33 | -1.33 | -1.33 | -1.32 | -1.31 | -1.36 | -1.36 | -1.39 | -1.40 | -1.42 | -1.42 | -1.43 | -1.37 | -1.40 | -1.43 | -1.40 | -1.43 | -1.42 | -1.41 | -1.42 | -1.43 | -1.44 | -1.45 | -1.43 |

Table 8: *continued.*

| Location | D11 Ms | | | | | | R1 Ms | | | | | | | | | S15 Ms | | | | | | SK1 Ms | | |
|---|---|---|---|---|---|---|---|---|---|---|---|---|---|---|---|---|---|---|---|---|---|---|---|---|
| *Day* | *2* | *2* | *2* | *2* | *2* | *2* | *1* | *1* | *1* | *1* | *1* | *1* | *1* | *1* | *1* | *1* | *1* | *1* | *1* | *1* | *1* | *1* | *1* | *1* |
| *Spot Nr.* | *168* | *169* | *191* | *192* | *214* | *215* | *295* | *128* | *129* | *291* | *292* | *293* | *294* | *130* | *131* | *102* | *103* | *266* | *267* | *268* | *269* | *208* | *209* | *346* |
| $SiO_2$ | 48.2 | 46.9 | 47.8 | 47.6 | 47.9 | 47.4 | 47.8 | 48.2 | 48.3 | 48.3 | 48.3 | 48.2 | 48.3 | 48.2 | 48.3 | 48.0 | 47.8 | 47.8 | 47.9 | 48.1 | 47.8 | 46.2 | 46.7 | 47.8 |
| $Al_2O_3$ | 32.9 | 34.3 | 33.6 | 33.9 | 33.6 | 34.0 | 35.4 | 35.6 | 35.5 | 35.2 | 35.2 | 35.3 | 35.2 | 35.5 | 35.4 | 35.1 | 35.2 | 35.0 | 34.9 | 34.8 | 34.9 | 36.0 | 35.3 | 34.7 |
| $K_2O$ | 12.4 | 12.2 | 12.0 | 11.9 | 11.9 | 11.9 | 11.7 | 11.2 | 11.2 | 11.7 | 11.7 | 11.7 | 11.8 | 11.1 | 11.3 | 11.1 | 11.3 | 11.6 | 11.8 | 11.5 | 11.8 | 12.4 | 12.5 | 11.7 |
| $Na_2O$ | 0.7 | 0.7 | 0.6 | 0.7 | 0.7 | 0.7 | 0.8 | 0.8 | 0.8 | 0.7 | 0.7 | 0.7 | 0.7 | 0.8 | 0.7 | 0.8 | 0.7 | 0.7 | 0.7 | 0.8 | 0.7 | 0.5 | 0.4 | 0.6 |
| CaO | b.d | 0.0 | 0.0 | 0.0 | 0.0 | 0.0 | b.d | b.d | 0.0 | 0.0 | b.d | b.d | 0.0 | 0.0 | 0.0 | b.d | 0.0 | b.d | b.d | b.d | 0.0 | 0.0 | 0.0 | 0.0 |
| MgO | 0.7 | 0.7 | 0.7 | 0.7 | 0.7 | 0.8 | 0.7 | 0.7 | 0.7 | 0.7 | 0.7 | 0.7 | 0.7 | 0.7 | 0.7 | 0.6 | 0.6 | 0.6 | 0.5 | 0.6 | 0.6 | 0.5 | 0.5 | 0.5 |
| MnO | 0.0 | 0.0 | 0.0 | 0.0 | 0.0 | 0.0 | 0.0 | 0.0 | 0.0 | 0.0 | 0.0 | 0.0 | 0.0 | 0.0 | 0.0 | 0.0 | 0.0 | 0.0 | 0.0 | 0.0 | 0.0 | 0.0 | 0.0 | 0.0 |
| FeO | 4.4 | 4.4 | 4.4 | 4.3 | 4.3 | 4.4 | 3.1 | 2.8 | 2.9 | 2.9 | 2.9 | 2.9 | 2.9 | 3.1 | 3.1 | 3.9 | 3.9 | 3.8 | 3.8 | 3.8 | 3.8 | 3.8 | 3.9 | 4.0 |
| Li | 73 | 73 | 66 | 64 | 63 | 63 | 32 | 30 | 31 | 33 | 33 | 32 | 34 | 35 | 34 | 32 | 32 | 35 | 29 | 32 | 35 | 65 | 65 | 63 |
| $^{85}Rb$ | 497 | 574 | 579 | 571 | 567 | 538 | 882 | 935 | 924 | 969 | 973 | 1028 | 1037 | 857 | 867 | 917 | 917 | 910 | 915 | 899 | 900 | 1335 | 1352 | 1420 |
| $^{86}Sr$ | 3 | 3 | 3 | 3 | 3 | 3 | 1 | 0 | 0 | 1 | 1 | 0 | 0 | 1 | 1 | 1 | 1 | 1 | 1 | 1 | 1 | 0 | 0 | 0 |
| Ba | 27 | 28 | 29 | 29 | 31 | 29 | 8 | 3 | 3 | 4 | 4 | 3 | 3 | 6 | 6 | 13 | 15 | 16 | 16 | 15 | 17 | 2 | 3 | 2 |
| Cs | 13 | 13 | 13 | 12 | 13 | 12 | 126 | 172 | 164 | 186 | 189 | 225 | 230 | 124 | 126 | 143 | 141 | 143 | 144 | 139 | 137 | 27 | 28 | 28 |
| Ta | 4 | 4 | 4 | 5 | 5 | 5 | 19 | 26 | 26 | 30 | 29 | 34 | 34 | 21 | 19 | 20 | 19 | 20 | 21 | 20 | 21 | 12 | 12 | 12 |
| total | 99.27 | 99.19 | 99.20 | 99.19 | 99.19 | 99.19 | 99.50 | 99.51 | 99.51 | 99.51 | 99.52 | 99.52 | 99.52 | 99.46 | 99.50 | 99.55 | 99.55 | 99.55 | 99.55 | 99.55 | 99.55 | 99.44 | 99.43 | 99.42 |
| Number of ions based on 11 O | | | | | | | | | | | | | | | | | | | | | | | | |
| Si | 3.09 | 3.00 | 3.06 | 3.05 | 3.07 | 3.04 | 3.05 | 3.07 | 3.08 | 3.08 | 3.08 | 3.07 | 3.08 | 3.08 | 3.08 | 3.07 | 3.06 | 3.06 | 3.06 | 3.07 | 3.06 | 2.95 | 2.99 | 3.07 |
| $^{IV}Al$ | 0.91 | 1.00 | 0.94 | 0.95 | 0.93 | 0.96 | 0.95 | 0.93 | 0.92 | 0.92 | 0.92 | 0.93 | 0.92 | 0.92 | 0.92 | 0.93 | 0.94 | 0.94 | 0.94 | 0.93 | 0.94 | 1.05 | 1.01 | 0.93 |
| $\Sigma Z$ | 4.00 | 4.00 | 4.00 | 4.00 | 4.00 | 4.00 | 4.00 | 4.00 | 4.00 | 4.00 | 4.00 | 4.00 | 4.00 | 4.00 | 4.00 | 4.00 | 4.00 | 4.00 | 4.00 | 4.00 | 4.00 | 4.00 | 4.00 | 4.00 |
| $^{VI}Al$ | 1.57 | 1.58 | 1.61 | 1.61 | 1.61 | 1.60 | 1.71 | 1.75 | 1.75 | 1.73 | 1.73 | 1.72 | 1.72 | 1.75 | 1.75 | 1.72 | 1.71 | 1.69 | 1.69 | 1.69 | 1.69 | 1.66 | 1.65 | 1.69 |
| Fe | 0.23 | 0.23 | 0.23 | 0.23 | 0.23 | 0.23 | 0.16 | 0.15 | 0.16 | 0.15 | 0.15 | 0.16 | 0.15 | 0.17 | 0.16 | 0.21 | 0.21 | 0.20 | 0.20 | 0.20 | 0.20 | 0.20 | 0.21 | 0.21 |
| Li | 0.00 | 0.00 | 0.00 | 0.00 | 0.00 | 0.00 | 0.00 | 0.00 | 0.00 | 0.00 | 0.00 | 0.00 | 0.00 | 0.00 | 0.00 | 0.00 | 0.00 | 0.00 | 0.00 | 0.00 | 0.00 | 0.00 | 0.00 | 0.00 |
| Mn | 0.00 | 0.00 | 0.00 | 0.00 | 0.00 | 0.00 | 0.00 | 0.00 | 0.00 | 0.00 | 0.00 | 0.00 | 0.00 | 0.00 | 0.00 | 0.00 | 0.00 | 0.00 | 0.00 | 0.00 | 0.00 | 0.00 | 0.00 | 0.00 |
| Ti | 0.02 | 0.02 | 0.02 | 0.02 | 0.02 | 0.02 | 0.01 | 0.01 | 0.01 | 0.01 | 0.00 | 0.00 | 0.00 | 0.01 | 0.01 | 0.00 | 0.00 | 0.00 | 0.00 | 0.00 | 0.00 | 0.01 | 0.01 | 0.01 |
| Mg | 0.07 | 0.07 | 0.07 | 0.07 | 0.07 | 0.07 | 0.07 | 0.07 | 0.07 | 0.07 | 0.07 | 0.07 | 0.06 | 0.07 | 0.07 | 0.06 | 0.06 | 0.05 | 0.05 | 0.05 | 0.05 | 0.05 | 0.05 | 0.05 |
| $\Sigma Y$ | 1.89 | 1.92 | 1.94 | 1.94 | 1.94 | 1.94 | 1.95 | 1.98 | 1.98 | 1.96 | 1.96 | 1.95 | 1.95 | 1.99 | 1.98 | 1.99 | 1.98 | 1.96 | 1.95 | 1.96 | 1.95 | 1.92 | 1.92 | 1.96 |
| K | 1.01 | 0.99 | 0.98 | 0.97 | 0.97 | 0.97 | 0.95 | 0.91 | 0.91 | 0.95 | 0.95 | 0.96 | 0.96 | 0.91 | 0.92 | 0.91 | 0.92 | 0.95 | 0.96 | 0.94 | 0.96 | 1.01 | 1.02 | 0.96 |
| Na | 0.09 | 0.09 | 0.08 | 0.09 | 0.08 | 0.09 | 0.09 | 0.10 | 0.10 | 0.09 | 0.09 | 0.09 | 0.08 | 0.10 | 0.09 | 0.10 | 0.09 | 0.09 | 0.08 | 0.10 | 0.08 | 0.06 | 0.05 | 0.07 |
| Ca | b.d | 0.00 | 0.00 | 0.00 | 0.00 | 0.00 | b.d | b.d | 0.00 | 0.00 | b.d | b.d | 0.00 | 0.00 | 0.00 | b.d | 0.00 | b.d | b.d | b.d | 0.00 | 0.00 | 0.00 | 0.00 |
| Rb | 0.00 | 0.00 | 0.00 | 0.00 | 0.00 | 0.00 | 0.00 | 0.00 | 0.00 | 0.00 | 0.00 | 0.00 | 0.00 | 0.00 | 0.00 | 0.00 | 0.00 | 0.00 | 0.00 | 0.00 | 0.00 | 0.01 | 0.01 | 0.01 |
| $\Sigma X$ | 1.11 | 1.08 | 1.06 | 1.06 | 1.06 | 1.06 | 1.05 | 1.02 | 1.02 | 1.04 | 1.04 | 1.05 | 1.05 | 1.01 | 1.02 | 1.01 | 1.02 | 1.04 | 1.05 | 1.04 | 1.05 | 1.08 | 1.07 | 1.04 |
| mgli | 0.06 | 0.07 | 0.07 | 0.07 | 0.07 | 0.07 | 0.06 | 0.07 | 0.07 | 0.06 | 0.06 | 0.06 | 0.06 | 0.06 | 0.06 | 0.05 | 0.05 | 0.05 | 0.05 | 0.05 | 0.05 | 0.04 | 0.04 | 0.04 |
| feal | -1.31 | -1.33 | -1.35 | -1.35 | -1.35 | -1.34 | -1.54 | -1.59 | -1.58 | -1.57 | -1.57 | -1.56 | -1.56 | -1.57 | -1.57 | -1.50 | -1.50 | -1.48 | -1.48 | -1.49 | -1.48 | -1.45 | -1.44 | -1.47 |

Table 8: *continued.*

| Location | Sk1 Ms | | | V5 Ms | | | | | | L1 Ms | | | | | R2 Ms | | | | | | S7 Ms | | | S20 |
|---|---|---|---|---|---|---|---|---|---|---|---|---|---|---|---|---|---|---|---|---|---|---|---|---|
| Day | 1 | 1 | 1 | 1 | 1 | 1 | 1 | 1 | 1 | 1 | 1 | 1 | 1 | 1 | 1 | 1 | 1 | 1 | 1 | 1 | 1 | 1 | 1 | 1 |
| Spot Nr. | 347 | 348 | 349 | 94 | 141$^E$ | 142$^E$ | 143$^E$ | 144$^E$ | 145$^E$ | 94 | 95 | 242 | 243 | 318 | 150 | 151 | 296 | 152 | 153 | 297 | 122 | 123 | 270 | 265 |
| SiO2 | 47.7 | 47.9 | 47.4 | 47.0 | 47.0 | 47.2 | 46.8 | 46.8 | 46.6 | 46.5 | 48.3 | 47.7 | 47.9 | 47.7 | 47.1 | 46.9 | 47.3 | 47.5 | 47.5 | 47.4 | 47.2 | 47.7 | 47.7 | 47.6 |
| Al2O3 | 34.7 | 34.5 | 35.0 | 38.7 | 39.2 | 39.1 | 39.3 | 39.2 | 39.7 | 37.0 | 34.7 | 35.7 | 35.3 | 35.7 | 35.6 | 35.5 | 35.1 | 35.2 | 35.1 | 35.0 | 36.3 | 35.6 | 35.4 | 34.1 |
| K2O | 11.9 | 11.7 | 12.0 | 10.5 | 10.0 | 10.1 | 10.2 | 10.3 | 10.1 | 11.8 | 12.2 | 12.0 | 12.4 | 12.1 | 11.7 | 11.8 | 11.8 | 11.8 | 11.8 | 12.1 | 12.0 | 11.9 | 12.2 | 11.9 |
| Na2O | 0.6 | 0.6 | 0.5 | 0.6 | 0.7 | 0.7 | 0.7 | 0.6 | 0.6 | 0.5 | 0.3 | 0.4 | 0.3 | 0.5 | 0.7 | 0.7 | 0.6 | 0.6 | 0.6 | 0.5 | 0.6 | 0.5 | 0.5 | 0.5 |
| CaO | 0.0 | b.d | 0.0 | 0.0 | 0.0 | 0.0 | 0.0 | 0.0 | 0.0 | 0.0 | 0.0 | b.d | 0.0 | 0.0 | b.d | 0.0 | 0.0 | b.d | b.d | 0.0 | 0.0 | b.d | 0.0 | b.d |
| MgO | 0.5 | 0.5 | 0.5 | 0.4 | 0.5 | 0.5 | 0.5 | 0.5 | 0.5 | 0.5 | 0.7 | 0.5 | 0.5 | 0.5 | 0.7 | 0.7 | 0.7 | 0.6 | 0.7 | 0.6 | 0.6 | 0.7 | 0.6 | 0.6 |
| MnO | 0.0 | 0.0 | 0.0 | 0.0 | 0.0 | 0.0 | 0.0 | 0.0 | 0.0 | 0.0 | 0.0 | 0.0 | 0.0 | 0.0 | 0.0 | 0.0 | 0.0 | 0.0 | 0.0 | 0.0 | 0.0 | 0.0 | 0.0 | 0.0 |
| FeO | 4.1 | 4.1 | 4.0 | 2.2 | 2.1 | 1.9 | 1.9 | 2.1 | 2.0 | 3.0 | 3.2 | 3.1 | 3.0 | 3.0 | 3.6 | 3.7 | 3.8 | 3.6 | 3.7 | 3.7 | 2.8 | 3.1 | 3.0 | 4.0 |
| Li | 63 | 66 | 55 | 19 | 25 | 18 | 24 | 21 | 22 | 24 | 24 | 27 | 15 | 22 | 37 | 35 | 33 | 28 | 36 | 33 | 31 | 34 | 32 | 27 |
| $^{85}$Rb | 1435 | 1444 | 1340 | 641 | 655 | 661 | 659 | 657 | 868 | 762 | 527 | 676 | 701 | 712 | 601 | 620 | 607 | 611 | 622 | 609 | 557 | 540 | 520 | 390 |
| $^{86}$Sr | 0 | 0 | 0 | 3 | 1759 | 1425 | 1287 | 2155 | 2009 | 4 | 8 | 7 | 9 | 6 | 4 | 6 | 6 | 5 | 4 | 7 | 4 | 6 | 16 | 15 |
| Ba | 2 | 2 | 2 | 20 | 16 | 15 | 18 | 18 | 10 | 19 | 87 | 30 | 31 | 21 | 44 | 34 | 40 | 32 | 33 | 41 | 16 | 51 | 38 | 448 |
| Cs | 29 | 30 | 25 | 18 | 18 | 18 | 17 | 19 | 39 | 23 | 34 | 23 | 22 | 22 | 10 | 11 | 10 | 10 | 10 | 11 | 20 | 20 | 17 | 36 |
| Ta | 12 | 13 | 11 | 5 | 6 | 6 | 6 | 7 | 17 | 7 | 7 | 8 | 7 | 12 | 5 | 7 | 6 | 9 | 7 | 6 | 6 | 6 | 8 | 8 |
| total | 99.42 | 99.42 | 99.42 | 99.48 | 99.44 | 99.44 | 99.44 | 99.43 | 99.45 | 99.42 | 99.43 | 99.42 | 99.38 | 99.43 | 99.40 | 99.39 | 99.39 | 99.42 | 99.37 | 99.37 | 99.46 | 99.43 | 99.44 | 98.88 |
| Number of ions based on 11 O | | | | | | | | | | | | | | | | | | | | | | | | |
| Si | 3.06 | 3.07 | 3.04 | 3.00 | 2.99 | 3.00 | 2.98 | 2.98 | 2.96 | 2.97 | 3.09 | 3.05 | 3.06 | 3.05 | 3.01 | 3.00 | 3.03 | 3.03 | 3.04 | 3.03 | 3.01 | 3.04 | 3.05 | 3.06 |
| $^{IV}$Al | 0.94 | 0.93 | 0.96 | 1.00 | 1.01 | 1.00 | 1.02 | 1.02 | 1.04 | 1.03 | 0.91 | 0.95 | 0.94 | 0.95 | 0.99 | 1.00 | 0.97 | 0.97 | 0.96 | 0.97 | 0.99 | 0.96 | 0.95 | 0.94 |
| ΣZ | 4.00 | 4.00 | 4.00 | 4.00 | 4.00 | 4.00 | 4.00 | 4.00 | 4.00 | 4.00 | 4.00 | 4.00 | 4.00 | 4.00 | 4.00 | 4.00 | 4.00 | 4.00 | 4.00 | 4.00 | 4.00 | 4.00 | 4.00 | 4.00 |
| $^{VI}$Al | 1.67 | 1.67 | 1.68 | 1.90 | 1.93 | 1.93 | 1.92 | 1.92 | 1.94 | 1.74 | 1.71 | 1.74 | 1.72 | 1.73 | 1.69 | 1.67 | 1.67 | 1.69 | 1.68 | 1.67 | 1.74 | 1.72 | 1.71 | 1.64 |
| Fe | 0.22 | 0.22 | 0.22 | 0.12 | 0.11 | 0.10 | 0.10 | 0.11 | 0.10 | 0.16 | 0.17 | 0.16 | 0.16 | 0.16 | 0.19 | 0.20 | 0.20 | 0.19 | 0.20 | 0.20 | 0.15 | 0.17 | 0.16 | 0.22 |
| Li | 0.00 | 0.00 | 0.00 | 0.00 | 0.00 | 0.00 | 0.00 | 0.00 | 0.00 | 0.00 | 0.00 | 0.00 | 0.00 | 0.00 | 0.00 | 0.00 | 0.00 | 0.00 | 0.00 | 0.00 | 0.00 | 0.00 | 0.00 | 0.00 |
| Mn | 0.00 | 0.00 | 0.00 | 0.00 | 0.00 | 0.00 | 0.00 | 0.00 | 0.00 | 0.00 | 0.00 | 0.00 | 0.00 | 0.00 | 0.00 | 0.00 | 0.00 | 0.00 | 0.00 | 0.00 | 0.00 | 0.00 | 0.00 | 0.00 |
| Ti | 0.01 | 0.01 | 0.01 | 0.01 | 0.01 | 0.01 | 0.01 | 0.01 | 0.01 | 0.01 | 0.01 | 0.01 | 0.01 | 0.01 | 0.01 | 0.01 | 0.01 | 0.01 | 0.01 | 0.01 | 0.01 | 0.01 | 0.01 | 0.04 |
| Mg | 0.05 | 0.05 | 0.05 | 0.04 | 0.05 | 0.04 | 0.04 | 0.04 | 0.04 | 0.05 | 0.07 | 0.05 | 0.05 | 0.05 | 0.06 | 0.06 | 0.06 | 0.06 | 0.06 | 0.06 | 0.06 | 0.07 | 0.06 | 0.06 |
| ΣY | 1.95 | 1.95 | 1.95 | 2.07 | 2.10 | 2.09 | 2.08 | 2.09 | 2.09 | 1.97 | 1.97 | 1.97 | 1.95 | 1.95 | 1.96 | 1.95 | 1.95 | 1.96 | 1.96 | 1.95 | 1.95 | 1.97 | 1.95 | 1.96 |
| K | 0.97 | 0.96 | 0.98 | 0.85 | 0.82 | 0.82 | 0.83 | 0.84 | 0.82 | 0.96 | 0.99 | 0.98 | 1.01 | 0.98 | 0.95 | 0.97 | 0.97 | 0.96 | 0.96 | 0.98 | 0.97 | 0.97 | 0.99 | 0.97 |
| Na | 0.07 | 0.08 | 0.06 | 0.07 | 0.09 | 0.09 | 0.09 | 0.07 | 0.08 | 0.07 | 0.04 | 0.05 | 0.04 | 0.06 | 0.08 | 0.08 | 0.08 | 0.08 | 0.08 | 0.07 | 0.07 | 0.06 | 0.06 | 0.07 |
| Ca | 0.00 | b.d | 0.00 | 0.00 | 0.00 | 0.00 | 0.00 | 0.00 | 0.00 | 0.00 | 0.00 | b.d | 0.00 | 0.00 | b.d | 0.00 | 0.00 | b.d | b.d | 0.00 | 0.00 | b.d | 0.00 | b.d |
| Rb | 0.01 | 0.01 | 0.01 | 0.00 | 0.00 | 0.00 | 0.00 | 0.00 | 0.00 | 0.00 | 0.00 | 0.00 | 0.00 | 0.00 | 0.00 | 0.00 | 0.00 | 0.00 | 0.00 | 0.00 | 0.00 | 0.00 | 0.00 | 0.00 |
| ΣX | 1.05 | 1.05 | 1.05 | 0.93 | 0.90 | 0.91 | 0.92 | 0.91 | 0.91 | 1.03 | 1.03 | 1.03 | 1.05 | 1.05 | 1.04 | 1.05 | 1.05 | 1.04 | 1.04 | 1.05 | 1.05 | 1.03 | 1.05 | 1.04 |
| mgli | 0.04 | 0.05 | 0.04 | 0.04 | 0.04 | 0.04 | 0.04 | 0.04 | 0.04 | 0.05 | 0.07 | 0.05 | 0.05 | 0.05 | 0.06 | 0.06 | 0.06 | 0.06 | 0.06 | 0.06 | 0.05 | 0.06 | 0.06 | 0.06 |
| feal | -1.45 | -1.45 | -1.45 | -1.77 | -1.80 | -1.82 | -1.80 | -1.80 | -1.82 | -1.57 | -1.52 | -1.56 | -1.55 | -1.56 | -1.48 | -1.45 | -1.45 | -1.48 | -1.47 | -1.45 | -1.57 | -1.54 | -1.54 | -1.39 |

Spot Nr.$^E$ = excluded due to bad 4:1 relationship (IV-ions/monovalent-ions)

Table 8: *continued.*

| | S22 Ms | | | Leucosome Ms | | | | | | | | | | | | | D11 Bt | | | | | | L1 Bt | |
|---|---|---|---|---|---|---|---|---|---|---|---|---|---|---|---|---|---|---|---|---|---|---|---|---|
| *Day* | *1* | *1* | *1* | *1* | *1* | *1* | *1* | *1* | *1* | *1* | *1* | *1* | *1* | *1* | *1* | *1* | *2* | *2* | *2* | *2* | *2* | *2* | *1* | *1* |
| *Spot Nr.* | *98* | *99* | *263* | *210* | *211* | *350* | *351* | *352* | *353* | *354* | *324* | *325* | *326* | *327* | *206* | *207* | *170* | *171* | *193* | *194* | *216* | *217* | *154* | *155* |
| SiO2 | 47.1 | 47.2 | 47.2 | 47.6 | 46.7 | 47.3 | 47.2 | 46.8 | 48.5 | 47.5 | 46.9 | 47.0 | 47.2 | 47.1 | 44.8 | 45.0 | 35.5 | 36.0 | 36.2 | 36.6 | 36.5 | 35.9 | 37.7 | 38.0 |
| Al2O3 | 35.7 | 35.6 | 35.3 | 34.2 | 35.5 | 34.8 | 34.8 | 34.8 | 33.0 | 34.2 | 35.3 | 35.1 | 35.2 | 34.9 | 37.2 | 36.5 | 15.8 | 15.5 | 15.7 | 15.6 | 15.8 | 15.5 | 17.4 | 17.0 |
| K2O | 11.4 | 11.4 | 11.9 | 12.1 | 11.9 | 11.7 | 11.7 | 11.9 | 12.5 | 11.8 | 12.0 | 12.0 | 11.9 | 12.2 | 12.5 | 12.5 | 10.8 | 10.7 | 10.7 | 10.6 | 10.4 | 10.6 | 11.0 | 11.1 |
| Na2O | 0.8 | 0.8 | 0.6 | 0.7 | 0.7 | 0.7 | 0.7 | 0.7 | 0.5 | 0.7 | 0.6 | 0.6 | 0.5 | 0.4 | 0.6 | 0.5 | 0.1 | 0.1 | 0.1 | 0.0 | 0.0 | 0.0 | 0.1 | 0.1 |
| CaO | b.d | b.d | b.d | 0.0 | 0.0 | b.d | b.d | b.d | b.d | 0.0 | 0.0 | b.d | b.d | b.d | b.d | b.d | 0.0 | 0.0 | 0.0 | 0.0 | 0.0 | 0.0 | 0.0 | 0.0 |
| MgO | 0.6 | 0.6 | 0.6 | 0.7 | 0.7 | 0.7 | 0.7 | 0.7 | 0.6 | 0.7 | 0.6 | 0.6 | 0.6 | 0.6 | 0.6 | 0.7 | 8.6 | 8.5 | 8.4 | 8.3 | 8.4 | 8.3 | 6.7 | 6.7 |
| MnO | 0.0 | 0.0 | 0.0 | 0.0 | 0.0 | 0.0 | 0.0 | 0.0 | 0.0 | 0.0 | 0.0 | 0.0 | 0.0 | 0.0 | 0.0 | 0.0 | 0.8 | 0.8 | 0.8 | 0.8 | 0.8 | 0.8 | 0.4 | 0.4 |
| FeO | 3.8 | 3.8 | 3.7 | 3.8 | 3.8 | 3.9 | 4.0 | 4.1 | 3.9 | 4.1 | 3.5 | 3.5 | 3.4 | 3.7 | 3.2 | 3.6 | 25.2 | 25.2 | 24.9 | 24.9 | 24.8 | 25.7 | 23.7 | 23.6 |
| Li | 54 | 50 | 47 | 77 | 70 | 70 | 73 | 75 | 75 | 74 | 61 | 58 | 59 | 71 | 69 | 74 | 240 | 228 | 222 | 198 | 188 | 199 | 119 | 133 |
| $^{85}$Rb | 614 | 606 | 605 | 389 | 382 | 408 | 411 | 416 | 426 | 411 | 396 | 399 | 409 | 402 | 380 | 387 | 1141 | 1137 | 1133 | 1141 | 1116 | 1147 | 834 | 844 |
| $^{86}$Sr | 2 | 2 | 2 | 18 | 17 | 19 | 20 | 21 | 20 | 21 | 21 | 22 | 22 | 20 | 19 | 19 | 0 | 0 | 0 | 0 | 1 | 1 | 0 | 0 |
| Ba | 13 | 12 | 14 | 567 | 600 | 648 | 626 | 657 | 616 | 651 | 1086 | 1140 | 1120 | 1043 | 1006 | 1019 | 24 | 25 | 23 | 25 | 25 | 24 | 360 | 370 |
| Cs | 91 | 89 | 88 | 9 | 9 | 10 | 9 | 9 | 9 | 8 | 15 | 15 | 16 | 17 | 15 | 17 | 96 | 101 | 95 | 103 | 100 | 106 | 58 | 60 |
| Ta | 14 | 13 | 14 | 7 | 8 | 8 | 8 | 8 | 7 | 7 | 5 | 4 | 5 | 4 | 4 | 5 | 12 | 11 | 12 | 11 | 12 | 12 | 11 | 13 |
| total | 99.37 | 99.38 | 99.37 | 99.18 | 99.24 | 99.23 | 99.09 | 99.05 | 99.06 | 99.01 | 98.85 | 98.84 | 98.85 | 98.90 | 98.96 | 98.87 | 96.84 | 96.86 | 96.84 | 96.85 | 96.81 | 96.85 | 96.89 | 96.88 |
| Number of ions based on 11 O | | | | | | | | | | | | | | | | | | | | | | | | |
| Si | 3.01 | 3.01 | 3.02 | 3.05 | 2.98 | 3.03 | 3.02 | 2.99 | 3.11 | 3.05 | 3.00 | 3.01 | 3.02 | 3.02 | 2.85 | 2.87 | 2.71 | 2.75 | 2.76 | 2.79 | 2.78 | 2.75 | 2.88 | 2.91 |
| $^{IV}$Al | 0.99 | 0.99 | 0.98 | 0.95 | 1.02 | 0.97 | 0.98 | 1.01 | 0.89 | 0.95 | 1.00 | 0.99 | 0.98 | 0.98 | 1.15 | 1.13 | 1.29 | 1.25 | 1.24 | 1.21 | 1.22 | 1.25 | 1.12 | 1.09 |
| ΣZ | 4.00 | 4.00 | 4.00 | 4.00 | 4.00 | 4.00 | 4.00 | 4.00 | 4.00 | 4.00 | 4.00 | 4.00 | 4.00 | 4.00 | 4.00 | 4.00 | 4.00 | 4.00 | 4.00 | 4.00 | 4.00 | 4.00 | 4.00 | 4.00 |
| $^{VI}$Al | 1.69 | 1.69 | 1.68 | 1.63 | 1.65 | 1.65 | 1.64 | 1.62 | 1.60 | 1.63 | 1.66 | 1.66 | 1.68 | 1.65 | 1.65 | 1.62 | 0.13 | 0.15 | 0.17 | 0.19 | 0.21 | 0.14 | 0.45 | 0.44 |
| Fe | 0.20 | 0.20 | 0.20 | 0.20 | 0.20 | 0.21 | 0.22 | 0.22 | 0.21 | 0.22 | 0.19 | 0.19 | 0.18 | 0.20 | 0.17 | 0.19 | 1.60 | 1.61 | 1.59 | 1.59 | 1.59 | 1.64 | 1.52 | 1.51 |
| Li | 0.00 | 0.00 | 0.00 | 0.00 | 0.00 | 0.00 | 0.00 | 0.00 | 0.00 | 0.00 | 0.00 | 0.00 | 0.00 | 0.00 | 0.00 | 0.00 | 0.02 | 0.02 | 0.02 | 0.01 | 0.01 | 0.01 | 0.01 | 0.01 |
| Mn | 0.00 | 0.00 | 0.00 | 0.00 | 0.00 | 0.00 | 0.00 | 0.00 | 0.00 | 0.00 | 0.00 | 0.00 | 0.00 | 0.00 | 0.00 | 0.00 | 0.05 | 0.05 | 0.05 | 0.05 | 0.05 | 0.05 | 0.03 | 0.03 |
| Ti | 0.01 | 0.01 | 0.01 | 0.02 | 0.02 | 0.02 | 0.03 | 0.03 | 0.03 | 0.03 | 0.03 | 0.03 | 0.03 | 0.03 | 0.03 | 0.03 | 0.15 | 0.15 | 0.15 | 0.15 | 0.15 | 0.15 | 0.15 | 0.15 |
| Mg | 0.06 | 0.06 | 0.05 | 0.06 | 0.07 | 0.07 | 0.06 | 0.07 | 0.06 | 0.06 | 0.06 | 0.06 | 0.06 | 0.06 | 0.06 | 0.07 | 0.98 | 0.96 | 0.96 | 0.95 | 0.96 | 0.94 | 0.76 | 0.76 |
| ΣY | 1.97 | 1.97 | 1.95 | 1.92 | 1.94 | 1.95 | 1.96 | 1.94 | 1.91 | 1.95 | 1.95 | 1.95 | 1.96 | 1.95 | 1.91 | 1.91 | 2.93 | 2.93 | 2.94 | 2.95 | 2.97 | 2.94 | 2.91 | 2.90 |
| K | 0.93 | 0.92 | 0.97 | 0.99 | 0.97 | 0.96 | 0.96 | 0.97 | 1.02 | 0.96 | 0.98 | 0.98 | 0.97 | 1.00 | 1.02 | 1.02 | 1.05 | 1.04 | 1.04 | 1.03 | 1.01 | 1.03 | 1.07 | 1.08 |
| Na | 0.10 | 0.10 | 0.08 | 0.09 | 0.09 | 0.09 | 0.09 | 0.09 | 0.07 | 0.09 | 0.07 | 0.07 | 0.07 | 0.05 | 0.07 | 0.07 | 0.01 | 0.01 | 0.01 | 0.01 | 0.01 | 0.01 | 0.01 | 0.01 |
| Ca | b.d | b.d | b.d | 0.00 | 0.00 | b.d | b.d | b.d | b.d | 0.00 | 0.00 | b.d | b.d | b.d | b.d | b.d | 0.00 | 0.00 | 0.00 | 0.00 | 0.00 | 0.00 | 0.00 | 0.00 |
| Rb | 0.00 | 0.00 | 0.00 | 0.00 | 0.00 | 0.00 | 0.00 | 0.00 | 0.00 | 0.00 | 0.00 | 0.00 | 0.00 | 0.00 | 0.00 | 0.00 | 0.01 | 0.01 | 0.01 | 0.01 | 0.01 | 0.01 | 0.00 | 0.00 |
| ΣX | 1.03 | 1.03 | 1.05 | 1.08 | 1.06 | 1.05 | 1.04 | 1.06 | 1.09 | 1.05 | 1.05 | 1.05 | 1.04 | 1.05 | 1.09 | 1.09 | 1.06 | 1.06 | 1.05 | 1.05 | 1.03 | 1.05 | 1.09 | 1.09 |
| mgli | 0.06 | 0.06 | 0.05 | 0.06 | 0.06 | 0.06 | 0.06 | 0.06 | 0.06 | 0.06 | 0.05 | 0.05 | 0.05 | 0.06 | 0.05 | 0.06 | 0.96 | 0.95 | 0.94 | 0.94 | 0.94 | 0.93 | 0.75 | 0.76 |
| feal | -1.48 | -1.48 | -1.46 | -1.40 | -1.43 | -1.42 | -1.40 | -1.37 | -1.37 | -1.38 | -1.44 | -1.44 | -1.46 | -1.42 | -1.45 | -1.39 | 1.68 | 1.66 | 1.62 | 1.60 | 1.58 | 1.70 | 1.25 | 1.25 |

Table 8: *continued.*

| Location | L1 Bt | | S20 Bt | | | S22 Bt | | | Leucosome Bt | | | | |
|---|---|---|---|---|---|---|---|---|---|---|---|---|---|
| Day | 1 | 1 | 1 | 1 | 1 | 1 | 1 | 1 | 2 | 2 | 2 | 2 | 2 |
| Sample Nr. | 298 | 299 | 100 | 101 | 264 | 262 | 96 | 97 | 172 | 173 | 195 | 196 | 218 |
| SiO2 | 37.7 | 37.1 | 37.4 | 37.5 | 39.2 | 38.1 | 37.2 | 37.2 | 35.4 | 35.1 | 36.0 | 36.1 | 36.0 |
| Al2O3 | 16.8 | 17.4 | 16.8 | 16.7 | 17.4 | 17.3 | 17.6 | 17.7 | 15.9 | 16.0 | 15.9 | 15.9 | 15.8 |
| K2O | 11.1 | 11.0 | 10.6 | 10.8 | 10.4 | 11.0 | 10.9 | 10.7 | 10.7 | 10.7 | 10.5 | 10.5 | 10.6 |
| Na2O | 0.1 | 0.1 | 0.1 | 0.1 | 0.1 | 0.1 | 0.1 | 0.1 | 0.0 | 0.0 | 0.0 | 0.0 | 0.0 |
| CaO | 0.0 | 0.0 | b.d | 0.0 | 0.0 | 0.0 | b.d | 0.0 | 0.0 | 0.0 | 0.0 | 0.0 | 0.0 |
| MgO | 6.6 | 6.6 | 6.9 | 6.8 | 6.7 | 7.0 | 7.2 | 7.1 | 9.0 | 9.2 | 9.0 | 9.0 | 8.9 |
| MnO | 0.4 | 0.4 | 0.4 | 0.4 | 0.3 | 0.4 | 0.4 | 0.4 | 0.5 | 0.5 | 0.5 | 0.5 | 0.5 |
| FeO | 24.1 | 24.0 | 24.1 | 24.0 | 22.8 | 23.0 | 23.5 | 23.7 | 24.9 | 24.9 | 24.6 | 24.6 | 24.6 |
| Li | 123 | 128 | 136 | 135 | 132 | 166 | 164 | 172 | 183 | 173 | 164 | 156 | 165 |
| [85]Rb | 867 | 850 | 641 | 663 | 569 | 663 | 660 | 666 | 698 | 683 | 680 | 669 | 675 |
| [86]Sr | 0 | 0 | 1 | 1 | 6 | 1 | 1 | 5 | 1 | 1 | 1 | 1 | 1 |
| Ba | 335 | 382 | 790 | 787 | 767 | 880 | 861 | 917 | 45 | 40 | 42 | 30 | 28 |
| Cs | 61 | 61 | 38 | 54 | 56 | 67 | 69 | 68 | 585 | 562 | 568 | 514 | 546 |
| Ta | 13 | 12 | 4 | 5 | 2 | 2 | 2 | 1 | 4 | 4 | 4 | 4 | 4 |
| total | 96.81 | 96.75 | 96.34 | 96.36 | 96.92 | 96.95 | 96.95 | 96.87 | 96.47 | 96.43 | 96.46 | 96.54 | 96.48 |
| Number of ions on the basis of 11 O | | | | | | | | | | | | | |
| Si | 2.89 | 2.84 | 2.87 | 2.88 | 3.00 | 2.90 | 2.84 | 2.84 | 2.69 | 2.67 | 2.74 | 2.74 | 2.74 |
| [IV]Al | 1.11 | 1.16 | 1.13 | 1.12 | 1.00 | 1.10 | 1.16 | 1.16 | 1.31 | 1.33 | 1.26 | 1.26 | 1.26 |
| ΣZ | 4.00 | 4.00 | 4.00 | 4.00 | 4.00 | 4.00 | 4.00 | 4.00 | 4.00 | 4.00 | 4.00 | 4.00 | 4.00 |
| [VI]Al | 0.41 | 0.41 | 0.39 | 0.39 | 0.56 | 0.46 | 0.42 | 0.43 | 0.12 | 0.10 | 0.17 | 0.17 | 0.16 |
| Fe | 1.55 | 1.54 | 1.55 | 1.54 | 1.46 | 1.47 | 1.50 | 1.51 | 1.59 | 1.58 | 1.57 | 1.56 | 1.57 |
| Li | 0.01 | 0.01 | 0.01 | 0.01 | 0.01 | 0.01 | 0.01 | 0.01 | 0.01 | 0.01 | 0.01 | 0.01 | 0.01 |
| Mn | 0.03 | 0.03 | 0.03 | 0.03 | 0.02 | 0.03 | 0.03 | 0.03 | 0.03 | 0.03 | 0.03 | 0.03 | 0.03 |
| Ti | 0.16 | 0.16 | 0.18 | 0.18 | 0.15 | 0.14 | 0.14 | 0.15 | 0.17 | 0.17 | 0.17 | 0.17 | 0.17 |
| Mg | 0.75 | 0.76 | 0.79 | 0.78 | 0.77 | 0.79 | 0.82 | 0.81 | 1.03 | 1.05 | 1.02 | 1.02 | 1.01 |
| ΣY | 2.90 | 2.90 | 2.94 | 2.93 | 2.97 | 2.91 | 2.92 | 2.94 | 2.94 | 2.94 | 2.97 | 2.97 | 2.95 |
| K | 1.08 | 1.08 | 1.04 | 1.06 | 1.01 | 1.07 | 1.06 | 1.04 | 1.04 | 1.04 | 1.02 | 1.02 | 1.03 |
| Na | 0.01 | 0.01 | 0.01 | 0.01 | 0.01 | 0.01 | 0.01 | 0.01 | 0.01 | 0.01 | 0.01 | 0.01 | 0.01 |
| Ca | 0.00 | 0.00 | b.d | 0.00 | 0.00 | 0.00 | b.d | 0.00 | 0.00 | 0.00 | 0.00 | 0.00 | 0.00 |
| Rb | 0.00 | 0.00 | 0.00 | 0.00 | 0.00 | 0.00 | 0.00 | 0.00 | 0.00 | 0.00 | 0.00 | 0.00 | 0.00 |
| ΣX | 1.10 | 1.09 | 1.05 | 1.07 | 1.03 | 1.09 | 1.07 | 1.06 | 1.05 | 1.05 | 1.03 | 1.03 | 1.04 |
| mgli | 0.74 | 0.75 | 0.78 | 0.77 | 0.76 | 0.78 | 0.81 | 0.80 | 1.01 | 1.03 | 1.01 | 1.01 | 1.00 |
| feal | 1.32 | 1.31 | 1.37 | 1.36 | 1.06 | 1.18 | 1.25 | 1.25 | 1.67 | 1.68 | 1.60 | 1.59 | 1.62 |

### 5.4.2. Feldspar

Together with quartz, K-feldspar is the most abundant mineral in pegmatites, it is therefore ideally suited for comparisons with other pegmatite provinces and locations. The analyzed feldspars were collected from 19 different type I and II pegmatites, always collecting one white milky and one salmon colored mineral grain if possible. A total of 16 plagioclase and 22 K-feldspar laser spots were measured. In the phase diagram for feldspars, the salmon-colored feldspars plot in the sanidine field and the milky grains plot in the albite (An: 0-10%) and oligoclase (An: 10-30%) fields. Plagioclase from type II pegmatites have an anorthite content about 10% higher than plagioclase from type I. However, a difference between Type I and II cannot be seen in the Kfsp samples.
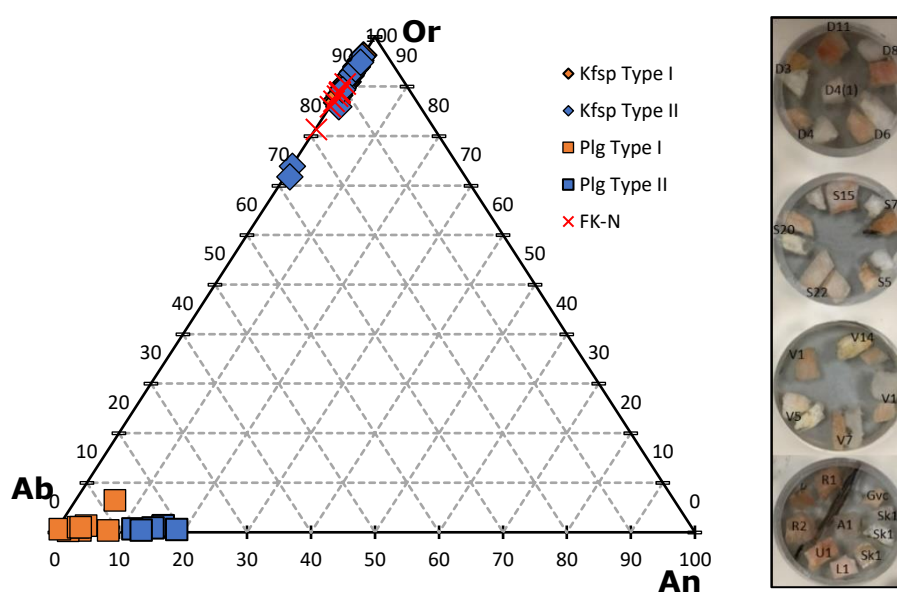


*Figure 18: Shown is the phase diagram for feldspar with plotted samples of Kfsp and Plg collected from type I and type II pegmatites, as well as the composition of FK-N standard. On the right side are all pugs for Feldspar shown, consisting of Plg (white) and Kfsp (salmon colored) from each sampled pegmatite.*

### 5.4.3. Garnet

Garnet is found exclusively in Type II pegmatites, where it occurs in clusters of 5-30 crystals, predominantly in the intermediate zone. A total of 10 garnets were cut in half and sampled from the rim to the core with a profile of 4 laser spots each. Two garnets from pegmatite D4 and D11 were sampled to see if garnets differ in composition within a pegmatite. Garnets from more highly fractionated pegmatites have a higher spessartine > almandine component, whereas garnets in less fractionated pegmatites have a higher almandine > spessartine component. Beryl occurs in D3, D4, D8 and D11 but not in V5, D6 and melt.

*Table 9: Shown are oxides, trace element concentrations and the stoichiometric mineral formula from the sampled garnets of the respective pegmatites*

| Samples | V5 core | V5 | V5 | V5 rim | D11 core | D11 | D11 | D11 rim | D8 core | D8 | D8 | D8 rim | D3 core | D3 | D3 | D3 rim | D4 core | D4 |
|---|---|---|---|---|---|---|---|---|---|---|---|---|---|---|---|---|---|---|
| SiO2 | 32.38 | 31.36 | 32.27 | 31.71 | 32.60 | 32.73 | 34.86 | 34.43 | 33.06 | 33.28 | 32.86 | 32.66 | 32.43 | 32.47 | 32.39 | 32.30 | 32.49 | 32.54 |
| Al2O3 | 18.93 | 18.88 | 18.82 | 18.83 | 18.74 | 18.63 | 18.72 | 18.71 | 18.58 | 18.49 | 18.33 | 18.47 | 18.69 | 18.67 | 18.66 | 18.99 | 18.67 | 18.83 |
| K2O | 0.00 | 0.00 | 0.00 | 0.00 | 0.00 | 0.00 | 0.00 | 0.00 | 0.01 | 0.00 | 0.00 | 0.00 | 0.00 | 0.00 | 0.00 | 0.00 | 0.00 | 0.00 |
| Na2O | 0.03 | 0.03 | 0.04 | 0.01 | 0.05 | 0.05 | 0.05 | 0.05 | 0.06 | 0.07 | 0.06 | 0.05 | 0.04 | 0.05 | 0.04 | 0.04 | 0.04 | 0.04 |
| CaO | 0.22 | 0.21 | 0.56 | 0.46 | 1.59 | 1.73 | 0.55 | 0.70 | 0.33 | 0.18 | 0.20 | 0.18 | 0.06 | 0.07 | 0.05 | 0.05 | 0.16 | 0.20 |
| MgO | 0.87 | 0.77 | 0.69 | 1.05 | 0.67 | 0.63 | 0.75 | 0.68 | 0.52 | 0.54 | 0.55 | 0.55 | 0.82 | 0.83 | 0.81 | 0.81 | 1.09 | 1.07 |
| MnO | 15.07 | 14.61 | 14.88 | 13.51 | 25.87 | 26.18 | 27.22 | 26.27 | 31.68 | 31.50 | 31.76 | 31.79 | 24.75 | 24.66 | 25.18 | 24.93 | 25.02 | 25.23 |
| FeO | 32.40 | 34.08 | 32.65 | 34.39 | 20.32 | 19.88 | 17.75 | 19.06 | 15.69 | 15.88 | 16.18 | 16.21 | 23.14 | 23.19 | 22.80 | 22.81 | 22.46 | 22.02 |
| Cr2O3 | 0.00 | 0.00 | 0.00 | 0.00 | 0.00 | 0.00 | 0.00 | 0.00 | 0.00 | 0.00 | 0.00 | 0.00 | 0.00 | 0.00 | 0.00 | 0.00 | 0.00 | 0.00 |
| TiO2 | 0.07 | 0.03 | 0.04 | 0.00 | 0.05 | 0.05 | 0.03 | 0.05 | 0.04 | 0.03 | 0.03 | 0.03 | 0.02 | 0.01 | 0.01 | 0.02 | 0.04 | 0.04 |
| ZnO | 0.00 | 0.00 | 0.01 | 0.01 | 0.01 | 0.01 | 0.01 | 0.01 | 0.01 | 0.02 | 0.02 | 0.02 | 0.02 | 0.02 | 0.02 | 0.02 | 0.01 | 0.01 |
| Y2O | 0.02 | 0.04 | 0.03 | 0.01 | 0.03 | 0.03 | 0.03 | 0.04 | 0.01 | 0.01 | 0.01 | 0.01 | 0.00 | 0.00 | 0.00 | 0.00 | 0.02 | 0.02 |
| total | 101.22 | 101.49 | 101.27 | 101.42 | 101.24 | 101.22 | 100.66 | 100.77 | 101.08 | 101.03 | 101.15 | 101.17 | 101.19 | 101.20 | 101.21 | 101.20 | 101.25 | 101.23 |
| Crystallochemical formular (apfu) based on 12 oxygen | | | | | | | | | | | | | | | | | | |
| Si | 2.69 | 2.61 | 2.68 | 2.64 | 2.70 | 2.71 | 2.88 | 2.85 | 2.75 | 2.77 | 2.73 | 2.72 | 2.69 | 2.70 | 2.69 | 2.68 | 2.70 | 2.70 |
| Al | 1.85 | 1.85 | 1.85 | 1.85 | 1.83 | 1.82 | 1.82 | 1.83 | 1.82 | 1.81 | 1.80 | 1.81 | 1.83 | 1.83 | 1.83 | 1.86 | 1.82 | 1.84 |
| Ti | 0.00 | 0.00 | 0.00 | 0.00 | 0.00 | 0.00 | 0.00 | 0.00 | 0.00 | 0.00 | 0.00 | 0.00 | 0.00 | 0.00 | 0.00 | 0.00 | 0.00 | 0.00 |
| Y | 0.00 | 0.00 | 0.00 | 0.00 | 0.00 | 0.00 | 0.00 | 0.00 | 0.00 | 0.00 | 0.00 | 0.00 | 0.00 | 0.00 | 0.00 | 0.00 | 0.00 | 0.00 |
| Cr | 0.00 | 0.00 | 0.00 | 0.00 | 0.00 | 0.00 | 0.00 | 0.00 | 0.00 | 0.00 | 0.00 | 0.00 | 0.00 | 0.00 | 0.00 | 0.00 | 0.00 | 0.00 |
| Fe | 2.25 | 2.38 | 2.27 | 2.39 | 1.41 | 1.38 | 1.23 | 1.32 | 1.09 | 1.10 | 1.13 | 1.13 | 1.61 | 1.61 | 1.58 | 1.58 | 1.56 | 1.53 |
| Mn | 1.06 | 1.03 | 1.05 | 0.95 | 1.82 | 1.84 | 1.91 | 1.84 | 2.23 | 2.22 | 2.24 | 2.24 | 1.74 | 1.74 | 1.77 | 1.75 | 1.76 | 1.77 |
| Mg | 0.11 | 0.10 | 0.09 | 0.13 | 0.08 | 0.08 | 0.09 | 0.08 | 0.06 | 0.07 | 0.07 | 0.07 | 0.10 | 0.10 | 0.10 | 0.10 | 0.13 | 0.13 |
| Ca | 0.02 | 0.02 | 0.05 | 0.04 | 0.15 | 0.16 | 0.05 | 0.07 | 0.03 | 0.02 | 0.02 | 0.02 | 0.01 | 0.01 | 0.01 | 0.00 | 0.01 | 0.02 |
| Na | 0.01 | 0.01 | 0.01 | 0.00 | 0.01 | 0.01 | 0.01 | 0.01 | 0.01 | 0.01 | 0.01 | 0.01 | 0.01 | 0.01 | 0.01 | 0.01 | 0.01 | 0.01 |
| Total Z | 4.55 | 4.47 | 4.53 | 4.48 | 4.53 | 4.53 | 4.71 | 4.67 | 4.57 | 4.58 | 4.53 | 4.53 | 4.53 | 4.53 | 4.52 | 4.54 | 4.52 | 4.54 |
| Total X | 3.44 | 3.52 | 3.46 | 3.52 | 3.45 | 3.45 | 3.28 | 3.31 | 3.42 | 3.40 | 3.45 | 3.45 | 3.46 | 3.46 | 3.46 | 3.44 | 3.47 | 3.45 |
| total | 7.99 | 7.99 | 7.99 | 8.00 | 7.98 | 7.98 | 7.98 | 7.99 | 7.98 | 7.98 | 7.98 | 7.98 | 7.98 | 7.98 | 7.98 | 7.98 | 7.99 | 7.99 |
| Endmember | | | | | | | | | | | | | | | | | | |
| Alm | 38.33 | 35.82 | 38.73 | 38.07 | 13.25 | 12.69 | 18.77 | 19.58 | 1.98 | 2.81 | 0.00 | 0.00 | 14.98 | 15.22 | 13.75 | 15.41 | 12.98 | 13.43 |
| And | 0.46 | 0.56 | 1.62 | 1.44 | 4.82 | 5.22 | 1.60 | 2.03 | 0.90 | 0.45 | 0.53 | 0.45 | 0.13 | 0.18 | 0.12 | 0.11 | 0.35 | 0.49 |
| Grs | 0.00 | 0.00 | 0.00 | 0.00 | 0.00 | 0.00 | 0.00 | 0.00 | 0.00 | 0.00 | 0.00 | 0.00 | 0.00 | 0.00 | 0.00 | 0.00 | 0.00 | 0.00 |
| Prp | 3.59 | 3.18 | 2.84 | 4.33 | 2.76 | 2.58 | 3.08 | 2.80 | 2.13 | 2.22 | 2.04 | 1.90 | 3.40 | 3.41 | 3.35 | 3.36 | 4.50 | 4.41 |
| Sps | 35.38 | 34.38 | 34.95 | 31.70 | 60.53 | 61.26 | 63.57 | 61.40 | 74.38 | 73.96 | 74.68 | 74.74 | 58.14 | 57.91 | 59.16 | 58.52 | 58.63 | 59.07 |

| Samples | D4 | D4 rim | D4´ core | D4´ | D4´ | D4´ rim | D6 core | D6 | D6 | D6 rim | D11´ core | D11´ | D11´ | D11´ rim | S15 | Melt | Melt | melt |
|---|---|---|---|---|---|---|---|---|---|---|---|---|---|---|---|---|---|---|
| SiO2 | 32.63 | 32.30 | 32.37 | 32.42 | 32.69 | 32.56 | 34.34 | 34.49 | 35.35 | 33.85 | 32.65 | 32.64 | 33.30 | 32.43 | 31.48 | 34.60 | 34.68 | 35.00 |
| Al2O3 | 18.87 | 18.84 | 18.95 | 18.84 | 18.90 | 19.15 | 20.18 | 20.16 | 20.16 | 19.96 | 19.25 | 19.11 | 19.23 | 18.88 | 18.98 | 17.77 | 17.99 | 17.79 |
| K2O | 0.00 | 0.00 | 0.00 | 0.05 | 0.04 | 0.00 | 0.00 | 0.00 | 0.07 | 0.00 | 0.00 | 0.00 | 0.00 | 0.01 | 0.00 | b.d. | 0.00 | b.d. |
| Na2O | 0.02 | 0.04 | 0.02 | 0.04 | 0.04 | 0.01 | 0.00 | 0.00 | 0.31 | 0.00 | 0.05 | 0.06 | 0.05 | 0.05 | 0.04 | 0.00 | 0.01 | 0.02 |
| CaO | 0.15 | 0.41 | 0.15 | 0.21 | 0.29 | 0.12 | 10.16 | 9.98 | 9.86 | 10.33 | 1.09 | 0.56 | 1.63 | 0.50 | 0.18 | 0.33 | 0.39 | 0.34 |
| MgO | 1.11 | 0.98 | 0.45 | 0.44 | 0.48 | 0.59 | 0.29 | 0.29 | 0.28 | 0.29 | 0.69 | 0.71 | 0.62 | 0.66 | 0.81 | 1.44 | 1.39 | 1.34 |
| MnO | 23.93 | 25.14 | 28.81 | 28.95 | 28.30 | 27.34 | 13.12 | 13.26 | 12.88 | 13.64 | 26.62 | 26.70 | 25.62 | 26.58 | 27.15 | 22.74 | 22.74 | 22.67 |
| FeO | 23.15 | 22.17 | 19.17 | 18.99 | 19.18 | 20.17 | 21.87 | 21.79 | 21.05 | 21.89 | 19.52 | 20.13 | 19.45 | 20.61 | 21.25 | 22.98 | 22.69 | 22.71 |
| Cr2O3 | 0.00 | 0.00 | 0.00 | 0.00 | 0.00 | 0.00 | 0.00 | 0.00 | 0.00 | 0.00 | 0.00 | 0.00 | 0.00 | 0.00 | 0.00 | 0.00 | 0.00 | 0.00 |
| TiO2 | 0.06 | 0.06 | 0.04 | 0.03 | 0.03 | 0.02 | 0.01 | 0.01 | 0.01 | 0.01 | 0.06 | 0.05 | 0.04 | 0.05 | 0.06 | 0.05 | 0.08 | 0.07 |
| ZnO | 0.01 | 0.01 | 0.01 | 0.00 | 0.00 | 0.01 | 0.00 | 0.00 | 0.00 | 0.00 | 0.01 | 0.01 | 0.01 | 0.01 | 0.00 | 0.03 | 0.02 | 0.03 |
| Y2O | 0.00 | 0.01 | 0.01 | 0.00 | 0.00 | 0.00 | 0.02 | 0.03 | 0.03 | 0.03 | 0.03 | 0.04 | 0.04 | 0.03 | 0.00 | 0.01 | 0.00 | 0.01 |
| total | 101.17 | 101.27 | 101.19 | 101.14 | 101.08 | 101.12 | 100.87 | 100.84 | 100.67 | 101.02 | 101.17 | 101.17 | 101.02 | 101.02 | 101.43 | 100.81 | 100.78 | 100.70 |

Crystallochemical formular (apfu) based on 12 oxygen

| | D4 | D4 rim | D4´ core | D4´ | D4´ | D4´ rim | D6 core | D6 | D6 | D6 rim | D11´ core | D11´ | D11´ | D11´ rim | S15 | Melt | Melt | melt |
|---|---|---|---|---|---|---|---|---|---|---|---|---|---|---|---|---|---|---|
| Si | 2.70 | 2.68 | 2.69 | 2.70 | 2.72 | 2.71 | 2.78 | 2.79 | 2.85 | 2.74 | 2.70 | 2.71 | 2.75 | 2.69 | 2.62 | 2.87 | 2.87 | 2.90 |
| Al | 1.84 | 1.84 | 1.86 | 1.85 | 1.85 | 1.88 | 1.92 | 1.92 | 1.91 | 1.91 | 1.88 | 1.87 | 1.87 | 1.85 | 1.86 | 1.73 | 1.75 | 1.74 |
| Ti | 0.00 | 0.00 | 0.00 | 0.00 | 0.00 | 0.00 | 0.00 | 0.00 | 0.00 | 0.00 | 0.00 | 0.00 | 0.00 | 0.00 | 0.00 | 0.01 | 0.00 | 0.01 |
| Y | 0.00 | 0.00 | 0.00 | 0.00 | 0.00 | 0.00 | 0.00 | 0.00 | 0.00 | 0.00 | 0.00 | 0.00 | 0.00 | 0.00 | 0.00 | 0.00 | 0.00 | 0.00 |
| Cr | 0.00 | 0.00 | 0.00 | 0.00 | 0.00 | 0.00 | 0.00 | 0.00 | 0.00 | 0.00 | 0.00 | 0.00 | 0.00 | 0.00 | 0.00 | 0.00 | 0.00 | 0.00 |
| Fe | 1.60 | 1.54 | 1.33 | 1.32 | 1.33 | 1.40 | 1.48 | 1.47 | 1.42 | 1.48 | 1.35 | 1.40 | 1.34 | 1.43 | 1.48 | 1.59 | 1.57 | 1.57 |
| Mn | 1.68 | 1.77 | 2.03 | 2.04 | 1.99 | 1.92 | 0.90 | 0.91 | 0.88 | 0.94 | 1.87 | 1.87 | 1.79 | 1.87 | 1.91 | 1.59 | 1.59 | 1.59 |
| Mg | 0.14 | 0.13 | 0.06 | 0.06 | 0.06 | 0.08 | 0.04 | 0.04 | 0.04 | 0.04 | 0.09 | 0.09 | 0.08 | 0.09 | 0.11 | 0.18 | 0.17 | 0.17 |
| Ca | 0.01 | 0.04 | 0.01 | 0.02 | 0.03 | 0.01 | 0.88 | 0.87 | 0.85 | 0.90 | 0.10 | 0.05 | 0.14 | 0.04 | 0.02 | 0.03 | 0.03 | 0.03 |
| Na | 0.00 | 0.01 | 0.00 | 0.01 | 0.01 | 0.00 | 0.00 | 0.00 | 0.05 | 0.00 | 0.01 | 0.01 | 0.01 | 0.01 | 0.01 | 0.00 | 0.00 | 0.00 |
| Total Z | 4.55 | 4.52 | 4.55 | 4.55 | 4.57 | 4.58 | 4.70 | 4.71 | 4.76 | 4.65 | 4.58 | 4.57 | 4.62 | 4.54 | 4.48 | 4.60 | 4.62 | 4.63 |
| Total X | 3.44 | 3.47 | 3.44 | 3.44 | 3.42 | 3.41 | 3.30 | 3.29 | 3.18 | 3.35 | 3.40 | 3.41 | 3.36 | 3.43 | 3.51 | 3.40 | 3.38 | 3.37 |
| total | 7.99 | 7.99 | 7.99 | 7.99 | 7.99 | 7.99 | 8.00 | 8.00 | 7.94 | 8.00 | 7.98 | 7.98 | 7.99 | 7.97 | 7.98 | 8.00 | 8.00 | 8.00 |

Endmember %

| | D4 | D4 rim | D4´ core | D4´ | D4´ | D4´ rim | D6 core | D6 | D6 | D6 rim | D11´ core | D11´ | D11´ | D11´ rim | S15 | Melt | Melt | melt |
|---|---|---|---|---|---|---|---|---|---|---|---|---|---|---|---|---|---|---|
| Alm | 16.63 | 12.91 | 8.07 | 7.49 | 10.09 | 12.41 | 32.07 | 32.68 | 32.87 | 29.10 | 13.78 | 13.08 | 18.69 | 12.12 | 6.66 | 20.87 | 22.36 | 23.16 |
| And | 0.26 | 1.01 | 0.33 | 0.53 | 0.76 | 0.30 | 7.49 | 7.39 | 3.55 | 9.08 | 3.05 | 1.52 | 4.68 | 1.33 | 0.34 | 0.71 | 0.92 | 0.76 |
| Grs | 0.00 | 0.00 | 0.00 | 0.00 | 0.00 | 0.00 | 21.82 | 21.42 | 24.79 | 20.75 | 0.00 | 0.00 | 0.00 | 0.00 | 0.00 | 0.00 | 0.00 | 0.00 |
| Prp | 4.81 | 4.24 | 1.94 | 1.93 | 2.10 | 2.57 | 1.22 | 1.23 | 1.18 | 1.22 | 3.00 | 3.07 | 2.70 | 2.87 | 3.51 | 5.94 | 5.73 | 5.52 |
| Sps | 56.02 | 58.89 | 67.74 | 68.09 | 66.49 | 64.17 | 29.97 | 30.29 | 29.30 | 31.20 | 62.22 | 62.50 | 59.78 | 62.44 | 63.75 | 53.15 | 53.10 | 53.00 |
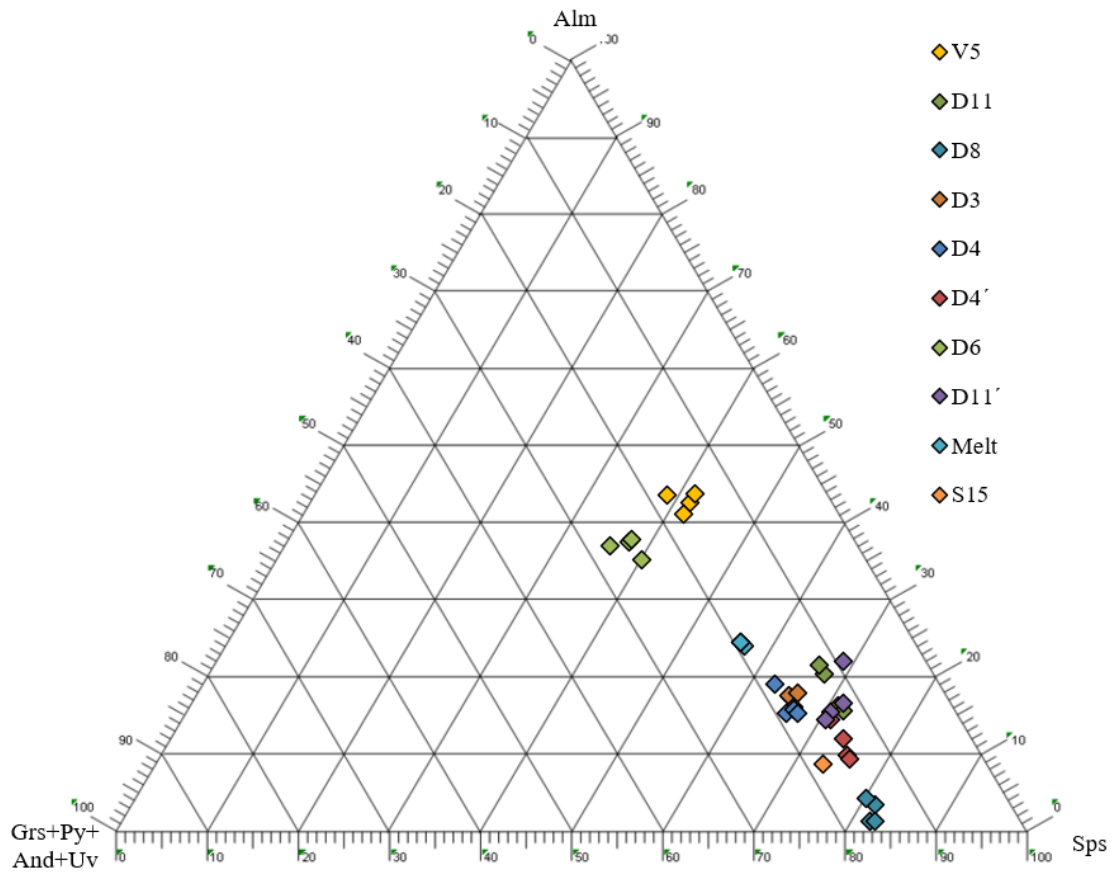
*Figure 19: Ternary diagram for the Alm—Sps—(Grs-And -Uv + Prp) proportions with major garnet end-members.*

Garnets from pegmatite V5 and D6, which do not have beryl, have the highest almandine component (see figure 19). Three spots were measured on three different crystals within the melt sample. The sampled garnet from pegmatite D6 shows an unusually high concentration of CaO (>9%; see Table 9). However, the signal is homogeneous and does not indicate inclusions within the garnet crystal, which would lead to an increased Ca concentration. The highest proportions in spessartine (Sps>0.68) are shown by garnets from the fractionated pegmatites D8, D11 and D4.

## 5.5. Fractionation of incompatible elements

### 5.5.1. Mica

To study the incompatible trace element enrichment in the samples, as well as the impact of the degree of fractionation on our results, the potential correlations between various incompatible elements are investigated. Plotting Ba/Rb versus Rb/Sr for Type I and II pegmatites as well as for mica grains from leucosomes provides a fractionation trend between these three sample types, where Sk1, D3 and D8 (all Type II) show to be the most fractionated samples with Rb/Sr ranging from 1300- 15400 and Ba/Rb ratio

ranging between 0.0009-0.045 (see figure 20). On the opposite side are the more primitive type I barren show Rb/Sr ratios of 20-300 and Ba/Rb ratios of 0.053 to 2.384. Leucosome muscovites have an even higher Ba/Rb ratio of 1.45-2.86. Between the Ba/Rb ratio of 0.1 and 0.01 pegmatites of both types are found with a Rb/Sr ratio of 34 to 3724. From a Ba/Rb ratio of < 0.1 only muscovite samples of type II are found, where Sk1, R1, S15, D3 and D8 are the highest fractionated pegmatites with the lowest Ba/Rb ratio of 0.0009 (Type II; D8). To ensure comparability, in addition to the samples from this study, 32 sample spots on a Högsbo-Ms standard have been included, which have Ba/Rb ratios of 0.00031 to 0.00165 an Rb/Sr ratio of 3100-7100.
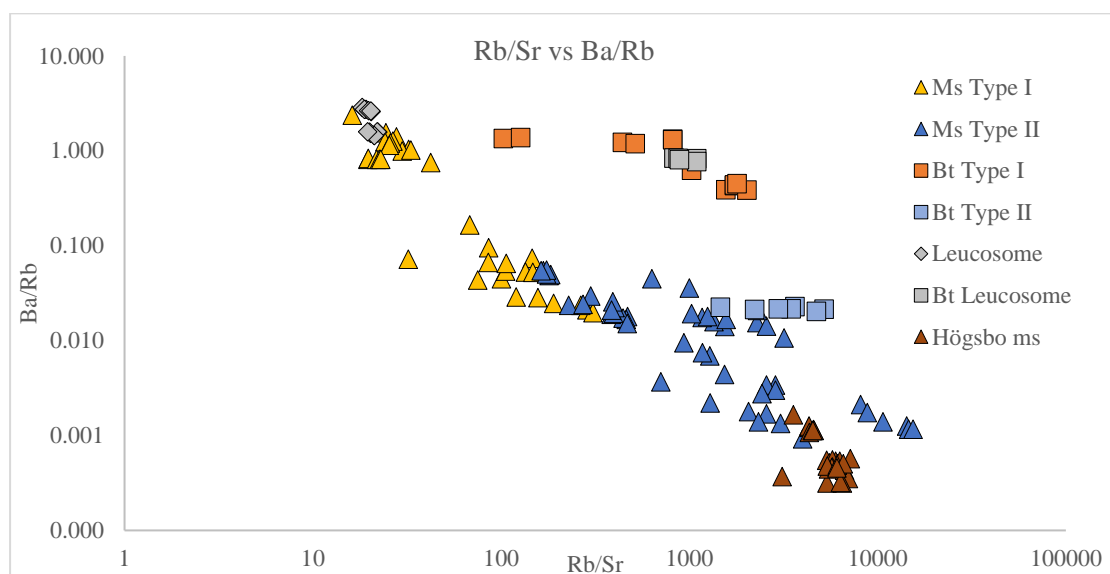


*Figure 20: Shown are ratios of Rb/Sr to Ba/Rb in muscovite and biotite from Type I and Type II pegmatites, as well as from leucosomes of the SLM Fm. For comparison of a strongly fractionated pegmatite, the Högsbo ms is additionally presented. The Rb/Sr ratio is calculated from the $^{85}Rb$ and $^{86}Sr$ isotopes.*

The K/Rb ratio in micas is commonly used as an indicator of pegmatite melt fractionation and evolution (Černý et al. 1985). In figure 21 Li, Ba, Ta, and Cs from all measured muscovite samples are plotted against K/Rb. The K/Rb ratio decreases with increasing fractionation to ~ 50 in the Donsö pegmatites and shows a maximum in the leucosome and Type I samples of ~ 300. Lithium does not fractionate in type I and type II muscovites, nor in biotite samples from type I and type II pegmatites. Rather, lithium is slightly depleted in the pegmatite samples, compared to the leucosome samples. Lithium concentration in muscovites from type I and II ranges from 6-80 ppm, while Li concentration from leucosome muscovites is around 70 ppm. Biotite exhibits consistent Li concentration in pegmatite and leucosome. Barium, on the other hand, fractionates strongly between leucosome, type I and type II pegmatite. The higher the fractionation

degree, the less Ba has been measured in the mica. Ba concentrations in Leucosome Muscovite samples range from 600-1140 ppm, type I pegmatites have 12- 839 ppm Ba, and type II pegmatites have 2-70 ppm Ba. Ta and Cs fractionate similarly between leucosome, type I and type II pegmatites from ~ 10 ppm in type I and leucosome muscovites to a maximum of 118 ppm Ta and 225 ppm Cs in type II pegmatites (highest in D3). Figure 22 shows only muscovite samples from type II pegmatites. If Ba/Rb and K/Rb represent the fractionation of incompatible elements most sensitively (Taylor 1963, Cherny, 1985), D3 and Sk1 are the highest fractionated sampled pegmatites in this study. The similar K/Rb ratios of D3 and D8 (~60), of R1 and S15 (~95) or D4 and D6 (~145) are noticeable. Thus, the presence of beryl is not an indicator of higher fractionation, as Sk1, R1 and D6 do not have beryl.
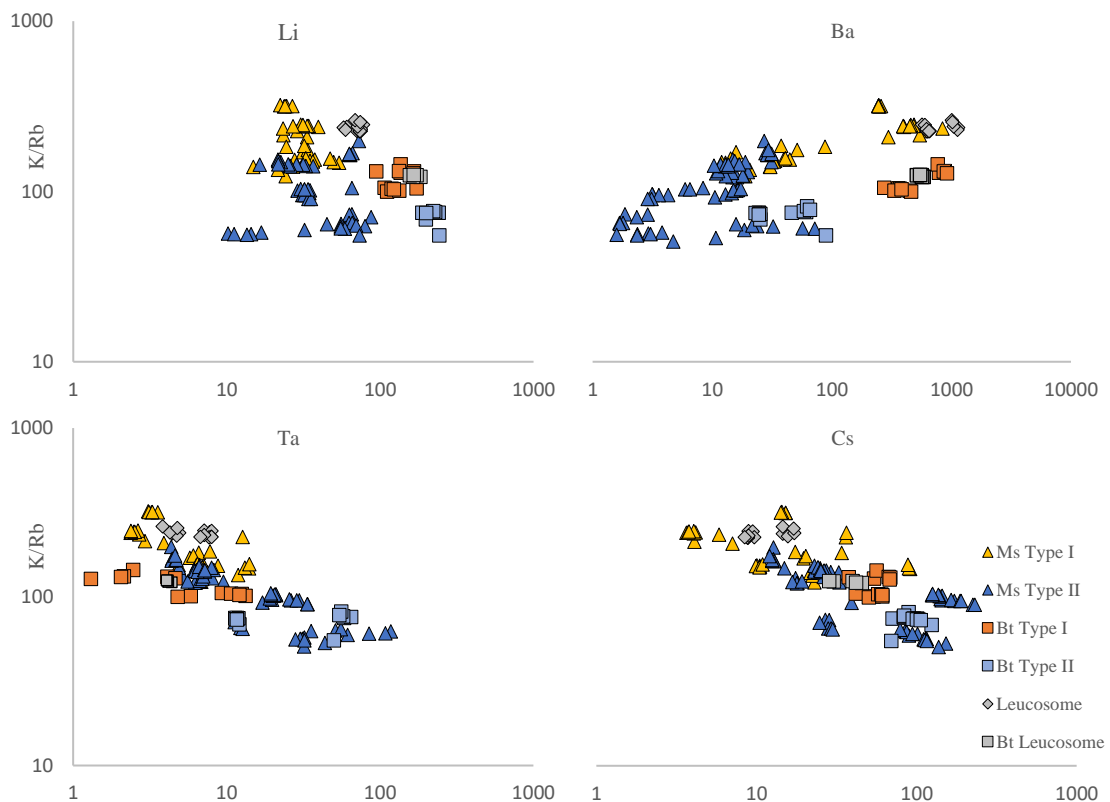


*Figure 21: Li, Ba, Ta and Cs concentrations in muscovite and biotite of type I and type II pegmatites, as well as of leucosomes samples plotted against K/Rb.*
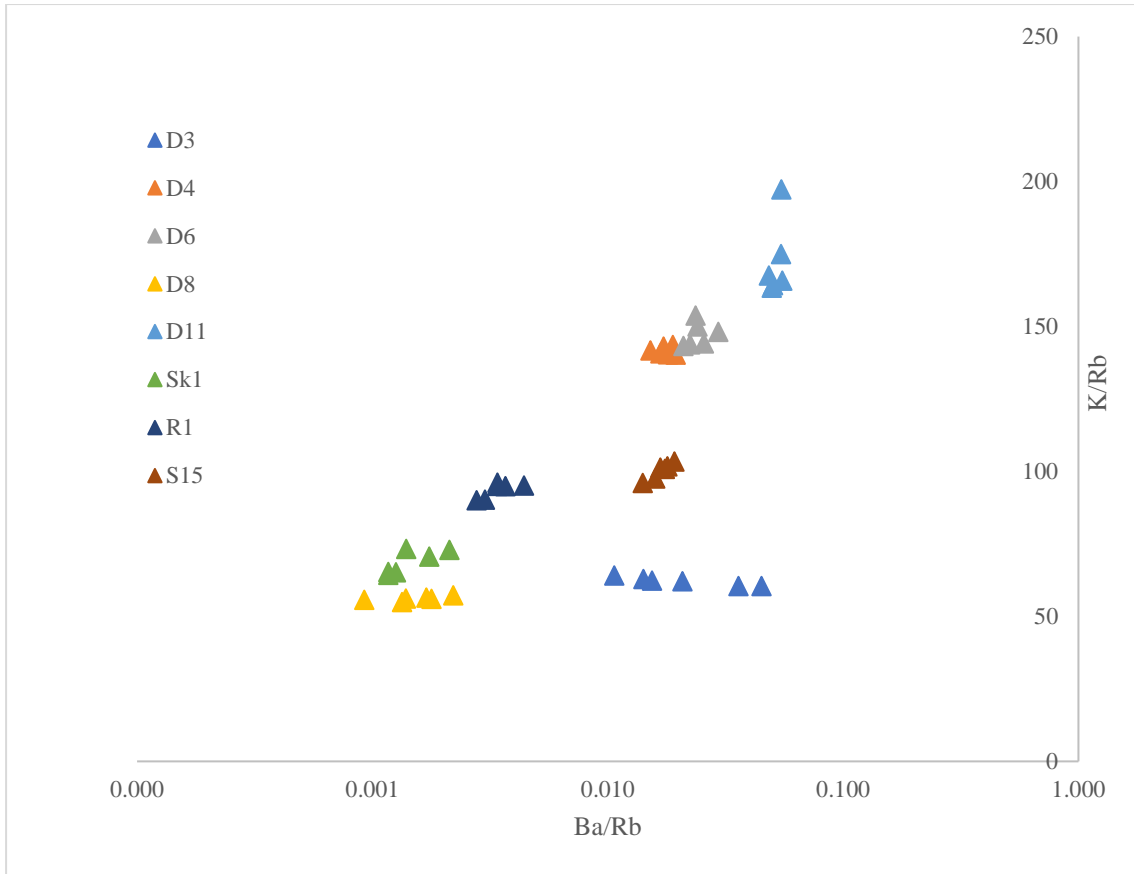
*Figure 22: Ba/Rb ratio plotted against K/Rb of highest fractionated pegmatites in muscovite samples.*

### 5.5.2. Garnet

Within the studied garnets, the Fe/Mn ratio decreases, the iron and magnesium content decreases, and the manganese content increases due to the increasing fractionation of the pegmatite melt. Garnets from pegmatites from the island of Donsö (D3, D4, D8 and D11), the garnet from pegmatite S15 and garnets within the melt show a significantly increased Mn concentration compared to garnets from pegmatite V5 and D6 (see figure 24).
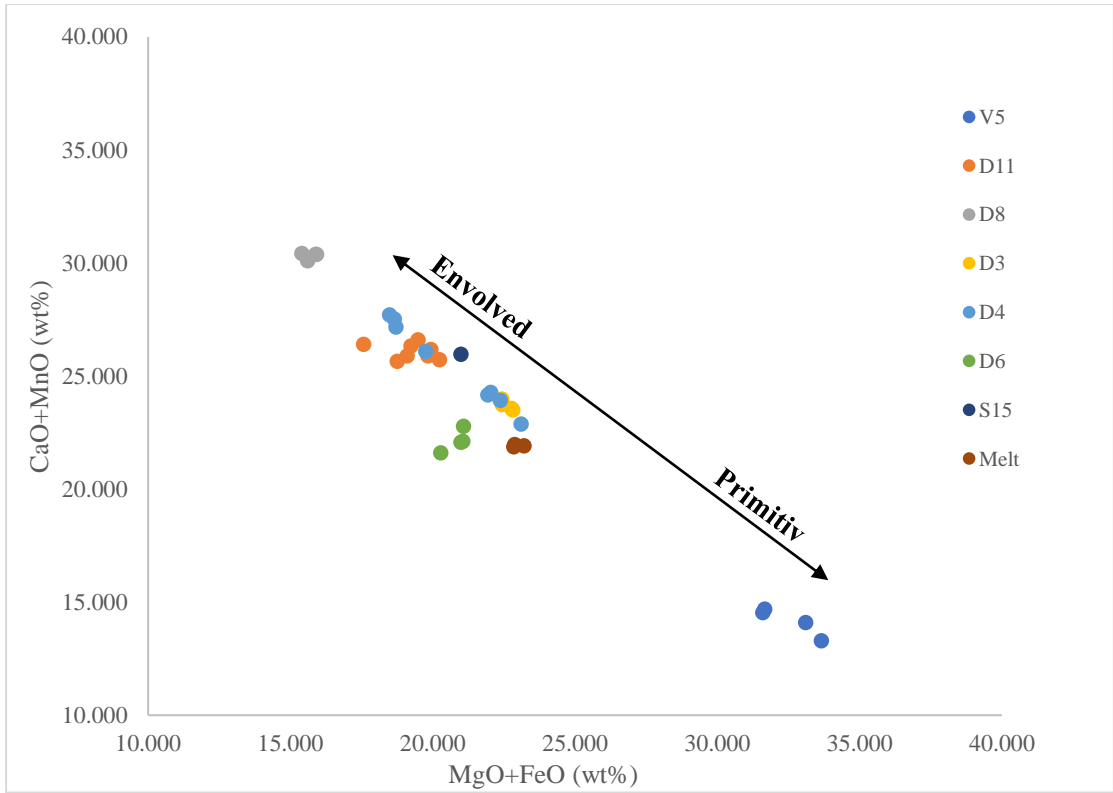
*Figure 23: Shown is the oxide composition from MgO+FeO (wt%) to CaO+MnO (wt%) of the sampled garnets from Type II pegmatites and the melt within the SLM Fm.*
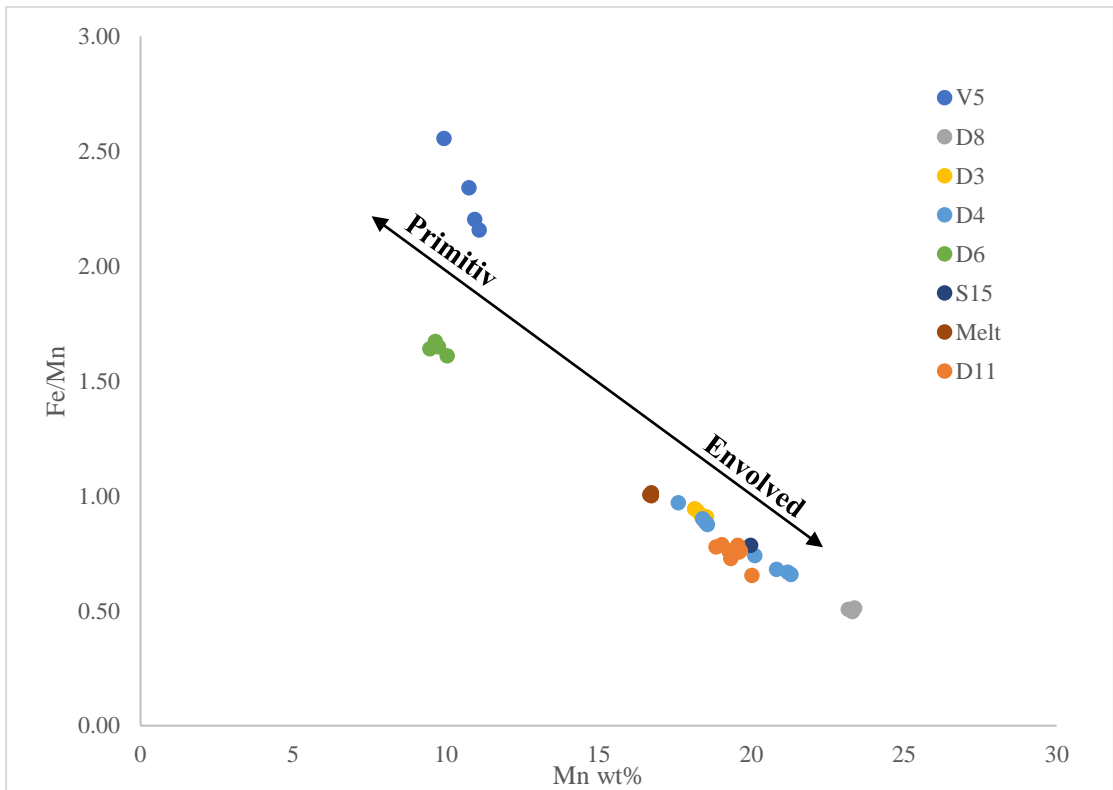


*Figure 24: The Mn wt% concentration is plotted against the Fe/Mn ratio in garnets of the sampled Type II pegmatites and the melt within the SLM Fm.*

### 5.5.3 Comparison of LA-ICP-MS and pXRF data on K-feldspar

Comparing the results of the pXRF analysis on Kfsp measured in the field with the LA-ICP-MS data obtained in the laboratory shows that the ratios (e.g. Rb/Sr) and concentrations (e.g. Ba ppm) show a clear difference between fractionated and primitive pegmatites, especially over the amount of analysis points. In figure 25 the pXRF data were compared with the LA-ICP-MS data and two highlighted pegmatites (Type I: Langholmen and Type II Skeppstadsholmen). It is important to note that the Kfsp grains measured by pXRF in field do not always correspond to the K-feldspars sampled in the laboratory and thus the comparison is between randomly distributed mineral grains within the pegmatite bodies.
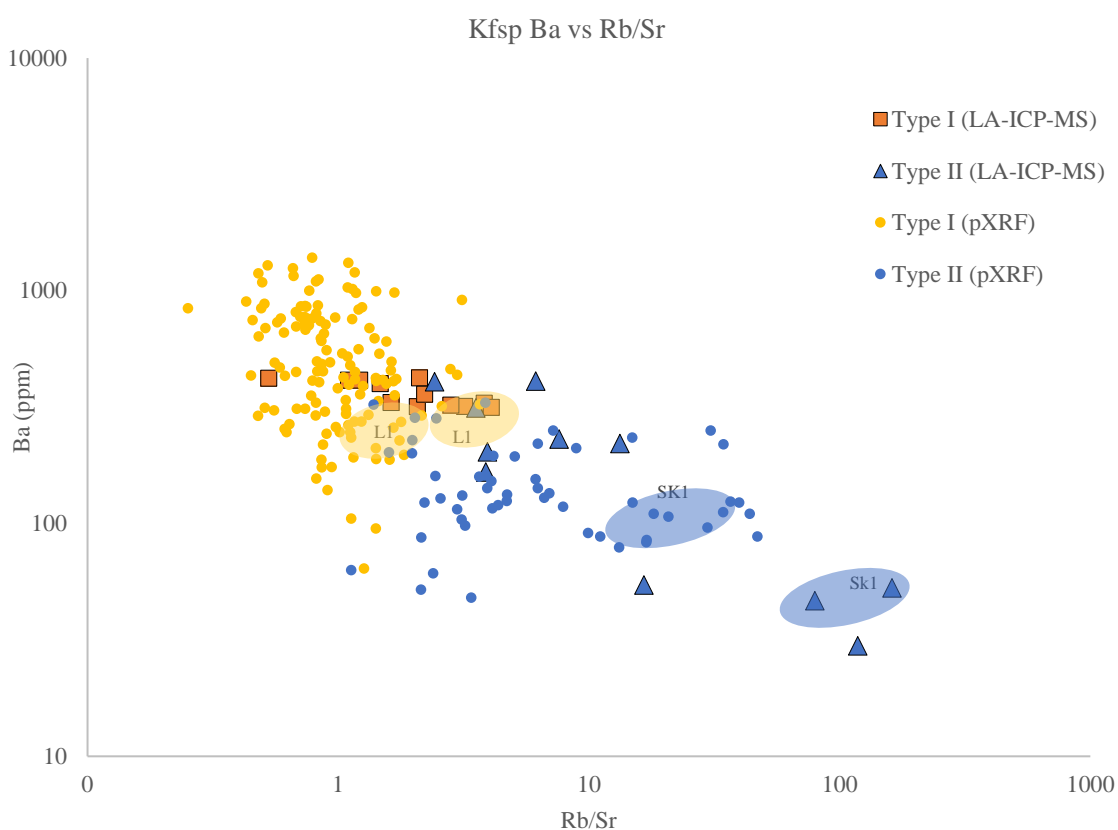


*Figure 25: Shown is the comparison of Ba vs Rb/Sr from pXRF field data with LA-ICP-MS data measured in the laboratory for all Type I and II pegmatites. Highlighted are two pegmatites: Sk1 and L1 for direct comparison. The exact data of the two pegmatites can be found in table 10.*

*Table 10: Comparison of pXRF and LA-ICP-MS data based on pegmatite Sk1 and L1*

| Skeppstad-sholmen pXRF | K (wt%) | Rb (ppm) | Sr (ppm) | Ba (ppm) | Rb/Sr | Ba vs Rb/Sr | K vs Rb/Sr |
|---|---|---|---|---|---|---|---|
| 1 | 8.62 | 551 | 18 | 110 | 31 | 3.59 | 0.28 |
| 2 | 9.54 | 544 | 30 | 110 | 18 | 6.07 | 0.53 |
| 3 | 9.74 | 658 | 15 | 112 | 44 | 2.55 | 0.22 |
| 4 | 9.1 | 619 | 18 | 96 | 34 | 2.79 | 0.26 |
| 5 | 8.54 | 684 | 23 | 124 | 30 | 4.17 | 0.29 |
| 6 | 9.23 | 515 | 14 | 88 | 37 | 2.39 | 0.25 |
| 7 | 7.8 | 471 | 10 | 120 | 47 | 2.55 | 0.17 |
| X̄ | *9* | *577* | *18* | *109* | *34* | *3.44* | *0.29* |
| **LA-ICP-MS** | | | | | | | |
| 1 | 11.54 | 779 | 10 | 47 | 80 | 0.59 | 0.14 |
| 2 | 16.94 | 1049 | 6 | 53 | 162 | 0.33 | 0.10 |
| X̄ | *14* | *914* | *8* | *50* | *121* | *0.46* | *0.12* |
| **Langholmen pXRF** | | | | | | | |
| 1 | 9.55 | 295 | 168 | 290 | 1.76 | 165.15 | 5.44 |
| 2 | 7.89 | 274 | 236 | 311 | 1.16 | 267.87 | 6.81 |
| 3 | 8.13 | 206 | 132 | 243 | 1.56 | 155.71 | 5.21 |
| 4 | 8.28 | 193 | 116 | 247 | 1.66 | 148.46 | 4.98 |
| 5 | 8 | 267 | 218 | 468 | 1.22 | 382.11 | 6.53 |
| 6 | 8.94 | 272 | 200 | 227 | 1.36 | 166.91 | 6.57 |
| X̄ | *8* | *251* | *178* | *298* | *1* | *214.37* | *5.92* |
| **LA-ICP-MS** | | | | | | | |
| 1 | 16.04 | 487 | 127 | 241 | 3.83 | 62.93 | 4.19 |
| 2 | 14.98 | 474 | 116 | 293 | 4.07 | 71.83 | 3.68 |
| X̄ | *16* | *480* | *122* | *267* | *4* | *67.38* | *3.93* |

Table 10 shows that potassium in K-feldspar is detected by pXRF at < 10 wt%, while potassium is measured at ~ 14 wt% by the ICP-MS. The same can be seen for rubidium, which results in higher Rb/Sr ratios in the ICP-MS measurements. Barium concentrations are relative consistent between the two instruments.

## 5.6. Geochronology

*Day 1 (211217)*

On the first day muscovite, biotite, K-feldspar and Plagioclase samples from the locations: Langholmen, Styrsö, Rivö, Skeppstadsholmen and Leucosome from the SLM were analyzed. The Mica-Mg nanopowder standard of Hogmalm et al. (2017) was used as an internal primary standard, as well as secondary muscovite and biotite standards with documented literature ages, such as Mica-Fe, Högsbo-Ms, La-Posta Bt, McClure-Bt, and Wilson Prom.-Bt (see Table 11). The results of the isotopic data measurement are summarized in Table 11 and consist of the amount of analysis per standard, the used initial $^{87}Sr/^{86}Sr$ ratio, the range of Rb and Sr mass fractions, as well as ratios for $^{87}Rb/^{86}Sr$ and $^{87}Sr/^{86}Sr$. The single spot 2s precision (random uncertainties) for the $^{87}Rb/^{86}Sr$ and $^{87}Sr/^{86}Sr$ ratios are also reported. The weighted mean (2s) represents the age of all individual spots combined. As $^{87}Sr/^{87}Rb$ is determined simultaneously with

$^{87}$Rb/$^{86}$Sr and $^{87}$Sr/$^{86}$Sr, it is possible to calculate the error correlation coefficient for each analysis (Schmitz & Schoene, 2007). All micas investigated in this study are less likely to be affected to P/A issues, as they have high Rb mass fractions, with analysis of $^{85}$Rb in analogue mode. All analyses of standard samples and samples from the pegmatites presented in this study were taken from a single muscovite/biotite grain, except for D4 and D11 Ms with two grains (Day 2). The laser spots were placed in different areas along the crystal for each measurement session. Since a precise initial $^{87}$Sr/$^{86}$Sr ratio is assumed to be negligible at extreme $^{87}$Rb/$^{87}$Sr ratios, the initial $^{87}$Sr/$^{86}$Sr ratio of $0.715 \pm 0.015$ (typical for enriched magmatic rocks) from Rösel & Zack, 2022 was used in this study.

*Table 11: Calculated ages of Mica-Mg, Mica-Fe, Högsbo-Ms, La Posta-Bt, McClure-Bt and Wilson Prom.-Bt reported in other studys compared with data from this study ensure the accuracy of our data.*

| Standard | Mica-Mg | Mica-Fe | Högsbo-Ms | La Posta Bt | McClure Bt | Wilsons Prom. Bt |
|---|---|---|---|---|---|---|
| Published ages (in Ma) | $519.4 \pm 6.5$[1] | $307.6 \pm 0.4$[2] | $1029 \pm 1.7$[3] $1037 \pm 11$[1] | $91.6 \pm 1.2$[1] | $523.98 \pm 0.12$[4] $523.26 \pm 1.27$[4] $523.51 \pm 2.09$[4] $523.2 \pm 1.8$[5] | $395 \pm 4$[6] $391 \pm 14$[7] |
| Initial $^{87}$Sr/$^{86}$Sr | $0.72607 \pm 0.0007$ | $0.72607 \pm 0.0007$ | $0.72000 \pm 0.0001$ | $0.7063 \pm 0.0012$ | $0.70369 \pm 0.00002$ | - |
| **Results in this study** | | | | | | |
| *n* | 24 | 9 | 24 | 7 | 8 | 8 |
| Rb (ppm) | 1393-1476 | 2294-2546 | 4002-4155 | 356-528 | 597-659 | 1132-1352 |
| Sr (ppm) | 25-27 | 0.2-0.4 | 0.6-1.3 | 1.0-37 | 2.2-4.2 | 0.4-12 |
| Initial $^{87}$Sr/$^{86}$Sr | 0.72607 | 0.72607 | 0.72 | 0.7063 | 0.70369 | 0.715 |
| $^{87}$Rb/$^{86}$Sr (2s) | $154.76 \pm 0.6$ | $24900 \pm 2100$ | $18210 \pm 700$ | $440 \pm 180$ | $550 \pm 88$ | $2500 \pm 2000$ |
| f$^{87}$Sr (mean) | 39% | 0.7% | 0.3% | 43% | 14% | 7% |
| $^{87}$Sr/$^{86}$Sr (2s) | $1.85 \pm 0.002$ | $107.9 \pm 9.2$ | $265 \pm 11$ | $1.34 \pm 0.27$ | $4.63 \pm 0.7$ | $15 \pm 11$ |
| Weighted mean (2s) | $519.4 \pm 2.2$ | $307.5 \pm 1.1$ | $1037 \pm 1.3$ | $92.0 \pm 1.9$ | $523.1 \pm 2.6$ | $393.6 \pm 2.3$ |
| MSWD | 0.81 | 0.22 | 0.031 | 1.7 | 0.38 | 0.55 |

(Rb-Sr ms nano-powder)[1], (Ar-Ar biotite)[2], (Pb-Pb Mn-columbite)[3], (compiled age)[1], (U-Pb zircon)[4,6], (U-Pb titanite)[4], (U-Pb apatite)[4], (Ar-Ar hornblende)[5], (K-Ar Biotite)[7] [1]Hogmalm et al. (2017); [2]Grove & Harrison (1996); [3]Romer & Smeds (1994); [1]Zack & Hogmalm (2016), [4]Schoene & Bowring (2006), [5]Spell & McDougall (2003), [6]Elburg (1996), [7]Richards & Singleton (1981)

Table 11 shows the used standards with the $^{87}$Sr/$^{87}$Rb ages established in this study. Comparing the ages obtained from this study with the ages from previous studies, a high equivalency can be observed in all standards. Due to this high precision and a repetitive measurement sequence between standards and samples (8 standards - 10

samples - 8 standards - etc.), it can be assumed that the calculated weighted mean (2s) ages of the pegmatite samples are also very precise.

*Table 12: Calculated ages of Muscovites and Biotites from sampled Pegmatites.*

| Sample | S22 | S22_bt | SK1 | R1 | R2 | L1 | L1_bt | S15 | Leuco ms |
|---|---|---|---|---|---|---|---|---|---|
| *n* | 3 | 3 | 6 | 4 | 5 | 3 | 4 | 6 | 8 |
| Rb (ppm) | 605-604 | 660-666 | 1335-1444 | 857-1037 | 601-622 | 527-762 | 834-867 | 899-917 | 380-426 |
| Sr (ppm) | 2.0-2.3 | 0.8-5.2 | 0.1-0.2 | 0.3-1.4 | 4-7 | 4-9 | 0.4-0.5 | 0.6-0.8 | 17-22 |
| Initial $^{87}Sr/^{86}Sr$ | 0.715 | 0.715 | 0.715 | 0.715 | 0.715 | 0.715 | 0.715 | 0.715 | 0.715 |
| $^{87}Rb/^{86}Sr$ (2s) | 801 ± 54 | 1300 ± 1000 | 29500 ± 7700 | 5400 ± 1200 | 299 ± 61 | 340 ± 95 | 5560 ± 290 | 3540 ± 460 | 56 ± 2 |
| $f^{87}Sr$ (mean) | 3.9% | 2.4% | 0.01% | 0.5% | 9% | 7% | 0.1% | 0.8% | 7% |
| $^{87}Sr/^{86}Sr$ (2s) | 18.3 ± 1.2 | 20 ± 13 | 650 ± 170 | 120 ± 26 | 6.8 ± 1.2 | 8.2 ± 2 | 77 ± 3.5 | 78 ± 10 | 1.94 ± 0.05 |
| Weighted mean (2s) | 1557 ± 10 | 950 ± 0.7 | 1552 ± 0.9 | 1549 ± 1.4 | 1556 ± 6.5 | 1553 ± 5.4 | 968 ± 4.3 | 1552 ± 1.5 | 1552 ± 5.2 |
| MSWD | - | - | 0.005 | - | 0.2 | - | - | 0.014 | 0.21 |

The samples presented in *Table 12* are muscovite and biotite (bt) grains from the respective pegmatites, barren and leucosomes. Rb mass fraction ranges from 527 ppm to 1444 ppm (or >1500000 cps), resulting in the Mica-Mg standard being used as the primary internal standard here as well. The common $^{86}Sr$, used here as a proxy for the total common Sr fraction, ranges between 0.1-9 ppm in the pegmatite micas and between 17 and 19 ppm in the leucosome muscovite. The radiogenic $^{87}Sr$ constitutes for >90%, majority >99%, of the present strontium (see $f^{87}Sr$, table 12). The $^{87}Sr/^{87}Rb$ ages for muscovite from pegmatites S22, Sk1, R1, R2, L1 and S15, which include type 1 and 2 pegmatites, give a minimum weighted mean cooling age of 1549 ± 1.4 Ma 2s (R1) and a maximum of 1557 ± 10 Ma 2s (S22). The average cooling age for all pegmatites is 1553 ± 4.8 Ma 2s. The calculated MSWD is <1 for all samples (only possible with n>5). The $^{87}Sr/^{87}Rb$ ages determined for biotite from pegmatites S22 and L1 give a weighted mean cooling age of 950 ± 0.7 Ma 2s ($^{87}Sr/^{87}Rb$ = 0.01323-0.01352) for S22 and 968 ± 4.3 Ma 2s ($^{87}Sr/^{87}Rb$ = 0.01342-0.01388) for L1. The $^{87}Sr/^{87}Rb$ age for muscovite from Leuscome sample gives a cooling age of 1552 ± 5.2 Ma 2s with an MSWD of 0.21 and a much lower $^{87}Rb/^{86}Sr$ (2s) of 56 ± 2 compared to the Muscovites from the pegmatites. Isochron calculation from 45 spots on muscovites from pegmatite: L1, S22, S15, R1, R2 and Sk1 yields an initial $^{87}Sr/^{86}Sr$ ratio of 0.713 ± 0.015 and an age of 1556 ± 14.9 1s Ma with a low MSWD of 0.033 (see figure 26).
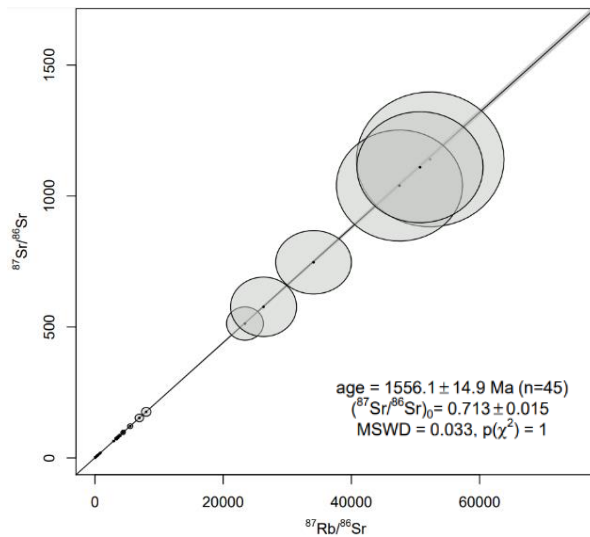
*Figure 26: Isochron plot from day 1 analyses showing the 45 muscovite analyses from pegmatite L1, S5, S22, S15, R1, R2 and Sk1.*
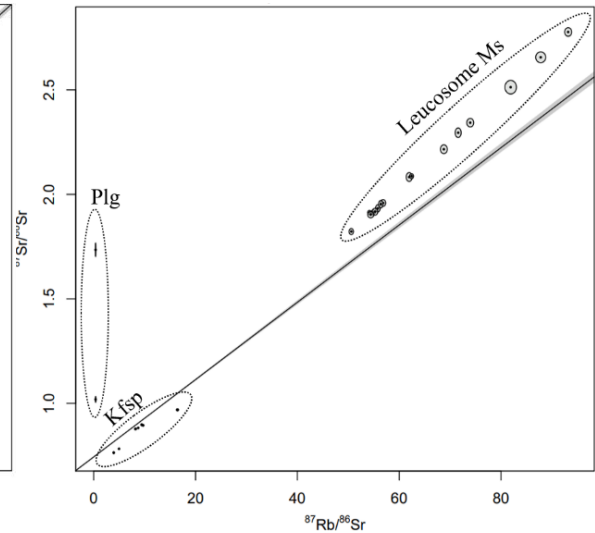
*Figure 27: Isochron plot from day 1 showing the Leucosome and S5 muscovite together with 8 Kfsp and 3 Plg analyses.*

Figure 27 shows 8 spots (2 per grain) on K-feldspar from pegmatite L1, R1, R2 and Sk1 and 3 spots from pegmatite Sk1 on plagioclase together with Leucosome and S5 muscovite in an isoplot. The 3 plagioclase spots and the 8 Kfsp spots are not on the isochron.
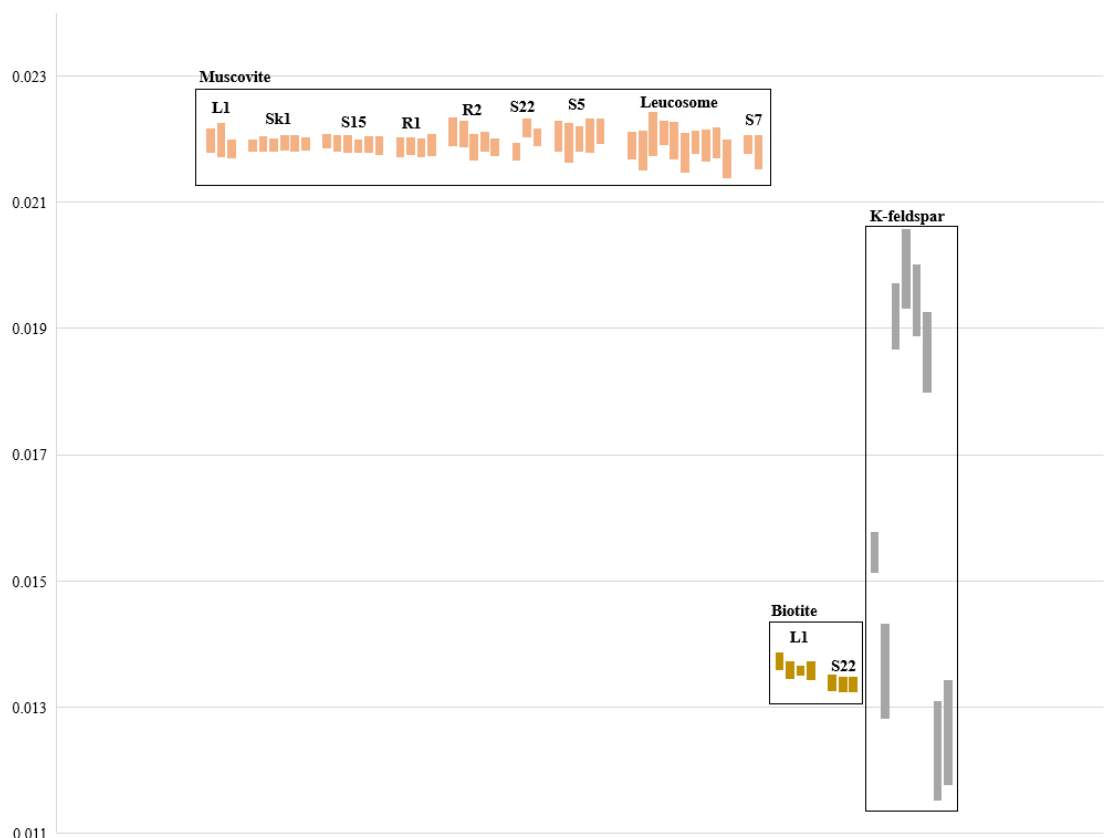


*Figure 28: Ms, Bt and Kfsp individual $^{87}Sr/^{87}Rb$ ratios of single spots.*

Figure 28 shows a homogeneous spread of all individual muscovite $^{87}Sr/^{87}Rb$ ratios in the range of ~ 0.022. Bitotite $^{87}Sr/^{87}Rb$ ratios are also quite homogeneous among themselves but in the range of ~ 0.014. K-feldspar $^{87}Sr/^{87}Rb$ ratios are very heterogeneous and are therefore not considered in the age dating. The same applies to plagioclase of Sk1 with $^{87}Sr/^{87}Rb$ ratios of 0.00057-8.1.

*Day 2 (220831)*

On the second day the samples from the island of Donsö were analyzed together with the standards Mica-Mg, Mica-Fe, Högsbo-Ms and Wilsons Prom.-Bt. As well as a biotite grain from the SLM were analyzed. The calculated $^{87}Sr/^{87}Rb$ ages for Mica-Fe, Högsbo-Ms and Wilson's Prom.-Bt. could be reproduced as well (see table 13). The laser spots were placed in different areas along the grains for each measurement session. Data reduction for all pegmatite samples was carried out using the initial Sr of 0.715 ± 0.015 (typical for enriched magmatic rocks) from Rösel & Zack, 2022.

*Table 13: Calculated ages of Mica-Mg, Mica-Fe, Högsbo-Ms and Wilson Prom.-Bt reported in other studys compared with data from this study to ensure the accuracy of our data.*

| Standard | Mica-Mg | Mica-Fe | Högsbo-Ms | Wilsons Prom. Bt |
|---|---|---|---|---|
| Published ages (in Ma) | 519.4 ± 6.5[1] | 307.6 ± 0.4[2] | 1029 ± 1.7[3] 1037 ± 11[1] | 395 ± 4[6] 391 ± 14[7] |
| Initial $^{87}Sr/^{86}Sr$ | 0.72607 ± 0.0007 | 0.72607 ± 0.0007 | 0.72000 ± 0.0001 | - |
| **Results in this study** | | | | |
| *n* | 20 | 8 | 6 | 8 |
| Rb (ppm) | 1289-1453 | 2208-2473 | 2946-3350 | 1065-1197 |
| Sr (ppm) | 22-24 | 0.2-0.9 | 0.6-0.8 | 0.3-3.0 |
| Initial $^{87}Sr/^{86}Sr$ | 0.72607 | 0.72607 | 0.72 | 0.715 |
| $^{87}Rb/^{86}Sr$ (2s) | 154.57 ± 0.4 | 16000 ± 4500 | 11940 ± 330 | 2500 ± 2000 |
| f$^{87}Sr$ (mean) | 39% | 0.7% | 0.4% | 7% |
| $^{87}Sr/^{86}Sr$ (2s) | 1.85 ± 0.004 | 70 ± 20 | 175 ± 4.2 | 15 ± 11 |
| Weighted mean (2s) | 519.4 ± 1.6 | 308.5 ± 0.53 | 1035 ± 3.2 | 393.6 ± 2.3 |
| MSWD | 0.84 | 0.013 | 0.37 | 0.55 |

(Rb-Sr ms nano-powder)[1], (Ar-Ar biotite)[2], (Pb-Pb Mn-columbite)[3], (compiled age)[1], (U-Pb zircon)[4,6], (U-Pb titanite)[4], (U-Pb apatite)[4], (Ar-Ar hornblende)[5], (K-Ar Biotite)[7] [1]Hogmalm et al. (2017); [2]Grove & Harrison (1996); [3]Romer & Smeds (1994); [1]Zack & Hogmalm (2016), [4]Schoene & Bowring (2006), [5]Spell & McDougall (2003), [6]Elburg (1996), [7]Richards & Singleton (1981)

The Rb mass fraction ranges from 680 ppm to 1755 ppm (or >1500000 cps), so that the mica Mg standard is also used as the primary internal standard here. The common $^{86}Sr$, ranges from 0.2-3.3 ppm in the pegmatite mica and from 0.6 to 0.8 ppm in the leucosomal biotite. The radiogenic $^{87}Sr$ accounts for >90 % of the strontium present (see f$^{87}Sr$,

table 14). The $^{87}Sr/^{87}Rb$ ages for muscovite from pegmatites D3, D4, D6, D8 and D11 result entirely in a weighted mean cooling age of 1520 Ma 2s with a calculated error of 6.4 Ma 2s. The calculated MSWD is between 0.011 in D8 and 0.41 in D6, which is again below the predicted analytical uncertainty. The average cooling age for the biotite analyzed from pegmatite D11 is $945 \pm 6.4$ 2s Ma with an $^{87}Rb/^{86}Sr$ (2s) ratio of $5900 \pm 2100$ 2s and an MSWD of 1.3. For the biotite from the leucosome of the SLM, a cooling age of $951 \pm 8.2$ 2s Ma with an $^{87}Rb/^{86}Sr$ (2s) ratio of $2740 \pm 170$ 2s was determined. D3, D4, D6, D8 and D11 muscovite $^{87}Sr/^{87}Rb$ ratios including the internal error are plotted in figure 29. The 26 spots on seven different muscovite grains (D4 and D11 consist of 2 grains), result in an isochrone with an initial $^{87}Sr/^{86}Sr$ $0.71 \pm 0.34$ and an $^{87}Sr/^{87}Rb$ age of $1522 \pm 37.6$ Ma 2s (see figure 30).

*Table 14: Calculated ages of Muscovites and Biotites from sampled Donsö pegmatites.*

| Sample | D3 | D4 | D6 | D8 | D11 | D11_bt | Leuco_bt |
|---|---|---|---|---|---|---|---|
| $n$ | 5 | 5 | 6 | 5 | 5 | 6 | 5 |
| Rb (ppm) | 1484-1600 | 680-711 | 629-666 | 1699-1755 | 497-579 | 1116-1147 | 669-698 |
| Sr (ppm) | 0.5-2.5 | 1.5-1.8 | 1.7-2.7 | 0.4-1.3 | 3.0-3.3 | 0.2-0.8 | 0.6-0.8 |
| Initial $^{87}Sr/^{86}Sr$ | 0.715 | 0.715 | 0.715 | 0.715 | 0.715 | 0.715 | 0.715 |
| $^{87}Rb/^{86}Sr$ (2s) | $5700 \pm 1200$ | $1170 \pm 51$ | $810 \pm 140$ | $5100 \pm 1200$ | $459 \pm 8.9$ | $5900 \pm 2100$ | $2740 \pm 170$ |
| $f^{87}Sr$ (mean) | 0.5% | 2.8% | 3.5% | 0.5% | 6.8% | 0.5% | 2% |
| $^{87}Sr/^{86}Sr$ (2s) | $122 \pm 25$ | $26 \pm 1$ | $18.2 \pm 3.3$ | $110 \pm 26$ | $10.57 \pm 0.19$ | $78 \pm 27$ | $37.3 \pm 2.5$ |
| Weighted mean (2s) | $1520 \pm 2.4$ | $1520 \pm 4$ | $1520 \pm 6.4$ | $1520 \pm 0.9$ | $1520 \pm 3.4$ | $945 \pm 6.4$ | $951 \pm 8.2$ |
| MSWD | 0.054 | 0.17 | 0.41 | 0.011 | 0.094 | 1.3 | 1.6 |
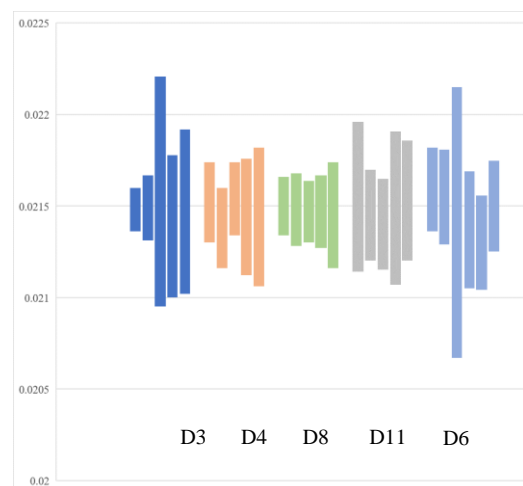


*Figure 29: Donsö Pegmatite Day 2 individual $^{87}Sr/^{87}Rb$ ratios of single spots on muscovite.*
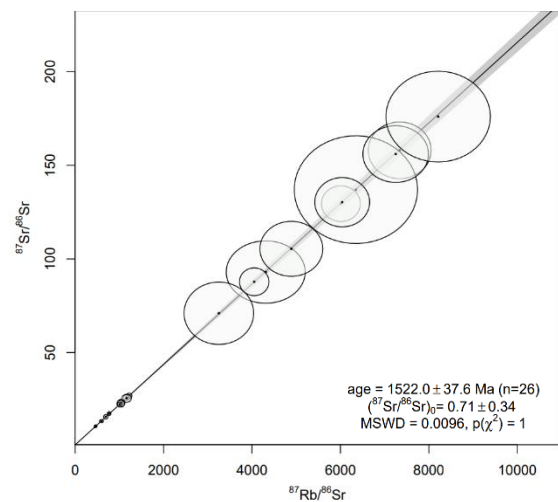
*Figure 30: Donsö Pegmatite Day 2 isoplot including 26 spots on muscovite (see table 14 & 15)*

The muscovite grains from Donsö pegmatites are quite homogeneous with relatively small age spread for the individual $^{87}Sr/^{87}Rb$ ratios (see figure 29). To determine the impact of the used initial $^{87}Sr/^{86}Sr$ on the calculated ages, the calculation was carried out with $^{87}Sr/^{86}Sr$ 0.715 ± 0.015 (typical for enriched magmatic rocks) and 0.730 ± 0.030 (for crustal rocks; Rösel & Zack, 2022) for the homogeneous muscovites and a biotite from the Donsö pegmatites and then the deviation of the ages was determined (see Table 15). The use of the 0.715 $^{87}Sr/^{86}Sr$ versus the 0.730 $^{87}Sr/^{86}Sr$ results in a maximum relative $^{87}Sr/^{87}Rb$ deviation of 0.14%, which in absolute ages corresponds to a maximum difference of 3 Ma 2s (D11 3-5). The mean deviation of the $^{87}Sr/^{87}Rb$ ages is 0.06%, which corresponds to < 1 Ma 2s. This value is within the internal error of 6.4 2s Ma.

*Table 15: A comparison is shown between the calculated $^{87}Sr/^{87}Rb$ and $^{87}Sr/^{87}Rb$ ages using two different assumptions of the initial $^{87}Sr/^{86}Sr$: 0.715 ± 0.015 (typical for enriched magmatic rocks) and 0.730 ± 0.030 (for crustal rocks).*

| initial $^{87}Sr/^{86}Sr$ | | 0.730 ± 0.030 | | 0.715 ± 0.015 | | Deviation | |
|---|---|---|---|---|---|---|---|
| Sample nr. | Spot nr. | $^{87}Sr/^{87}Rb$ | $^{87}Sr/^{87}Rb$ age | $^{87}Sr/^{87}Rb$ | $^{87}Sr/^{87}Rb$ age | $^{87}Sr/^{87}Rb$ | $^{87}Sr/^{87}Rb$ age |
| D3_1 | 160 | 0.02148 | 1521 | 0.02148 | 1521 | 0.00% | 0.01% |
| D3_2 | 161 | 0.02149 | 1521 | 0.02149 | 1522 | 0.00% | 0.07% |
| D3_3 | 183 | 0.02157 | 1528 | 0.02158 | 1528 | 0.05% | 0.00% |
| D3_4 | 206 | 0.02139 | 1515 | 0.02139 | 1515 | 0.00% | 0.00% |
| D3_5 | 207 | 0.02147 | 1520 | 0.02147 | 1521 | 0.00% | 0.07% |
| D4_1 | 162 | 0.0215 | 1523 | 0.02152 | 1524 | 0.09% | 0.07% |
| D4_2 | 163 | 0.02137 | 1513 | 0.02138 | 1514 | 0.05% | 0.07% |
| D4_3 | 185 | 0.02153 | 1525 | 0.02154 | 1525 | 0.05% | 0.00% |
| D4_4 | 186 | 0.02142 | 1517 | 0.02144 | 1518 | 0.09% | 0.07% |
| D4_5 | 208 | 0.02143 | 1517 | 0.02144 | 1518 | 0.05% | 0.07% |
| D8_1 | 166 | 0.02149 | 1522 | 0.0215 | 1522 | 0.05% | 0.00% |
| D8_2 | 167 | 0.02147 | 1520 | 0.02148 | 1521 | 0.05% | 0.07% |
| D8_3 | 189 | 0.02146 | 1520 | 0.02147 | 1520 | 0.05% | 0.00% |
| D8_4 | 190 | 0.02147 | 1520 | 0.02147 | 1520 | 0.00% | 0.00% |
| D8_5 | 213 | 0.02145 | 1519 | 0.02145 | 1519 | 0.00% | 0.00% |
| D11_1 | 168 | 0.02152 | 1524 | 0.02155 | 1526 | 0.14% | 0.13% |
| D11_2 | 169 | 0.02142 | 1517 | 0.02145 | 1519 | 0.14% | 0.13% |
| D11_3 | 191 | 0.02137 | 1513 | 0.0214 | 1516 | 0.14% | 0.20% |
| D11_4 | 192 | 0.02146 | 1519 | 0.02149 | 1522 | 0.14% | 0.20% |
| D11_5 | 215 | 0.0215 | 1522 | 0.02153 | 1525 | 0.14% | 0.20% |
| D11_bt_1 | 170 | 0.01336 | 950 | 0.01336 | 950 | 0.00% | 0.00% |
| D11_bt_2 | 171 | 0.01343 | 954.7 | 0.01343 | 954.8 | 0.00% | 0.01% |
| D11_bt_3 | 193 | 0.01338 | 951 | 0.01338 | 952 | 0.00% | 0.11% |
| D11_bt_4 | 194 | 0.01328 | 944 | 0.01328 | 944 | 0.00% | 0.00% |
| D11_bt_5 | 216 | 0.01309 | 931 | 0.0131 | 931 | 0.08% | 0.00% |
| D11_bt_6 | 217 | 0.01321 | 939.4 | 0.01321 | 939.6 | 0.00% | 0.02% |
| D6_1 | 164 | 0.02158 | 1528 | 0.02159 | 1529 | 0.05% | 0.07% |
| D6_2 | 165 | 0.02153 | 1525 | 0.02155 | 1526 | 0.09% | 0.07% |
| D6_3 | 187 | 0.02138 | 1514 | 0.02141 | 1516 | 0.14% | 0.13% |
| D6_4 | 188 | 0.02135 | 1512 | 0.02137 | 1514 | 0.09% | 0.13% |
| D6_5 | 210 | 0.02128 | 1507 | 0.0213 | 1508 | 0.09% | 0.07% |
| D6_6 | 211 | 0.02149 | 1522 | 0.0215 | 1523 | 0.05% | 0.07% |

# 6. Discussion

The initial assumption that there are two types of pegmatite was based on their internal mineralogy. Pegmatites containing garnets were designated as Type II in the following. Fractionation indicators such as ratios of compatible and incompatible elements within the crystal chemistry of K-feldspar like Ba/Rb and Rb/Sr support this initially simple division between Type I and II pegmatites (see figure 15 & 16). The handheld XRF proved to be a useful tool as a fast exploration method, where concentrations of Rb, Sr and Ba could be used to indicate the degree of fractionation quickly and reliably. The comparison of analytical instruments from field analyses with pXRF and laboratory analyses with ICP-MS shows that with the cheaper and faster pXRF a good estimation of the fractionation degree can be made. In particular, the large data set of different K-feldspars within the pegmatite body offers a clear advantage over ICP-Ms when it comes to a cost-effective and fast exploration method. There are several explanations for the offset between the two methods. The main reason is certainly that the mineral grains analyzed in the field are different from those measured in the laboratory with LA-ICP-MS. Another reason for the deviation can be explained by the fact that pXRF measures the total concentration of the elements and the mass spectrometer detects isotope fractions, which are then extrapolated to the total concentration. Furthermore, the precision and accuracy are significantly higher with ICP-MS, especially at low concentrations, which is noticeable with ratios of two elements (e.g., Rb/Sr) compared to pXRF.

Looking at the fractionation indicators within muscovites, a difference can also be seen within the ratios of Ba/Rb, K/Rb and Rb/Sr, which reinforces the assumption that there are two different types of pegmatites. However, in muscovites from type II pegmatites where beryl, chrysoberyl or minerals of the columbite group, which are used in various classification methods as indicators for rare-element pegmatites, occur, no significant change within these fractionation indicators could be found. This problem is certainly one of the reasons why it is difficult to classify pegmatites and recent studies classify them exclusively based on mineralogy and texture. According to the classification of from Černý et al. 2012 and Wise et al. 2022, D3, D4, D8, D11 and S15 can be classified as rare element pegmatites of group 1 due to the presence of beryl and columbite (descripted in D3 by Smeds, 1990), with muscovite, almandine, and biotite as rock-forming minerals (no distinction between DPA and RMG). All other pegmatites on the

islands of Styrsö, Vrangö, Rivö and Langholmen are classified as primitive barren according to wise 2022. The mica, garnet and feldspar chemistry alone does not allow any conclusions as to whether the pegmatites were formed from residual melting of the granites or by partial melting of the host rocks in situ. Nevertheless, the almost identical ratios of K/Rb, Ba/Rb and Rb/Sr as well as the Li, Cs, Ta and Ba concentrations between muscovite and biotite from leucosomes of the SLM migmatite and the primitive barren are remarkably similar, indicating an anatectic origin at least for the formation of the barren (type I).

Assuming that the Ba/Rb ratio can represent the degree of fractionation most sensitively, the pegmatites Sk1 (0.001-0.0022) and D8 (0.00092 to 0.0022) are the highest fractionated pegmatites found in this study with Ba/Rb ratios close to the level of the Högsbo pegmatite (0.0003 to 0.0016), Timmerhult (0.0003 to 0.1), Skuleboda (0.0025 to 0.0045) and Gundlebo (0.00007 to 0.0016), which are classified as rare element pegmatites (Jansson, 2018). Sk1 exhibits a high degree of fractionation within the muscovite geochemistry, but is not further distinguished mineralogically from other, less fractionated barren containing garnet, muscovite, feldspar, and quartz. It is also noticeable that mobile lithophilic elements such as Li are depleted in the Muscovites from higher fractionated pegmatites compared to less fractionated pegmatites or have a consistently low concentration in all samples (see figure 17). An argument for the anatectic model as the origin of the rare element pegmatites is the low content of Li, Cs and Ta in mica, in the presence of beryl and columbite, which are indicators of higher fractionated pegmatites. With steady differentiation from a large pluton, these elements should be significantly enriched, while in DPA pegmatites the composition of the host rock has a major influence on the mineralogy. The absence of lithium in the metasediment could be controlled by the high mobility of Li during sedimentation. Here, a comparison with the pegmatites originating from the Hisingen Suite would be a useful next step.

Fractionation parameters such as Fe/Mn and Mn wt% within the garnets show the same fractionation trends as the biotite samples. The Fe/Mn ratio decreases, the iron and magnesium content decreases, and the manganese content increases due to the increasing fractionation of the pegmatite melt. Garnets from the sampled melt have similar spessartine > almandine components as the fractionated pegmatites. This would mean that granodioritic melt pools, as they occur in the SLM, are already fractionated according to Fe/Mn. The trigger for the pegmatite formation would therefore probably be the

fluid content. This separation of the pegmatitic fluid from the felsic melt can be observed on Vrangö (see figure 14 A & B). It is also possible that the melt pool occurrence in the SLM fm. represents a later intrusion of the Hisingen suite at about 1520 Ma, as the migrating melt crosscuts foliation and migmatisation (see figure 9 B & 14 C).

A weakness of the sampling method used in this study is that muscovite, biotite, garnet, and K-feldspar were taken from different zones of the pegmatites, making comparisons difficult. An indication for this problem was already discovered with the pXRF that Ba, Rb, Sr concentrations as well as most likely Li, Cs, Ta, Nb, etc. can vary within the pegmatite bodies. Therefore, it is recommended to sample minerals from the same area in future research. A suitable mineral for this would be quartz from the core or intermediate zone, as quartz always occurs and these zones are easy to find, which is examined for trace elements such as Li, Cs, Be, Ti (high Li and low Ti = higher fractionation). Trace element studies in quartz from highly fractionated pegmatites showed that quartz crystals within the border and wall zone have the same primitive pattern as barren pegmatites (Müller et al. 2021). Therefore, it can be assumed that the same pattern also applies to K-feldspar, muscovite, and biotite, assuming a crystallization sequence from the boundary to the core, which can be assumed based on the depth estimate. Another advantage of quartz sampling is that genetic correlations can be established from the concentrations of Al, Li, Ti, Ge, B, Be and Ga (Götze et al. 2021).

In situ Rb/Sr dating of the primary and secondary standards was able to reproduce the published ages during day 1 and day 2 for Högsbo-Ms 1037±11 Ma (Hogmalm et al. 2016), La Posta-Bt granodiorite 91.6 Ma (Zack & Hogmalm, 2016), Mica-Fe with $307.6 \pm 0.4$ Ma (Grove & Harrison, 1996), McClure-Bt $523.98 \pm 0.12$ Ma (Schoene & Bowring, 2006), and Wilson Prom. -Bt $395 \pm 4$ Ma (Elburg, 1996) with the corresponding initial $^{87}Sr/^{86}Sr$ with a high accuracy.

The geochemically (4:1 ratio see 5.4.1 Mica) sorted muscovite grains from all pegmatites and both days are quite homogeneous (Figures 28 & 29). This is reflected in the well constrained age and relatively small age spread for the individual $^{87}Sr/^{87}Rb$ age determinations (Table 12 & 14). The $^{87}Sr/^{87}Rb$ muscovite ages are considered acceptable despite their low MSWD due to the great structural and geochemical homogeneity of the grains. This would only mean that the age is accurate, but the potential error is overestimated and less reliable. K-feldspar and plagioclase from pegmatites L1, R1, R2

and Sk1 were not included in the age calculations due to their high heterogeneity (see figures 27 & 28). The isoplots (Figures 26 & 30) show that muscovites from different pegmatites plot along the isochron, while plagioclase and K-feldspars do not plot on the isochron. This reinforces the assumption that $^{87}Sr/^{87}Rb$ ages of muscovites are more robust and could indicate a resetting of the Rb/Sr system in Kfsp and Plg at the same time. The influence of the initial $^{87}Sr/^{86}Sr$ ratio examined in table 15 shows that, especially at high $^{87}Sr/^{87}Rb$ ratios, the difference between 0.715 and 0.730 results in a negligible difference on the individual spot age of max. 0.14%, i.e., < 3 Ma, which is within the internal error of ± 6.4 2s Ma.

Table 11 and 13 show a summary of the ages obtained in this study. The ages of the primitive barren pegmatites indicate emplacement around 1553 Ma, with minimum and maximum ages of 1547-1562 Ma, considering the error, in agreement with the DG2 event at 1.56-1.54 Ga (Åhäll & Connelly 2008; Austin Hegardt et al. 2010). Migmatisation of the SLM is restricted at Nordön by the amphibolite intrusion at 1547 ± 11 Ma and sets a minimum age of migmatisation at 1536 Ma (Hegardt, 2010). Ackevall (2016) proposes, based on U-Pb dating on 21 zircon margins from the Lotsutkiken intrusion at 1552 ± 5 Ma, to limit the migmatisation of the SLM to 1547 Ma. The dated muscovites from barren L1 (1553 ± 5.4 Ma), R2 (1556 ± 6.2 Ma), S22 (1557 ± 10 Ma) and the Leucosome sample (1552 ± 5.2 Ma) support these results and set the minimum end of migmatisation at 1547 Ma. The end of migmatisation can be justified by the observation that the studied pegmatites were not metamorphic overprinted. Only beryl crystals in the younger Donsö pegmatites show an internal deformation, which, however, could also have been formed during the crystallization within a stress field.

A correlation between the degree of fractionation and the cooling age of the barren can been established (see figure 27). The younger barrens R1 (1549 ± 1.4 2s Ma), Sk1 (1552 ± 0.9 2s Ma) and S15 (1552 ± 1.5 2s Ma) exhibit garnets in their internal mineralogy and increased Ba/Rb and Rb/Sr ratios, as well as increased concentrations of Ta and Cs. The older barrens L1 (1553 ± 5.4 2s Ma), R2 (1556 ± 6.2 2s Ma) and S22 (1557 ± 10 2s Ma) are more primitive in their geochemistry and mineralogy. This could be explained by steady fractionation of incompatible elements and later cooling.

The heat source for the anatexis of the Stora Le-Marstrand Formation during the Gothian orogeny is thought to be mafic underplating and associated gabbro intrusions,

which in turn would be a source of regional mafic magmatism in the Idefjorden terrane at 1555 - 1553 Ma. Melt experiments show that melting of amphibolite tends to produce tonalitic melt compositions (Rapp et al. 1991). For the granitic pegmatite melts to originate from amphibolites the melts either underwent fractionation during melt movement or have a mixed melt source of amphibolitic and more felsic compositions, which in this case originate from the felsic part of the SLM. This hypothesis was supported by Ackevall (2016), who assumes that the felsic components of the Lotsutkiken intrusion originated from the Stora Le-Marstrand Formation. The resulting felsic melt is probably the source melt for the spawned primitive pegmatites in the SLM, which therefore have an anatectic origin. The different degrees of fractionation, which are due to the mineralogy of the barren and the isotope ratios Ba/Rb, K/Rb and Rb/Sr, can therefore only be explained by melt movement, combined with continuous fractionation of the incompatible elements and the composition of the source material. The younger, beryl-bearing Donsö pegmatites D3, D4, D6, D8 and D11, are intruded in a short time span around $1520 \pm 6.4$ 2s Ma. These pegmatites show a slightly higher degree of fractionation in the isotopic ratios of Ba/Rb, Rb/Sr and K/Rb than the average barren pegmatites on the other islands. However, no correlation between the different ages and the element concentration of Li, Cs, Ba and Ta could be observed in muscovite from both events (figure 31). Rather, it seems that both pegmatite clusters were formed from the same source at different times. In this case, only the melt formation within the SLM comes into question. Since the Hisingen Suite is thought to have formed as S-type granites from the SLM at 1.59-1.52 Ma, the Hisingen Suite could be the parent body for the Donsö pegmatites. Ackevall (2016) has dated monazites from an unfoliated granodiorite at Lotsutkiken/Vrangö to $1524 \pm 10$ Ma and suggests a metamorphic event at the end of the Hisingen Suite intrusion series. However, this metamorphic event is not seen in the older type I pegmatites on the evidence of deformation. Nevertheless, local melting of the SLM by re-underplating of mafic intrusions could provide a heat source and causes the formation of a new pegmatite generation around 1520 Ma. This would not explain the different mineralogy (beryl & columbite) of the Donsö pegmatites, which is rather an indication of lager melt accumulation and higher fractionation. The SLM fm. is the source material in each case, a constant element concentration at different degrees of fractionation would be a possible explanation for the formation of the rare element pegmatites and barrens. Fractionation within this pegmatite field is therefore significantly dependent on the melt volume, fluid content and melt movement of the same protolith.

A rather interesting phenomenon is that the younger (1520 ± 6.4 Ma) pegmatites were found exclusively on the island of Donsö. In addition, no typical concentric zoning was observed with increasing distance from the pluton (Hisingen Suite, east direction). Rather, it seems that the pegmatites found on Donsö are a local phenomenon.
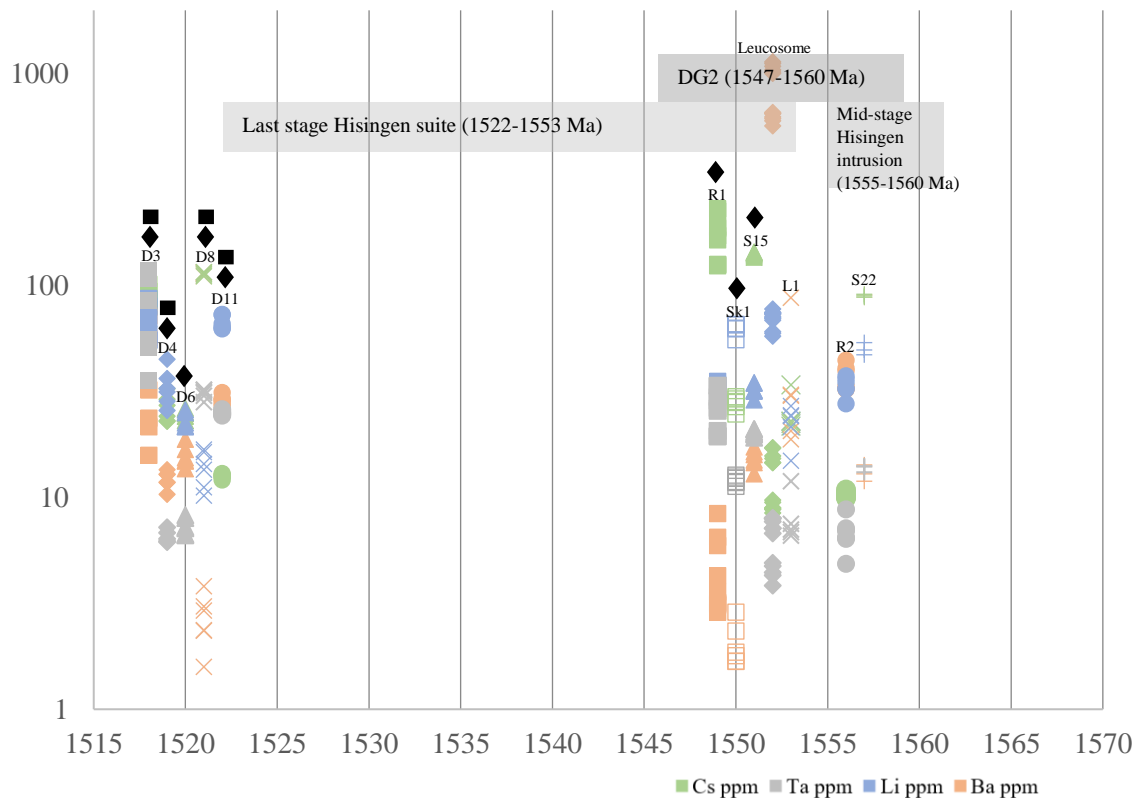


*Figure 31: Shown are the dated muscovites representative of the respective pegmatite plotted against the concentrations (ppm) of Cs, Ta, Li and Ba. The ages of D3, D4, D6, D8, D11(1520 ± 6.4 2s Ma) and Sk1 (1552 ± 0.9 2s Ma) have been slightly age offset for visual reasons. Garnet (♦) and beryl (■) bearing pegmatites are marked.*

The dated biotites from the Leucosome sample, as well as pegmatite samples from L1, D11 and S22 give a cooling age of 938 to 973 Ma, which falls within the end of the Sveconorwegian orogeny and the exhumation of the Idefjorden terrane at 980-940 Ma (Bingen et. al. 2021). Biotite has a closure temperature for Rb-Sr of 300-350 °C and can therefore be used here as an exhumation age. Because the same fractionation trends can be seen in muscovite and biotite (see figure 20 & 21), a cogenetic crystallization of both phases, from the same parent melt with different closure temperatures can be assumed.

## Future Research

This study shows that the pegmatites in the archipelago off Gothenburg may be a very exciting study area for the question, which has been discussed for several years, whether rare element pegmatites can also form as direct products of anatexis. Therefore, we recommend that future studies address the following open questions. As beryl crystals were also found in the Hisingen suite pegmatites within the drill cores on the mainland and the last stage of the Hisingen intrusion overlaps with the age of the Donsö pegmatites, a comparison of the Donsö pegmatites with the Hisingen series pegmatites would be a useful next step. Further we recommend trace element comparisons between garnet, columbite, mica and beryl from the 1520 Ma old pegmatites and the Sveconorwegian pegmatites (Högsbo, Timmerhult, Skuleboda, Skantorp, Hisingen Amazonite pegmatite). It is possible that the Sveconorwegian pegmatites also originated from the SLM due to the similar mineralogy. Another simpler task would be the search for columbite minerals in pegmatite D3, as Smed (1990) seems to have described columbite only based on the observation of a mineral collector (Dan Johansson 1988-1989). This could be combined with a broader mineral search in the beryl-bearing pegmatites, where larger quantities of pegmatite material, of different zones, will have to be extracted. The total rock composition would significantly facilitate the classification according to Wise 2022. It would also be interesting to investigate micas from the SLM from largely undeformed areas to strongly deformed areas to draw conclusions about the melt formation (muscovite breakdown), as well as P-T conditions in the pegmatites with e.g., garnet-biotite-muscovite-plagioclase geothermobarometers. To better understand more about resetting, cooling, and crystallization ages and the limitations and advantages of different dating methods (muscovite/biotite: Rb-Sr, K-Ar, Ar-Ar, garnet: Lu-Hf, Sm-Nd, U-Pb, and columbite: U-Pb), a comprehensive dating on the same pegmatite would be a useful next step.

# 7. Conclusiones

I. The calculated crystallization/cooling ages from Muscovites of the primitive barren make sense in the context of the DG2 deformation event at 1.56–1.54 Ga (Åhäll & Connelly, 2008; Austin Hegardt et al., 2010) and associated migmatisation with a calculated age of 1547-1562 Ma, including the 2s error. Therefore, the primitive barrens L1, Sk1, S15, S22, R1 and R2 can be assigned to the deformation event and have a high probability of having an anatectic origin.

II. Due to similar geochemical fractionation indicators, such as Ba/Rb, Rb/Sr and trace element concentrations like Li, Ta, and Cs between the Leucosome sample from the SLM Fm. and the primitive barren pegmatites, it is likely that these barrens originate from the partial melt (DPA) of the SLM fm.

III. The calculated muscovite ages of 1552 ± 5.2 2s Ma of the Leucosome sample from the SLM Fm. support this assumption and limit the migmatisation to 1547 Ma, which supports the results of Ackevall, 2016.

IV. The beryl-bearing rare element pegmatites D3, D4, D6, D8 and D11 on the island of Donsö, yield calculated cooling ages of 1520 ± 6.4 2s Ma. Due to the small age range of the individually calculated $^{87}Sr/^{87}Rb$ ages, it can be assumed that these rare element pegmatites are of cogenetic origin.

V. A correlation between the degree of fractionation and the cooling age of the barren has been identified. Younger barrens R1 (1549 ± 1.4 2s Ma), Sk1 (1552 ± 0.9 2s Ma) and S15 (1552 ± 1.5 2s Ma) exhibit garnets in their internal mineralogy and increased Ba/Rb and Rb/Sr ratios, as well as increased concentrations of Ta and Cs. Older barrens L1 (1553 ± 5.4 2s Ma), R2 (1556 ± 6.2 2s Ma) and S22 (1557 ± 10 2s Ma) are more primitive in their geochemistry and mineralogy. This could be explained by steady fractionation of incompatible elements and later cooling. However, this observation must be considered with caution, as the sampling in different zones of the pegmatites could have led to a random correlation between age and fractionation degree.

VI. Without a comparison between the pegmatites of the Hisingen suite and the Donsö rare element pegmatites, it cannot be fully clarified whether these can be classified as DPA or RMG pegmatites. Due to calculated ages, it is likely that the last intrusion stage of the Hisingen suite represents the parental body. However, fractionation parameters such as Ba/Rb, Rb/Sr and trace element

concentrations of Li, Ta and Cs show a high similarity to the primitive barren. Which could indicate that the SLM Fm. is the source material in each case.

VII. Calculated $^{87}Sr/^{87}Rb$ ages of 938 to 973 Ma 2s in all biotite samples of the Leucosome from the SLM Fm. and primitive barren pegmatites L1 and S22, as well as from the rare element pegmatite D11 can be used as exhumation ages due to the lower closure temperature. This would mean that the area of the SLM Fm. west of Gothenburg reached a temperature of 300-350 °C at this time, which is consistent with the end of the Sveconorwegian orogeny.

VIII. Our results show that individual single spot ages can be determined with high accuracy using the initial $^{87}Sr/^{86}Sr$ ratios established by Rösel & Zack (2022) of: (1) 0.703 ± 0.003 (for mantle derived magmatic rocks), (2) 0.715 ± 0.015 (for enriched magmatic rocks) and (3) 0.730 ± 0.030 (for crustal rocks), which makes the Rb/Sr dating process much easier and faster, as there is no need to sample several phases.

IX. The handheld XRF is suitable for a rough estimate of the degree of fractionation. Barium, rubidium, and strontium provide a good insight into the degree of fractionation due to their strong variance between the pegmatites. Pb concentrations, however, do not vary between the fractionated and primitive pegmatites.

## Acknowledgements

# References

Åhäll, K.I., Connelly, J.N., 1998. Intermittent 1.53-1.13 Ga magmatism in western Baltica; age constraints and correlations within a postulated supercontinent. Precambrian Res. 92, 1–20.

Åhäll, K.I., Connelly, J.N., 2008. Long-term convergence along SWFennoscandia: 330 m.y. of Proterozoic crustal growth. Precambrian Res. 161, 452–474.

Andersen, T., Griffin, W., Jackson, S., Knudsen, T.-L., Pearson, N. 2004. Mid-Proterozoic magmatic arc evolution at the southwest margin of the Baltic Shield. Lithos, 73(3), 289-318.

Andersson, J., Söderlund, U., Cornell, D., Johansson, L., Möller, C., 1999. Sveconorwegian (- Grenvillian) deformation, metamorphism and leucosome formation in SW Sweden, SW Baltic Shield: constraints from a Mesoproterozoic granite intrusion. Precambrian Research 98, 151-171.

Austin Hegardt, E., Cornell, D.H., Hellström, F.A., Lundqvist, I., 2007. Emplacement age of the mid-Proterozoic Kungsbacka Bimodal Suite, SW Sweden. Geologiska Föreningen, 129, 227–234.

Austin Hegardt, E., 2010. Ph.D. thesis. Pressure, Temperature and Time Constraints on Tectonic Models for Southwestern Sweden. Department of Earth Science, University of Gothenburg, 1–91.

Barros R., Menuge J.F., 2016. The origin of spodumene pegmatites associated with the Leinster Granite in southeast Ireland. The Canadian Mineralogist, 54(4), 847-862.

Bergman, S., Stephens, M.B., Andersson, J., Kathol, B. & Bergman, T., 2012. Sveriges berggrund, skala 1:1 miljon [Bedrock Map of Sweden, Scale 1:1 Million]. Sveriges geologiska undersökning K 423.

Bergström, U., Stephens, M.B.,Wahlgren, C.H., 2020. Chapter 16 - Polyphase (1.6–1.5 and 1.1–1.0 Ga) deformation and metamorphism of Proterozoic (1.7–1.1 Ga) continental crust, Idefjorden terrane, Sveconorwegian orogen. Geological Society London Memoirs, 50, 397–434.

Beurlen, H., Thomas, R., Rodrigues da Silva, M.R., Müller, A., Rhede, D., Soares, D.R., 2014. Perspectives for Li- and Ta-Mineralization in the Borborema Pegmatite Province, NE-Brazil: A review, Journal of South American Earth Sciences, Volume 56, 110-127

Bingen, B., Viola, G., Möller, C., Vander Auwera, J., Antonin, L., Yi, K., 2020. The Sveconorwegian orogeny. Gondwana Research, 90, 273-313.

Bingen, B., Skår, Ø., Marker, M., Sigmond, E. M., Nordgulen, Ø., Ragnhildstveit, J., Mansfeld, J., Tucker, R. D. & Liégeois, J. P., 2005. Timing of continental building in the Sveconorwegian orogen, SW Scandinavia. Norwegian Journal of Geology, 85(1-2), 87-116.

Bingen, B., Nordgulen, Ø., Viola, G. 2008a. A four-phase model for the Sveconorwegian orogeny, SW Scandinavia. Norwegian Journal of Geology 88, 43–72.

Bingen, B., Davis, W.J., Hamilton, M.A., Engvik, A., Stein, H.J., Skår, Ø., Nordgulen, Ø., 2008b. Geochronology of high-grade metamorphism in the Sveconorwegian belt. S Norway: U-Pb, Th-Pb and Re-Os dat, 13-42.

Brewer, T.S., Menuge, J.F., 1998. Metamorphic overprinting of Sm-Nd isotopic systems in volcanic rocks: the Telemark Supergroup, southern Norway. Chemical Geology 145, 1–16.

Brotzen, O., 1961. On some age relations in the Pre-Cambrian of southwestern Sweden. Geologiska Föreningen, 83(3), 227-252.

Cameron, E.N., Jahns, R.H., McNair, A.H. and Page, L.R., 1949. Internal structure of granitic pegmatites. Economic Geology., Monograph, 2, pp. 115.

Černý, P., Burt, D. M., 1984, Paragenesis, crystallochemical characteristics, and geochemical evolution of micas in granite pegmatites: Reviews in Mineralogy, 13, 257-297.

Černý, P., Meintzer, R.E., Anderson, A.J., 1985. Extreme fractionation in rare-element granitic pegmatites; selected examples of data and mechanisms. The Canadian Mineralogist, 23(3), 381-421.

Černý P., 1991. Rare-element granite pegmatites. Part I: anatomy and internal evolution of pegmatite deposits. Part II: regional to global relationships and petrogenesis. Geoscience Canada, 18, 49-81.

Černý P. & Ercit T.S., 2005. The classification of granitic pegmatites revisited. The Canadian Mineralogist, 46(6), 2005-2026.

Černý P., London D., Novák M., 2012. Granitic pegmatites as reflections of their sources. Elements, 8, 289-294.

Chakoumakos, B.C., Lumpkin, G.R., 1990. Pressure-temperature constraints on the crystallization of the Harding pegmatite, Taos County, New Mexico. Canadian Mineralogist 28, 287–298.

Clark, G. S., Černý, P., 1987. Radiogenic 87Sr, its mobility, and the interpretation of Rb- Sr fractionation trends in rare-element granitic pegmatites. Geochimica et Cosmochimica Acta, 51(4), 1011-1018.

Cliff, R.A., 1985. Isotopic dating in metamorphic belts. J. Geological Society London, 142, 97-110.

Connelly, J.N., Åhäll, K.-I., 1996. The Mesoproterozoic cratonisation of Baltica – new age constraints from SW Sweden. In: BREWER, T.S. (ed.) Precambrian Crustal Evolution in the North Atlantic Region. Geological Society, London, Special Publications, 112, 261–273

Cornell, D. H., Årebäck, H., & Scherstén, A., 2000. Ion microprobe discovery of Archaean and Early Proterozoic zircon xenocrysts in southwest Sweden. Geologiska Föreningen, 122(4), 377-383.

Crouse, R.A., Černý, P., 1972. The Tanco pegmatite at Bernic Lake, Manitoba; I, geology and paragenesis. The Canadian Mineralogist, 11(3), 591-608.

Daly, J.S., 1978. PhD thesis. Geochemical and geochronological studies in the Stora Le-Marstrand belt of Orust SW Sweden. University of Keele, Keele, UK.

Del Moro A., Puxeddu M., Radicati di Brozolo F., Villa I. M., 1982. Rb-Sr and K-Ar ages on minerals at temperatures of 300 – 400°C from deep wells of the Larderello geothermal field (Italy). Contributions to Mineralogy and Petrology, 81, 340 –349.

Demartis, M., Pinotti, L.P., Coniglio, J.E., D'Eramo, F.J., Tubía, J.M., Arag'on, E., Agulleiro Insúa, L.A., 2011. Ascent and emplacement of pegmatitic melts in a major reverse shear zone (Sierras de C'ordoba, Argentina). Journal of Structural Geology, 33, 1334–1346.

Deveaud, S., Millot, R. and Villaros, A., 2015. The genesis of LCT-type granitic pegmatites, as illustrated by lithium isotopes in micas. Chemical Geology, 411, 97-111.

Devineau K., Champallier, R., Pichavant, M., 2020. Dynamic Crystallization of a Haplogranitic Melt: Application to Pegmatites, Journal of Petrology, 61, egaa054.

Dodson M. H., 1973. Closure temperature in cooling geochronological and petrological systems. Contributions to Mineral Petrology, 40, 259 –27.

Engvik, A.K., Bingen, B., Solli, A., 2016. Localized occurrences of granulite: P–T modeling, U–Pb geochronology and distribution of early-Sveconorwegian high-grade metamorphism in Bamble, South Norway, Lithos, Volumes 240–243, 84-103.

Elburg, M., 1996. U-Pb ages and morphologies of zircon in microgranitoid enclaves and peraluminous host granite: Evidence for magma mingling. Contributions to Mineralogy and Petrology.

Fei G., Menuge, J.F., Li, Y., Yang, J., Deng, Y., Chen, C., Yang, Y., Yang, Z., Qin, L., Zheng, L., Tang, W., 2020. Petrogenesis of the Lijiagou spodumene pegmatites in Songpan-Garze Fold Belt, West Sichuan, China: evidence from geochemistry, zircon, cassiterite and coltan U-Pb geochronology and Hf isotopic compositions. Lithos 364–365, 105555.

Fuchsloch, W. C., Nex, P. A. M., and Kinnaird, J. A., 2018. Classification, mineralogical and geochemical variations in pegmatites of the Cape Cross-Uis pegmatite belt, Namibia: Lithos, 296, 79-95.

Ginsburg A.I., Timofeyev, I.N., Feldman L.G., 1979. Principles of geology of the granitic pegmatites. Nedra, Moscow.

Gourcerol, B., Gloaguen, E., Melleton, J., Tuduri, J., Galiegue, X., 2019. Re-assessing the European lithium resource potential – a review of hard-rock resources and metallogeny. Ore Geology Reviews, 109, 494–519.

Götze, J., Pan, Y., & Müller, A., 2021. Mineralogy and mineral chemistry of quartz: A review. Mineralogical Magazine, 85(5), 639-664.

Grove M., Harrison T.M., 1996. [40]Ar diffusion in Fe-rich biotite. American Mineralogist, 81, 940–951.

Halliday A.N., J.P. Davidson, W. Hildreth, P. Holden, 1991. Modelling the petrogenesis of high Rb/Sr silicic magmas, Chemical Geology, 92, 107-114.

Harrison, T.M., Célérier, J., Aikman, A.B., Hermann, J., Heizler, M.T., 2009. Diffusion of [40]Ar in muscovite. Geochim. Cosmochim. Acta 2009, 73, 1039–1051.

Herzog, L. F., Pinson, W. H., Hurley, P. M., 1960. Rb-Sr analyses and age determinations of certain lepidolites, including an international interlaboratory comparison suite. American Journal of Science, 258(3), 191-208.

Hogmalm K.J. & Zack T., Karlsson A.K.O., Sjoqvist A.S.L., Schonberg, D.G., 2017. In situ Rb-Sr and K-Ca dating by LA-ICP-MS/MS: an evaluation of N2O and SF6 as reaction gases. Journal of Analytical Atomic Spectrometry, 32, 305-313.

Hugo, P.J., 1970. The pegmatites of the Kenhardt and Gordonia districts, Cape Province. Memoir of Geological Survey of South Africa, 58, pp. 94.

Hulsbosch, N., Hertogen, J., Dewaele, S., André, L. and Muchez, P., 2014. Alkali metal and rare earth element evolution of rock-forming minerals from the Gatumba area pegmatites (Rwanda): Quantitative assessment of crystal-melt fractionation in the regional zonation of pegmatite groups. Geochimica et Cosmochimica Acta, 132, 349-374.

Jahns R.H., Burnham C.W., 1969. Experimental studies of pegmatite genesis: I. A model for the derivation and crystallisation of granitic pegmatites. Economic Geology, 64, 843-864.

Jahns, R.H., Ewing, R.C., 1976. The Harding mine, Taos County, New Mexico. New Mexico Geological Society.

Jansson E., 2018. Master thesis. Application of in situ RB-Sr dating on Sveconorwegian rare element pegmatites, southwestern Sweden. University of Gothenburg.

Jäger, E., 1979. Introduction to Geochronology. In: Jäger, E., Hunziker, J.C. (eds) Lectures in Isotope Geology. Springer, Berlin, Heidelberg. SEITEN

Jenkin G. R. T., 1997. Mode effects on cooling rate estimates from Rb-Sr data. Geology 25, 907–910.

Jochum K.P., Willbold M., Raczek I., Stoll B. and Herwig K., 2005. Chemical characterisation of the USGS reference glasses GSA-1G, GSC-1G, GSD-1G, GSE-1G, BCR-2G, BHVO- 2G and BIR-1G using EPMA, ID-TIMS, ID-ICP-MS and LA-ICP-MS. Geostandards and Geoanalytical Research, 29, 285–302.

Johansson, L., Lind, A., Möller, C., 1991. Late Sveconorwegian (Grenville) high-pressure granulite facies metamorphism in southwest Sweden. Journal of Metamorphic Geology 9, 283-292.

Johansson, L., Kullerud, L., 1993. Late Sveconorwegian metamorphism and deformation in southwestern Sweden. Precambrian Research 64, 347-360.

Jonason, D., 2016. Bachelor's Essay. U-Pb radiometric dating and trace element characteristics of columbite from the Högsbo pegmatite quarry, south-western Sweden. Department of Earth Sciences, Gothenburg University.

Jochum, K.P., Weis, U., Stoll, B., Kuzmin, D., Yang, Q., Raczek, I., Jacob, D.E., Stracke, A., Birbaum, K., Frick, D.A., 2011. Determination of reference values for NIST SRM 610--617 glasses following ISO guidelines. Geostandards Geoanalytical Research, 35(4), 397–429.

Kolbe, P. , Taylor, S. R., 1966. Major and trace element relationships in granodiorites and granites from Australia and South Africa. Contributions to Mineralogy and Petrology, 12 (2). 202-222.

Kontak, D.J., Creaser, R.A., Heaman, L.M. and Archibald, D.A., 2005. U-Pb tantalite, Re-Os molybdenite, and 40Ar/39Ar muscovite dating of the Brazil Lake pegmatite, Nova Scotia: a possible shear-zone related origin for an LCT-type pegmatite. Atlantic Geology, 41, 17-29.

Konzett, J., Schneider, T., Nedyalkova, L., Hauzenberger, C., Melcher, F., Gerdes, A., Whitehouse, M., 2018. Anatectic granitic pegmatites from the Eastern Alps: A case of variable rare-metal enrichment during high-grade regional metamorphism - I: Mineral assemblages, geochemical characteristics, and emplacement ages: Canadian Mineralogist, 56(4),  555-602.

Lee, J.K.W., Williams, I.S., Ellis, D.J., 1997. Pb, U and Th diffusion in natural zircon. Nature, 390, 159–162.

Linnen R.L., Van Lichtervelde M., Černý P., 2012. Granitic pegmatites as sources of strategic minerals. Elements, 8, 275-280.

London, D., 1990. Internal differentiation of rare-element pegmatites: a synthesis of recent research. Geological Society of America Special Paper, 246, 35-50.

London D., 2005. Geochemistry of alkali and alkaline earth elements in ore-forming granites, pegmatites and rhyolites. In: Linnen R.L., Samson I.M. [eds] Rare element geochemistry and mineral deposits. Geological Association of Canada Short Course Notes 17, 17-43.

London D., 2008. Pegmatites. Canadian Mineralogist, Special Publication 10, 347 p.

London D., Kontak D.J. 2012. Granitic pegmatites: scientific wonders and economic bonanzas. Elements, 8, 257-261.

London D., Morgan VI G.B. 2012. The pegmatite puzzle. Elements, 8, 263-268.

London, D., 2014. A petrologic assessment of internal zonation in granitic pegmatites. Lithos, 184, 74-104.

London, D., 2018. Ore-forming processes within granitic pegmatites. Ore Geology Reviews, 101, 349-383.

Lundegardh P. H., 1953. Petrology of the Mölndal-Styrsö-Valland region in the vincinity of Gothenburg.

Marchal, K.L., Simmons, W.B., Falster, A.U., Webber, K.L., & Roda-Robles, E., 2014. Geochemistry, mineralogy, and evolution of Li-Al micas and feldspars from the Mount Mica Pegmatite, Maine, USA. Canadian Mineralogist 52, 221–233.

Martin, R. F., De Vito, C., 2005. The patterns of enrichment in felsic pegmatites ultimately depend on tectonic setting. The Canadian Mineralogist, 43 (6). 2027-2048

McCauley, A., Bradley, D.C., 2014. The global age distribution of granitic pegmatites. The Canadian Mineralogist 52 (2), 183–190.

Morgan VI, G., London, D., 1999. Crystallization of the Little Three layered pegmatite-aplite dike, Ramona District, California. Contrib Mineral Petrol 136, 310–330.

Morteani, G., Kostitsyn Y., Gilg H., Preinfalk C. and Razakamanana T., 2013. Geochemistry of phlogopite, diopside, calcite, anhydrite and apatite pegmatites and syenites of southern Madagascar: Evidence for crustal silicocarbonatitic (CSC) melt formation in a Panafrican collisional tectonic setting. International Journal of Earth Sciences, 102, 627–645.

Möller, C., 1998. Decompressed eclogites in the Sveconorwegian (-Grenvillian) orogen of SW Sweden: petrology and tectonic implications. Journal of metamorphic Geology 16, 641-656.

Möller, C., 1999. Sapphirine in SW Sweden: a record of Sveconorwegian (-Grenvillian) lateorogenic tectonic exhumation. Journal of Metamorphic Geology 17, 127-141.

Müller A., Romer R.L., Pedersen, R.B., 2017. The Sveconorwegian pegmatite province - thousands of pegmatites without parental granites. The Canadian Mineralogist, 55(2), 283-315.

Müller, A., Simmons, W., Beurlen, H., Thomas, R., Ihlen, P., Wise, M., Roda-Robles, E., Neiva, A., Zagorsky, V., 2018. A proposed new mineralogical classification system for granitic pegmatites – Part I: History and the need for a new classification. The Canadian Mineralogist, 60 (2): 203–227.

Müller, A., Keyser, W.et al., 2021. Quartzchemistry of granitic pegmatites: implications for classification, genesis and economics. Chemical Geology, 584, 120507.

Müller, Axel et al., 2022. GREENPEG – exploration for pegmatite minerals to feed the energy transition: first steps towards the Green Stone Age. Geological Society, London, Special Publications (2022), 526 (1)

Nabelek, P.I., Whittington, A.G., Sirbescu, M.L.C., 2010. The role of $H_2O$ in rapid emplacement and crystallization of granite pegmatites: resolving the paradox of large crystals in highly undercooled melts. Contributions to Mineralogy and Petrology, 160(3), 313-325.

Neiva, A.M.R., 2013. Micas, feldspars and columbite-tantalite minerals from the zoned granitic lepidolite subtype pegmatite at Namivo, Alto Ligonha, Mozambique. European Journal of Mineralogy 25, 967–985

Nicolaysen L.O., 1961. Graphic interpretations of discordant age measurements on metamorphic rocks. Annals of the New York Academy of Sciences (Geochronology of Rock Systems), 91, 198–206.

Norton, J.J., Redden, J.A., 1990. Relations of zoned pegmatites to other pegmatites, granite, and metamorphic rocks in the southern Black Hills, South Dakota. American Mineralogist, 75(5-6), 631-655.

O'Connor P.J., Gallagher V., Kennan P.S., 1991. Genesis of lithium pegmatites from the Leinster Granite margin, southeast Ireland: geochemical constraints. Geological Journal, 26, 295-305.

Paton C., Hellstrom J., Paul B., Woodhead J., Hergt J., 2011. Iolite: Freeware for the visualisation and processing of mass spectrometric data. Journal of Analytical Atomic Spectrometry, 26, 2508–2518.

Park, R.G., Åhäll, K.I., Boland, M.P., 1991. The Sveconorwegian shear-zone network of SW Sweden in relation to mid-Proterozoic plate movements. Precambrian Res. 49, 245–260.

Petersson, A., Scherstén, A., Andersson, J., Möller, C., 2013. Zircon U–Pb and Hf–isotops from the eastern part of the Sveconorwegian Orogen, SW Sweden: implications for the growth of Fennoscandia. Geological Society, London, Special Publications, 389., 389- 392.

Petersson, A., Scherstén, A., Bingen, B., Gerdes, A., Whitehouse, M.J., 2015. Mesoproterozoic continental growth: U-Pb-Hf-O zircon record in the Idefjorden Terrane, Sveconorwegian Orogen. Precambrian Res. 261, 75–95.

Rapp, R.P., Watson, E.B., Calvin, F., Miller, F.,1991. Partial melting of amphibolite/eclogite and the origin of Archean trondhjemites and tonalites, Precambrian Research, 51, Issues 1–4, 1-25.

Richards, J, Singleton, O.,1981. Palaeozoic Victoria, Australia: igneous rocks, ages and their interpretation. Journal of the Geological Society, 28, 395–421.

Roda-Robles, E., Villaseca, C., Pesquera, A., Gil-Crespo, P.P., Vieira, R., Lima, A. and Garate-Olave, I., 2018. Petrogenetic relationships between Variscan granitoids and Li-(FP)-rich aplite-pegmatites in the Central Iberian Zone: Geological and geochemical constraints and implications for other regions from the European Variscides. Ore Geology Reviews, 95, 408-430.

Romer R.L., Smeds S.-A., 1996. U-Pb columbite ages of pegmatites from Sveconorwegian terranes in southwestern Sweden. Precambrian Research, 76 (1-2), 15-30.

Rösel, D., Zack, T., 2022. LA-ICP-MS/MS Single-Spot Rb-Sr Dating. Geostandards and Geoanalytical Research, 46, 143-168.

Schoene B., Bowring, S.A., 2006. U-Pb systematics of the McClure Mountain syenite: Thermochronological constraints on the age of the 40Ar/39Ar standard MMhb. Contributions to Mineralogy and Petrology, 151, 615–630.

Shaw, R.A., Goodenough, K.M., Roberts, N.M.W., Horstwood, M.S.A., Chenery S.R., Gunn A.G., 2016. Petrogenesis of rare-metal pegmatites in high-grade metamorphic terranes: a case study from the Lewisian Gneiss Complex of north-west Scotland. Precambrian Research, 281, 338-362.

Simmons, W.B., Foord, E.E., Falster, A.U. and King, V.T., 1995. Evidence for an anatectic origin of granitic pegmatites, western Maine, USA. Geological Society of America Annual Meeting., New Orleans, LA, Abstracts Programme, 27, pp. 411.

Simmons, W.B., Foord, E.E. and Falster, A.U., 1996. Anatectic origin of granitic pegmatites, western Maine, USA. GAC-MAC Annual Meeting., Winnipeg, Abstracts Programme A, 87.

Simmons, W.B., Webber, K.L., Falster, A.U., & Nizamoff, J.W., 2003. Pegmatology – Pegmatite mineralogy, petrology and petrogenesis. Rubellite Press, New Orleans, Louisiana, 176.

Simmons, W., Webber K., 2008. Pegmatite genesis: state of the art. European Journal of Mineralogy, 20, 421-438.

Simmons W., Falster A., Webber K., Roda-Robles E., Boudreaux A.P., Grassi L.R. & Freeman G., 2016. Bulk composition of Mt. Mica pegmatite, Maine, USA: implications for the origin of an LCT type pegmatite by anatexis. The Canadian Mineralogist, 54(4), 1053-1070.

Smeds, S.A., 1990. Regional trends in mineral assemblages of Swedish Proterozoic granitic pegmatites and their geological significance, Geologiska Föreningen i Stockholm Förhandlingar, 112(3), 227-242.

Spell, T.L. and McDougall, I., 2003. Characterization and calibration of 40Ar/39Ar dating standards. Chemical Geology, 198, 189–211.

Stephens, M.B., Wahlgren, C.H., Weijermars, R., Cruden, A.R., 1996. Left lateral transpressive deformation and its tectonic implications, Sveconorwegian Orogen, Baltic Shield, Southwestern Sweden. Precambrian Res. 79, 261–279.

Stilling, A., Ćerný, P., Vanstone, P.J., 2006. The Tanco pegmatite at Bernic Lake, Manitoba. XVI. Zonal and bulk compositions and their petrogenetic significance. The Canadian Mineralogist, 44(3), 599-623.

Taylor, S. R., Heier, K. S., 1960. The petrological significance of trace element variations in feldspars. International geological congress. Report of the 21st session Norden, Copenhagen,14, 47–61.

Taylor S.R., Erlank, A.J., Gurney, J.J., 1967. K/Rb ratios in australites, Geochimica et Cosmochimica Acta, Volume 31, Issue 6, 953-960.

Taylor, B.E., Foord, E.F., & Friedrichsen, H., 1979. Stable isotope and fluid inclusion studies of gem-bearing granitic pegmatite-aplite dikes, san diego co., california. Contributions to mineralogy and petrology 68, 187–205.

Thomas, R., Webster, J.D. and Heinrich, W., 2000. Melt inclusions in pegmatite quartz: complete miscibility between silicate melts and hydrous fluids at low pressure. Contributions to Mineralogy and Petrology, 139(4), 394-401.

Thomas, R., Davidson, P., 2012. Water in granite and pegmatite-forming melts. Ore Geology Reviews, 46, 32-46.

Thomas, R., Davidson, P., Beurlen, H., 2012. The competing models for the origin and internal evolution of granitic pegmatites in the light of melt and fluid inclusion research. Mineralogy and Petrology, 106(1-2), 55-73.

Tischendorf, G., Förster, H.-J., Gottesmann, B., 2001. Minor-and trace-element composition of trioctahedral micas: a review. Mineralogical Magazine, 65, 249–276.

Villa I. M., 1998. Isotopic closure. Terra Nova 10, 42– 47.

Villa I.M., De Bi`evre P., Holden N.E. and Renne P.R., 2015. IUPAC-IUGS recommendation on the half-life of 87Rb. Geochimica et Cosmochimica Acta, 164, 382–385.

Viola, G., Henderson, I.H.C., Bingen, B., Hendriks, B.W.H., 2011. The Grenvillian-Sveconorwegian orogeny in Fennoscandia: Back-thrusting and extensional shearing along the "Mylonite Zone". Precambrian Res. 189, 368–388.

Wang, X.-D., Lindh, A., 1996. Temperature pressure investigation of the southern part of the Southwest Swedish Granulite Region. European Journal of Mineralogy 8, 51-67.

Webber K.L., Falster A.U., Simmons W.B. & Foord E.E., 1997. The role of diffusion-controlled oscillatory nucleation in the formation of Line Rock in pegmatite-aplite dikes. Journal of Petrology, 38(12), 1777-1791.

Webber K.L., Simmons W.B., Falster A.U. & Foord E.E. ,1999. Cooling rates and crystallization dynamics of shallow level pegmatite-aplite dikes, San Diego County, California. American Mineralogist, 84, 708-717.

Webber, K. L., Simmons, W. B., Falster, A. U., Hanson, S. L., 2019. Anatectic pegmatites of the Oxford County pegmatite field, Maine, USA. The Canadian Mineralogist, 57, 811-815.

Welin, E., Blomqvist, G., 1964. Age measurements on radioactive minerals from Sweden. Geologiska Foereningan i Stockholm. Foerhandlingar, 86(1), 33-50.

Wise, M.A. & Brown C.D. 2010. Mineral chemistry, petrology and geochemistry of the Sebago granite-pegmatite system, southern Maine, USA. Journal of Geosciences, 55, 3-26.

Wise, M.A., Müller, A., Simmons, W.B., 2022. A proposed new mineralogical classification system for granitic pegmatites. The Canadian Mineralogist. 60 (2): 229–248.

Yang, Y.-H., Wu F.-Y., Yang, J.-H., Chew, D.M., Xie L.-W., Chu, Z.-Y., Zhang, Y.-B. and Huang, C., 2014. Sr and Nd isotopic compositions of apatite reference materials used in U-Th–Pb geochronology. Chemical Geology, 385, 35–55.

Zack T., Hogmalm K.J., 2016. Laser ablation Rb/Sr dating by online chemical separation of Rb and Sr in an oxygen-filled reaction cell. Chemical Geology, 437, 120-133.